2013

Planar Organic Photovoltaic Devices

Feras Alzubi
University of Central Florida

PLANAR ORGANIC PHOTOVOLTAIC DEVICES

by

FERAS G. ALZUBI
MS. Ball State University 2008

A dissertation submitted in partial fulfillment of the requirements
for the degree of Doctor of Philosophy
in the Department of Physics
in the College of Sciences
at the University of Central Florida
Orlando, Florida

Summer Term
2013

Major Professor: Saiful I. Khondaker

ABSTRACT

Organic Photovoltaic devices (OPV) are considered to be attractive candidates for clean and renewable energy source because of their potential for low cost of fabrication, easy processing, and their mechanical flexibility. The device efficiency of OPV cells are limited by several factors. Among them are: (i) donor-acceptor interface, (ii) morphology of the materials, (iii) electrode-organic semiconductor (OSC) interface and (iv) device architecture such as active material thickness and electrode separation. Although, the donor-acceptor interface has been studied in detail, the commonly prevalent vertical OPV device structure does not allow a good understanding of the other key issues as the vertical structure limits one of the electrode to be a transparent electrode as well as introducing inseparable relation between the electrodes separation and the active material thickness. In addition, it is also well known that the charge transport in OSC is anisotropic and the charge mobility is better in lateral direction rather than vertical direction. In order to address some of these issues, we fabricated OPV devices in a planar device structure where cathode and anode of dissimilar metals are in-plane with each other and their photovoltaic behaviors were studied. We used poly(3-hexylthiophene) and [6,6]-pheny1 C_{61}-butyric acid methy1 ester (P3HT:PCBM) blend as an active material. In particular, we present a detailed study about the effects of the structural parameters such as the channel length, the active layer thickness, and the work function of the electrodes on the open circuit voltage (V_{oc}), short circuit current (I_{sc}), fill factor (FF) and the power conversion efficiency (PCE).

In order to determine the suitable anode and cathode for the planar organic photovoltaic (P-OPV) structure, we first fabricated and measured organic field effect transistor (OFET) devices with different contacts and studied the effect of barrier height at the

P3HT:PCBM/electrode interface on the device output and transport properties. The study showed a clear effect of varying the contact material on the charge injection mechanism and on the carriers mobilities. The results have also shown that Au with high hole mobility and on current in the p-channel can be used as an anode (holes extractor) in the P-OPV device while In, Cr, and Ti that showed a reasonable value of electron mobility can be good candidates for cathode (electron extractor). We also found that, Ag, Al, and Mg showed large barrier which resulted in large threshold voltage in the I-V curve making them undesired cathode materials in the P-OPV device.

We then fabricated P-OPV devices with Au as an anode material and varied the cathode material to study the effect of the interface between the P3HT:PCBM layer and the cathode material. When Al, Mg, or Ag used as a cathode material no PV behavior was observed, while PV behavior was observed for In, Cr, and Ti cathode materials. The PV behavior and the characteristic parameters including V_{oc}, I_{sc}, FF and PCE were affected by varying the cathode material. The results have shown that the P-OPV device performance can be affected by the cathode material depending on the properties and the work function of the metal.

We have also studied the effect of varying the P3HT:PCBM layer thickness at a fixed channel length for Cr and Ti cathode materials and Au as anode. While V_{oc} and FF values do not change, I_{sc} and PCE increase with increasing the layer thickness due to the increase of the light absorption and charges generation. Moreover, we studied the effect of varying the channel length at a fixed film thickness; and showed that the values of I_{sc} and PCE increase with decreasing channel length while V_{oc} and FF maintain the same value.

In this thesis we will also present the results on experimentally defining and testing the illuminated area in the P-OPV device by using different measurement set-ups and different

electrodes patterns. The results prove that the illuminated area in the P-OPV device is the area enclosed between the two electrodes. Lastly, we will present the effect of the P3HT:PCBM ratio on the P-OPV device performance. We show that 1:2 ratio is the optimized ratio for the P-OPV device. The detailed results in this thesis show a potential opportunity to help improving and understanding the design of OPV device by understanding the effects of the device structural parameters.

To my parents
And
To my lovely wife

ACKNOWLEDGMENTS

I am most indebted to my parents. Many great thanks and praise are due to my parents Ghazi M. Alzubi and Ameera S. Ramadan who are always the main source of my success in my life and I will never be able to repay for their endless patience and encouragement. My parents have been the most influential people in my life. Both of them are some of the hardest working people I know.

I'm also in deep debt to my great wife, Enas M. Alramadan for always encouraging me when I was frustrated or discouraged and sharing the PhD pressure with me. She supported me every day and appreciated the intense focus it takes to obtain a PhD. I could have not done it without her. All sacrifices and efforts from her have led me to this point so they will never be forgotten.

Support from my brothers and sisters: Mohammad, Musaab, Jehad, Manar, Manal, and Aryam through my entire education has been crucial for my success.

I would like to thank my advisor, Dr. Saiful Khondaker. Saiful spent countless hours sharing his wisdom with me. I have learned so much about science and life in general from him. He was very patient in pushing me to strive hard myself. He will always be a friend and an adviser to me. I would also like to thank Dr. Andre who has helped me though my PhD by numerous discussions on photovoltaics and articles writing. Also, many thanks and appreciations go to Dr. Patrick Schelling and Dr. Lee Chow for serving on my committee.

Finally, I would like to thank all of my lab members for making my PhD possible and enjoyable. It was a pleasure to work with M. Arif, Daeha, Biddut, Rakib, Udai and Nare. I thank them all for their support, help and scientific insights. The presented work in this thesis is supported by U.S. National Science Foundation (NSF) under Grant No. ECCS 0801924.

TABLE OF CONTENTS

LIST OF FIGURES

LIST OF TABLES

CHAPTER 1: INTRODUCTION

1.1 Motivation

Sunlight is the most available renewable source of energy known to human being. However, it is still one of the most poorly consumed renewable energy sources. The first realization of the photovoltaic effect which is a conversion of light into electricity was in 1839 by Alexandre-Edmond Becquerel. After 1954 when silicon (Si) photovoltaic (PV) cell with efficiency about 6% was produced at Bell Labs [1], efforts have been focused to increase the PV device efficiency and reduce the production cost through optimizing the device architecture and by utilizing various semiconducting materials such as silicon, cadmium sulphide, gallium arsenide, cadmium telluride, and indium phosphide. PV devices based on silicon are considered the most promising and developed solar cell technology [2] because of the complete understanding of processing Si material and the well matched absorption spectra of Si with solar spectrum. For the last few decades, PV devices with efficiencies up to 25% have been produced using crystalline Si material [3]. To reduce the high cost to produce such high efficiencies research has been focused on less expensive technologies such as the thin inorganic films [4]. However, these technologies are facing challenges such as producing flexible devices and an ineffective production-cost to output-power ratio. To overcome these challenges and due to the large interest to expand the PV technology and the need for more efficient and environmental source of energy, new semiconductor materials were surfaced. In 1970s Alan J. Heeger, Alan G. MacDiarmid, and Hideki Shirakawa groups established the transition from the organic photovoltaic (OPV) technology. Their discovery has provided a clean and easy processed source of energy and has a potential of low cost energy production. OPV devices are expected to produce energy with $ 0.49 / kWh assuming 5% device efficiency with 5 years life time; and $

0.07 / kWh assuming 15% efficiency [5] while Si based PV devices costs $ 0.65 per kiloWatt-hour [6]. This low projected price is because OPV cells can be produced in large scale using inexpensive solution-based techniques such as painting and spraying [7]. However, with all of these advantages of the OPV technology, the projected price and the device efficiency of the produced OPV cells have not yet reached the competition level with the inorganic one (Figure 1.1). Efforts now are paid more towards increasing this efficiency to more than 10% or increasing the device life time to more than 5 years in order for the OPV cells to be practical and to compete with the inorganic Si-based PV cells [8, 9, 10].

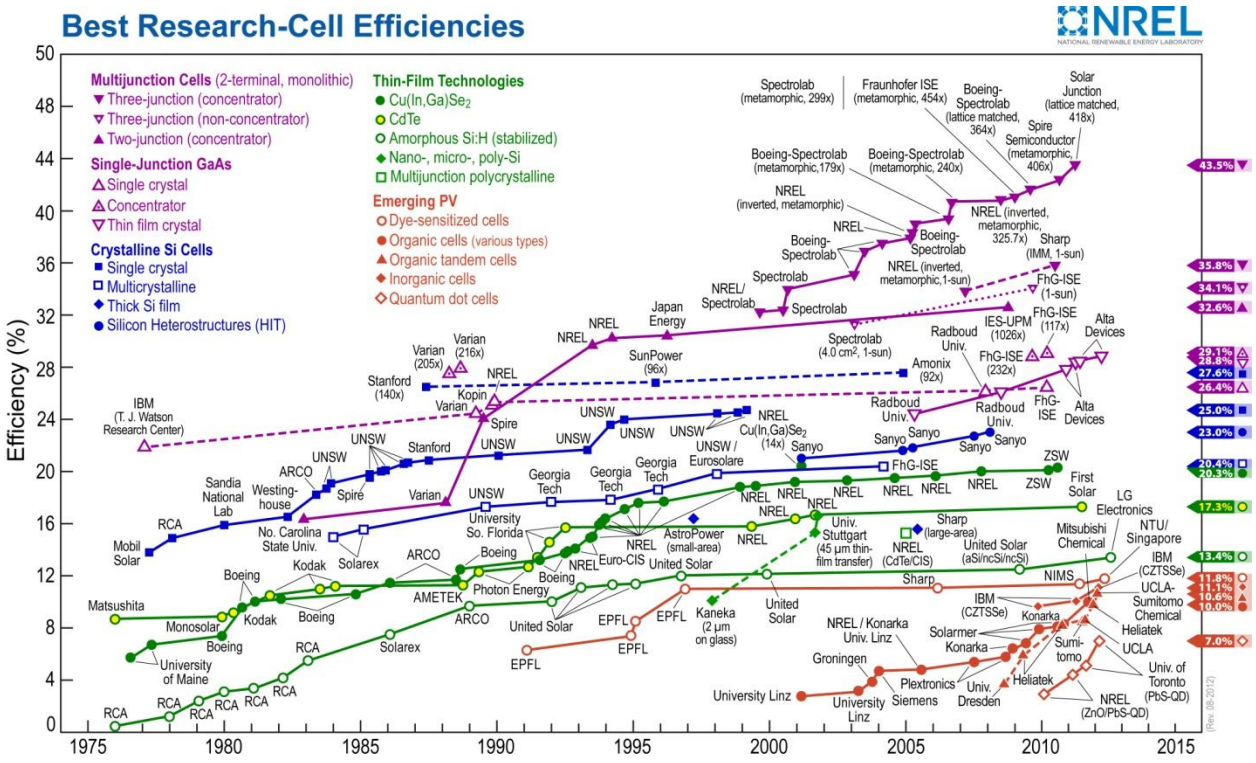

Figure 1.1 Best photovoltaic research efficiencies from 1976 to 2012 with organic PV technology showing low values [11].

The main reason for the slow progress of the OPV technology is the incomplete understanding of the design rule of OPV device which includes: (i) device architecture, (ii) the

choice of organic material, and (iii) the fabrication and synthesis parameters. Different routines to design a high efficiency organic solar cell have been tried such as using an active layer that consists of organic materials [12, 13], a mixture of organic and inorganic [14, 15], a mixture of high and low band gap polymers [16, 17], a polymer–polymer combination [18, 19]. In addition, various device structures such as inverted BHJ polymer solar cells [20], multilayer PV cell [21], and tandem cells [22] have been employed to understand and produce more efficient OPV device performance. Also, the performance of organic photovoltaic device can be further enhanced by engineering the active layer materials and their interfaces with the electrodes. The most stable optimized OPV device structure up to this point is made in a vertical geometry where an active layer (photo-active material) is sandwiched between a metallic electrode and a conducting transparent electrode (Indium Tin Oxide (ITO)) to transmit the light through (see Figure 1.2).

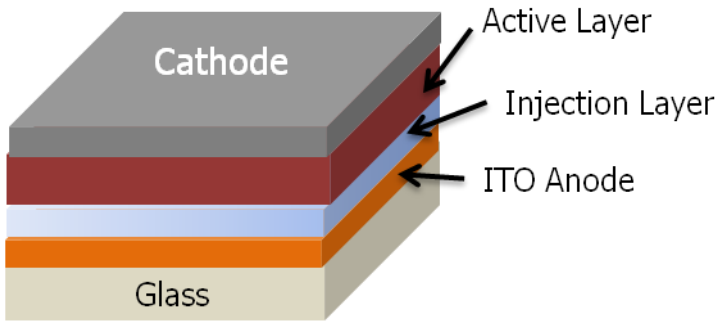

Figure 1.2 Vertical OPV device, the current most common PV device structure.

The structural nature of stacked layers in the vertical OPV device has introduced some limitations to the device performance, and the effect of some physical parameters cannot be addressed in the vertical OPV device because of its geometry as I discuss below.

First, an important limitation related with the vertical geometry is the fact that the active material thickness defines the electrodes separation which limits the light absorption that can be

increased by higher thickness. When increasing the thickness, the absorption path is increased leading to more photons absorption and more charge carriers generation [23]. However, the increase of thickness yields to the increase of the electrodes separation which decreases the carriers' mobilities and increases the probability of the free charges to recombine [24,25] which leads to a decrease in the PCE value (see Figure 1.3). Therefore, photovoltaic devices with vertical structure must have a limited active material thickness. As for the channel length, recent studies have indicated that a decrease in the charge recombination rate and an increase in the charges harvesting efficiency are related to short channel length (or small electrodes separation) which affects the PV device performance [26, 27]. However, the small electrodes separation cannot be achieved in the vertical geometry because the two electrodes are more likely to be shorted because of the creation of pine holes in the active layer during spin coating. In addition, a decrease in the electrodes separation leads to a poor light absorption in the active layer. Thus, independent optimizations of both channel length and thickness are highly expected to achieve high quality photovoltaic device.

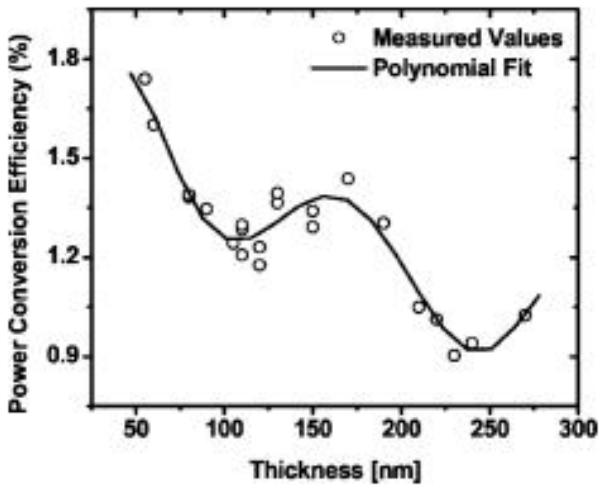

Figure 1.3 The variation of PCE in vertical OPV device with increasing the active layer thickness from ref [28].

Another limitation existed in the vertical OPV device geometry is the need for a transparent electrode, mostly ITO, which is an essential component in fabricating the device. Even though ITO was chosen because of its high transparency and good conductivity, it has a transparency of ~ 80% which can reduce the number of photons that can reach the active layer. Also, ITO with a conductivity in the range 10^5 S/m depending on its layer thickness is lower than the conductivity of metals about 10^7 S/m [29] which can affect the charge collection at the interface between the active material and the contacts. To overcome the related challenges, studies have been conducted to establish ITO free PV devices. For this purpose, different approaches are discussed in literature to substitute ITO electrode with mesh metallic electrodes [30, 31], ultra thin metal films [32, 33], and metallic nanowires [34, 35]. In these approaches, the vertical geometry was utilized with a higher metallic electrode conductivity which resulted in a gain in the conductivity. However, this gain was encountered because the high transparency of the ITO was compromised by the use of the metallic electrodes that are less transparent which led to low PCE values.

In vertical OPV device, because the active material is embedded in between a metallic layer and a not-fully transparent layer ITO, it is tough to examine the optical and morphological properties of the active layer by spectroscopic and microscopic tools. In addition, because of stacking layers structure of vertical OPV device the photon absorption will never be 100% because the active layer is embedded in a multilayer's structure with different refractive indices [36] and not fully transparent ITO electrode. Also, The stacked layer nature of the Vertical OPV device limits the study of the various interfaces in the device such as the acceptor/donor, acceptor/acceptor, active material/contact interfaces which play an important role in improving the PV device performance because these interfaces are responsible for the charge transport.

The charge transport plays an important role in the OPV device operation. Several techniques have been employed to understand the charge transport and recombination mechanisms in OPV devices; for example: transient photocurrent [37] and thin film field effect transistor [38]. Employing these techniques in the current vertical OPV device involves complex measurement set-ups that analyze the transient response of OPV device. The analyzed response also does not reflect the actual operation of the OPV device since it operates in a steady state and not a transient regime. In addition, the charge transport mechanism in the vertical structure is affected by the phase segregation of the components of the active material [39]. Donor and acceptor materials in the active layer are known to phase segregate vertically during the material spin coating and annealing which creates gradients of the concentrations of those materials in the vertical direction [40, 41]. This phase segregation is difficult to model because of its wide variation along the active layer depth.

In order to address the above issues that are difficult to be clearly understood in the vertical OPV device, a different device structure is required. The planar organic photovoltaic (P-OPV) device structure where the active material is deposited between two dissimilar metal electrodes that are patterned on a SiO_2 substrate has a great potential for understanding OPV device performance (see Figure 1.4).

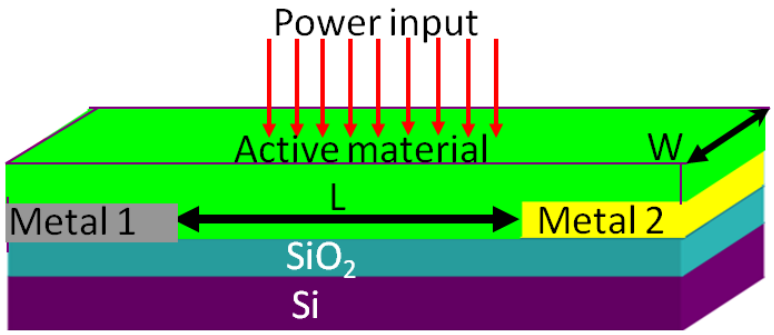

Figure 1.4 The planar organic photovoltaic device structure. Metal 1 and 2 are the two dissimilar electrodes, (L) is the channel length, and (W) is the channel width.

We utilize the P-OPV device structure to address several challenges resulted and can't be addressed by the use of the vertical geometry. By utilizing P-OPV device in this work, we were able to decouple the effect of the active layer thickness and the electrodes separation (channel length) as an advantage provided by the planar geometry. This allows us to independently control the active layer thickness and the channel length which has not been conducted before. We were able to study the effect of increasing the active layer thickness on the absorption and hence the device performance while keeping the electrodes separation fixed. On the other hand, we were able to investigate the effect of decreasing the channel length on the device performance without affecting the amount of the absorbed light in the film thickness. In addition, P-OPV device has the potential to be fabricated with few nm's channel length and investigate its related effect on the device performance with no fear of the electrodes to be shorted and affecting the light absorption.

Since in P-OPV the two electrodes are in plan, there is no need for a transparent electrode (ITO) because the light can be directly shinned on the active material. Utilizing this structural property of P-OPV we were able to study the effect of varying the contacts work function on the OPV device performance. This opens up the opportunity to fabricate the contacts from metals with higher conductivity than ITO and with different work functions. Varying the work function of the contacts leads to increasing or decreasing in the barrier height at the contact and active layer interface which can affect the OPV device characteristic parameters as we will see in this work. The fact that the active layer in P-OPV device is directly exposed to the light with no need to pass through multi layer structure makes it possible for the absorption to reach 100% because the light is not reflected of any stacking layers before reaching the active material. Also, this allows the study of film morphology and optical properties in transit with PV measurement.

P-OPV device also allows the study of the effect of the various interfaces such as the acceptor/donor, acceptor/acceptor, active-material/contact that exist in the device without affecting the device structure or performance. The study of such Interfaces that affect the charge transport in the device can help improving the device performance and add a deep insight to the device operation. In addition P-OPV can also be employed to address other issues such as the study of the charge transport and recombination in a steady state regime. In P-OPV device, PV behavior can be studied at the same time with charges recombination and transportation.

Vertical phase segregation effect has less influence in planar structure than in vertical because the charge transport in P-OPV is horizontally where no phase segregation gradients exist because of the constant component's concentration along the charge transportation path between the electrodes. Another advantage of using P-OPV device is that the FET mobility is expected to higher in plan than in vertical direction, this because π-orbital is responsible for the charge transport in the organic molecules chains. This orbital is distributed parallel to the substrate favoring the transport in that direction [[42], [43]] leading to anisotropic charge transport where the mobility along the backbone of the molecules chains is higher than along the vertical direction.

In addition, because of the recent high demand for flexible, portable, and multifunctional organic devices, the planar device structure can be an attractive to achieve those goals. Multi-functional planar organic-based devices have been recently reported; for example, field effect transistor (FET) that also works as light emitting diode (LED) [[44], [45]], and a solar cell that works as LED [[46]]. Also, recent reports on multifunctional organic-based devices have reported the fabrication of OPV device in a planar structure that can be used as a power source and an FET at the same time [[47], [48]]. However, those studies showed a low device performance including low PCE and mobility that can be a result of the use of (i) improper electrodes combination, (ii) non

optimized channel length, (iii) non optimized film thickness, and (iv) non optimized blending ratio. The investigations of these effects on the PV device performance can help to further improve the design of efficient OPV device.

1.2 Organization of the thesis

The background chapter discusses in details the photovoltaic effect and paying more focus to the history of organic photovoltaic devices and the evolution of the bulk hetrojunction material (BHJ). The general information about OPV device working mechanism, materials, and structure will be also discussed in this chapter. At the end, the characteristic parameters of a PV device will be introduced beside their effect on PV device performance.

After discussing the background, Chapter 3 will provide the information about the fabrication processes performed in our lab. This chapter will describe the fabrication of electrode patterns using electron beam lithography, organic solutions details, and experimental details for the fabrication OPV devices by spin coating mechanism, and measurement setups.

Chapter 4 reports performances of organic field effect transistors of the P3HT:PCBM blend with different metal electrodes. The mobility of these devices in addition to their output characteristics are reported and discussed as a tool to fabricate a functioning OPV planar device.

Chapter 5 will present detailed output, current-voltage, measurements on planar OPV with P3HT:PCBM (1:2 ratio) devices mainly to study the PV behavior of these devices. In contrast to the current vertical PV device, we show how the efficiency of OPV device is related to the device parameters, mainly electrodes separation and active layer thickness. In the same chapter, we also show that by utilizing the planar structure different metals can be used as electrodes and among those metals Cr and Ti have shown a good PV behavior.

Subsequently, in chapter 6 we will test the validity of the definition of the illuminated area in the planar PV device which is the area in-between the electrodes. This was performed by introducing two set of experiments: 1) comparing the efficiency values executed from up light shining with the ones from the bottom light shining and 2) studying the effect of the parasitic paths in the planar PV device.

Chapter 7 discusses the justification behind using P3HT:PCBM with 1:2 ratio in planar OPV device in this thesis while 1:1 ratio is known to be the optimized in vertical PV devices. This was done by comparing the efficiency values with other ratios and by discussing the effect of the used substrate, SiO_2, in the planar structure.

Chapter 8 shows the experimental strategies to enhance the efficiency in the planar structure by introducing the multi hole collector design which will enhance the collection of the hole carriers and by engineering the metal/organic interface through introducing a buffer layer at the interface. The final Chapter 9 draws the conclusions to this thesis in addition to suggesting the future directions and experiments related to this work.

CHAPTER 2: BACKGROUND

2.1 Photovoltaic device operational basics

An OPV device converts the solar illumination into photocurrent in four major processes: (i) Incident photons absorption and exciton generation (electron-hole pair), (ii) Exciton diffusion to the donor–acceptor interface, (iii) charges separation and transportation, and (iv) charges collection at the respective electrodes [[49]]. The four processes are illustrated in Figure 2.1 were LUMO is the lowest unoccupied molecular orbits, and HOMO is the highest occupied molecular orbits.

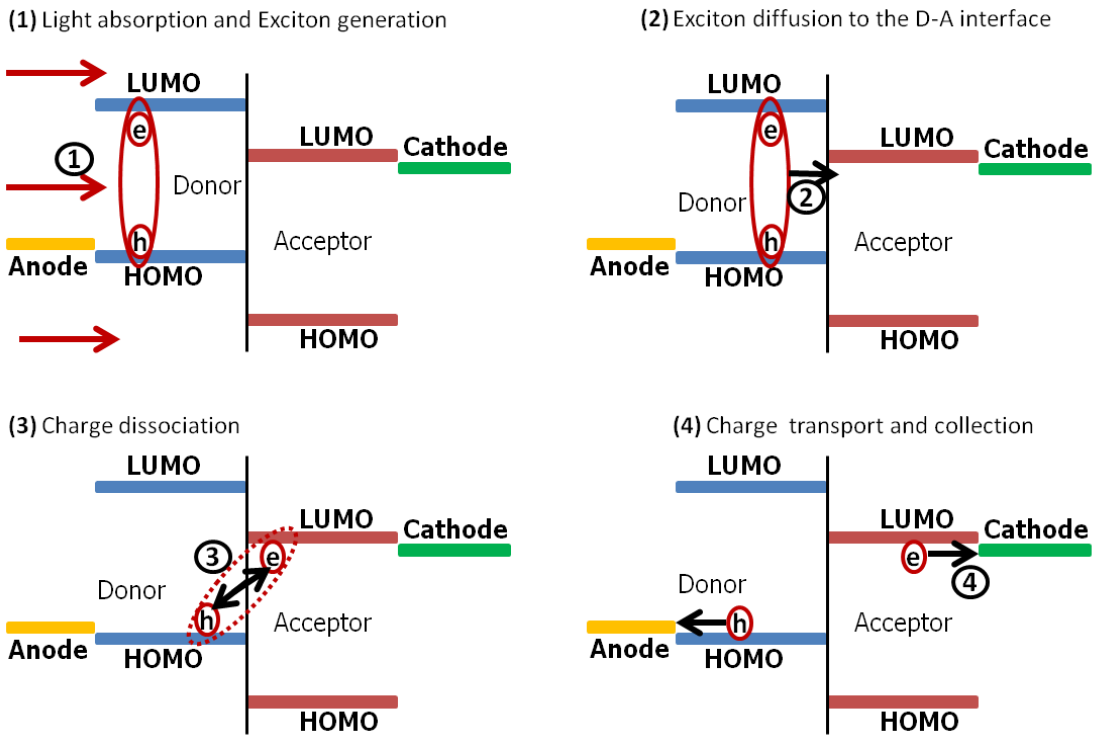

Figure 2.1 The four major processes occur when an OPV device is illuminated. Donor and acceptor are the organic components of the active layer material.

When the incident light reaches the active material in an OPV device then electron-hole pairs (Excitons) are created at the donor (p-type) material due to the electron transition from HOMO to LUMO level. The amount of the absorbed light in the active layer depends on the layer thickness and the absorption coefficient of the active material. The absorption efficiency (η_{abs}) is determined by the number of absorbed photons with respect to the incident one. This efficiency is also affected by other factors such as the absorption spectra of the active material and how well it matches the incident's light spectrum and the device architecture. The OPV cell responds to the light based on the absorption spectrum of the active layer material which depends on the chemical structure of that material (Figure 2.2).

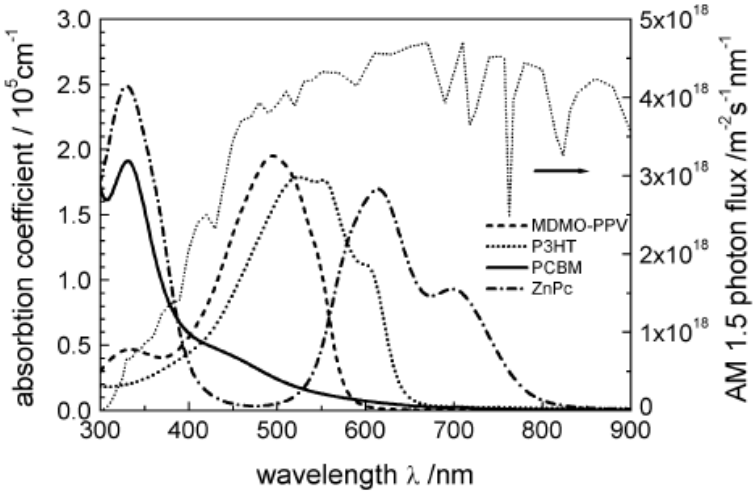

Figure 2.2 Absorption coefficients (represent the absorption spectra) of organic materials are compared to the standard solar spectrum ref [50].

In the second operational process, the generated excitons diffuse to the donor-acceptor interface. The efficiency of exciton diffusion in organic PV device is determined by the diffusion length of the exciton which is about ~ 10 nm in organic materials [51, 52]. Also, the morphology of the donor-acceptor interface affects the exciton diffusion process [53]. If the recombination process (hole-electron pair makes up an exciton back) doesn't occur during the diffusion process,

then the exciton with a binding energy 0.1-0.2 eV is dissociated (i.e the hole-electron pair is separated) at the interface due to the presence of the internal field at the donor-acceptor interface. Finally, the separated electrons and holes are then transferred through the donor and acceptor networks to the respective electrodes primarily by drift and diffusion processes [54]. Charge traps such as defect in the active layer morphology or dead ends in the networks of the donor and acceptor materials can lower the mobility of the transported charges. The most efficient collection of the separated charges at the contacts occurs when the work function of the cathode is less than LUMO of the acceptor and work function of the anode is larger than HOMO of the donor.

2.2 Current-Voltage (I-V) characteristics of OPV cell

The characteristic parameters that define the OPV device performance can be extracted from the current-voltage (*I-V*) curve of the measured devices. Figure 2.3 (a) shows a typical *I-V* curve for an idealized OPV device under illumination. From the curve in the Figure, short circuit current (I_{sc}) is at zero applied voltage. V_{oc} is the open circuit voltage which is a material property in case of organic materials. MPP is the maximum power point where the product of the current (I_{max}) and voltage (V_{max}) is maximum. A negative power indicates a power generation. The ratio of the maximum power to the multiplication of I_{sc} and V_{oc} determines the fill factor (FF) of the OPV device which is an indication of the device performance.

Figure 2.3 (b) shows the equivalent circuit for an OPV device that consists of current source, parallel resistance, and diode all connected in parallel and the three elements are connected in series with another resistance.

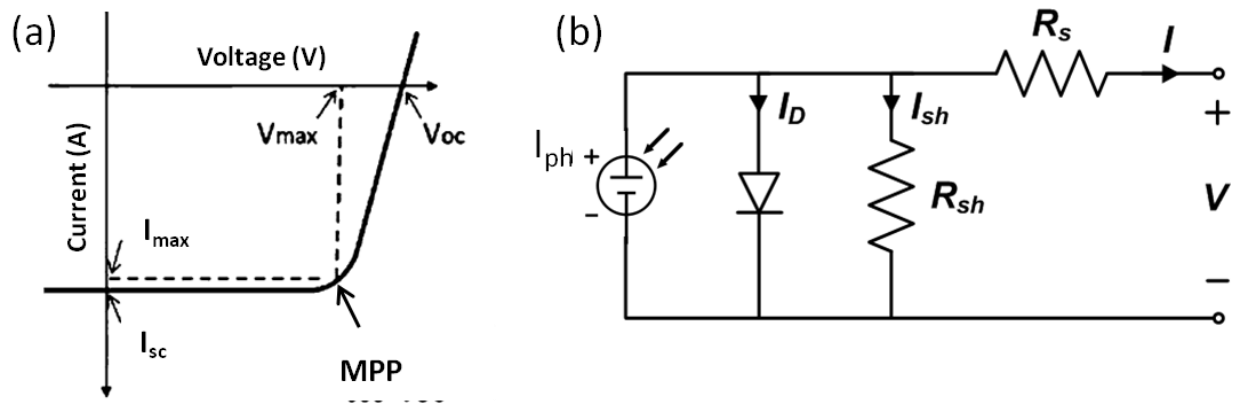

Figure 2.3 (a) Typical current-voltage (*I-V*) curve for an OPV device under illumination. (b) Equivalent PV device circuit with R_S: series resistance, R_{SH}: shunt resistance, I_D: dark current, I_{sh}, current pass through shunt resistance, and I_{ph}: photo current.

Under dark condition, the I-V curve resembles a diode behavior with small current in reverse bias and exponential behavior in the forward bias because the charge injection occurs in the forward bias. This diode like behavior is due to the energy barriers between the organic material and the contacts. When the device is illuminated, a photocurrent (I_{ph}) is created in the device; the superposition of the dark current and the photocurrent is the I-V characteristics under illumination which can be described by Shockley equation:

$$I = I_s \left[exp\left(\frac{qV}{nkT}\right) - 1 \right] - I_{ph} \qquad (2.1)$$

Where, I_s is the reverse saturated current, q is the elementary charge, k is Boltzmann constant, n is the ideality factor, and T is the temperature [55]. The photocurrent depends on the applied voltage in a real device, incident light intensity and spectrum.

The diode behavior of the OPV device under dark which represents the rectification behavior of the donor-acceptor heterojunctions is characterized by I_s and "n". The ideality factor is extracted from the slope of the exponential curve in the forward bias and it is equal to 1 in

ideal diode. Ideality factor value greater than one, indicates a low rectification at the donor-acceptor hetrojunctions due to many factors like recombination current. The values of "n" are normally greater than 1.6 for organic-based photovoltaic devices due to the charge recombination in the device.

After the illumination and photocurrent generation passes through the device and reaching the contacts, a series resistance (R_S) is created in the path of this current due to the finite resistance of the organic layers and the electrodes in addition to the contact resistance at the interfaces with the electrodes. The lower the series resistance the less power loss because more current will pass through the device. Finally, the shunt resistance (R_{SH}) accounts for the leakage current, charge recombination, and dead ends in the networks of the donor or acceptor. For an ideal OPV device, Rs=0 and $R_{SH}=\infty$; and for an actual OPV device R_s and R_{SH} can be calculated from the I-V curve the measured device as following:

$$R_S = \frac{1}{dI/dV} \; at \; I = 0 \tag{2.2}$$

$$R_{SH} = \frac{1}{dI/dV} \; at \; V = 0 \tag{2.3}$$

From the equivalent circuit model and after accounting for the Rs and R_{SH} the equation for the *I-V* characteristics of a photovoltaic device is derived as:

$$I = I_s \left[exp\left(\frac{qV - IR_s}{nkT}\right) - 1 \right] + \frac{V - IR_s}{R_{SH}} - I_{ph} \tag{2.4}$$

2.3 Characteristic parameters of OPV device

The parameters for OPV device that are extracted from the I-V curve of a device under known illumination intensity are called the characteristic parameters because they define and evaluate the device performance. Those parameters are mainly: open-circuit voltage (V_{oc}), short circuit current (I_{sc}), fill factor (FF), and the power conversion efficiency (PCE).

2.3.1 Open-circuit voltage

One of the main characteristic parameters that the performance of an OPV device depends on is the open circuit voltage (V_{oc}), the value of V_{oc} is determined when the current in the external circuit is equal to zero [56]. Since the current value is zero at this voltage, no power is produced. However, V_{oc} sets the boundary for the voltage values at which power can be produced. The nature of V_{oc} has been a crucial topic in the literature, a general definition of V_{oc} gives it the same value as the built in potential. This definition is accurate at low temperature and underestimating the built-in potential at room temperature [57,58]. In a metal/insulator/metal (MIM) device V_{oc} is equal to the difference between the work functions of the two electrodes' materials [59]. Various studies have experimentally proved this MIM definition of V_{oc} by studying OPV device made of ITO as one electrode and the other electrode was either aluminum (Al), magnesium (Mg) or calcium (Ca) [60, 61]. On the other hand in organic PV device, V_{oc} value is equal to the difference between the HOMO level of the donor and LUMO level of the acceptor.

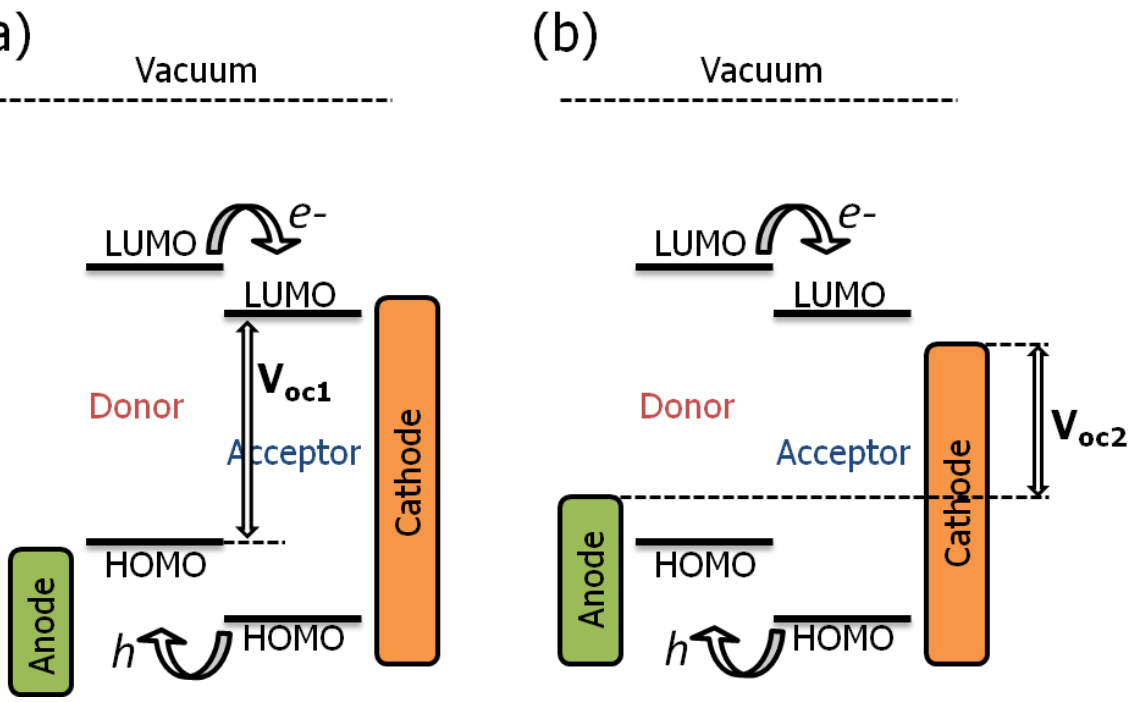

Figure 2.4 Energy band diagram of donor and acceptor materials with respect to the work functions of the metal contacts in OPV device. (a) ohmic-contacts case where difference between HOMO and LUMO levels of donor and acceptor is V_{oc1}. Non-ohmic contacts where difference between work functions of the electrodes is V_{oc2} according MIM theory.

Figure 2.4 shows the band structure of an OPV device including the HOMO and LUMO levels of the donor and acceptor materials and the work functions of the contacts. When the work-functions of the anode and cathode match the HOMO of the donor and the LUMO of the acceptor, respectively, then ohmic contacts are created as illustrated in Figure 2.4 (a). In this case, the maximum V_{oc} value is equal to V_{oc1} which is the difference between HOMO of the donor and LUMO of the acceptor, and V_{OC} is governed by the active material properties. On the other hand, when non-ohmic contacts are created as in Figure 2.4 (b) where the difference between the electrodes work functions is less than an not matching the LUMO-HOMO difference then the maximum V_{oc} value is V_{oc2}, according to MIM. Mihailetchi et al. have concluded that V_{oc} of a BHJ OPV device is governed by the electrodes work functions for a non-

ohmic contacts, and it is governed by the HOMO and LUMO levels of the donor and acceptor materials for ohmic contacts [62]. Scharber et al. have extracted a linear relation between V_{oc} value and ($|E^{Donor}HOMO|-|E^{PCBM}LUMO|$) and they proved that MIM is not valid to BHJ OPV devices [63]. V_{oc} value for a measured OPV device can be affected by many experimental or device parameters such as the dark current [64], light intensity, and chemical potentials [65, 66]. Brabec et al. have shown that V_{oc} depends on the acceptors' material strength, and it is not influenced by the work function difference [67]. Gadisa et al. measured V_{oc} of ITO/PEDOT:PSS/Polymer/LiF/Al OPV device with different conjugated polymers [68]. They showed that V_{oc} depends on the oxidation potential of the polymer as a result of varying the injection barrier when varying the polymer. Frohne et al. found that the doping level of the injection layer PEDOT:PSS layer can affect the value of V_{oc} [69]. Another group has introduced the fact that the morphology of the active layer material can affect the value of V_{oc} [70]. Koster et al. have found a dependency of V_{oc} on the intensity of incident light for polymer/fullerene BHJ OPV device [71].

2.3.2 Short-circuit current

The value of short-circuit current (I_{sc}) is extracted from the I-V curve when the applied voltage is zero i.e. the external applied electric field equals and opposes the internal electric field created by the OPV device. In ideal OPV device, I_{sc} has the same value as the photocurrent. However, several effects can lower the I_{sc} value from the ideal one such as the recombination process. The most device structural parameter that affects I_{sc} is the active layer thickness. Moule et al. showed that the performance of a BHJ OPV device highly depends on the thickness of the active layer, and I_{sc} dependency on the thickness is not BHJ material sensitive [72]. Hoppe et al.

have related the I_{sc} to the internal quantum efficiency by modeling the optical properties of BHJ OPV device made from MDMO:PPV/PCBM [73]. The most common active layer used in fabricating OPV device is made from PCBM blended with MDMO-PPV or P3HT. One limiting factor in such materials is the limited absorption. A P3HT layer with thickness 240 nm can absorb only 21% of the sun's incident photons [74] in the range between 350 and 650 nm. This low percentage of the absorption is due to the mismatch between the solar and P3HT absorption spectra.

The lower the band gap of a polymer, difference between the HOMO and LUMO levels, the more photons that can be absorbed in the polymer layer and the higher current value passes in the device. However, common polymers used in OPV field have relatively high band gaps more 1.8 eV [75]. This limitation can be overcome by introducing low band gap molecules that shift the polymers' absorption spectra more to the red part of the spectra. The use of low band gap polymers has been reported by many research groups [76, 77, 78, 79, 80]. Another way to overcome the absorption limitation is to increase the thickness of the active layer to absorb more photons and increase the I_{sc} value. However, increasing the thickness affects the carriers' mobility and the charges life time in the OPV device.

2.3.3 Fill factor

While V_{oc} and I_{sc} define the boundaries of power production in OPV device, the maximum power point (MPP) which is the product of maximum voltage (V_{max}) and current (I_{max}) will be always less (see Figure 2.6). How close is maximum power point to the limits of power production of I_{sc} and V_{oc} is indicated by the fill factor (FF) which is defined for an OPV device as ratio between the maximum power point to the product of V_{oc} and I_{sc}, see Figure 2.5 below:

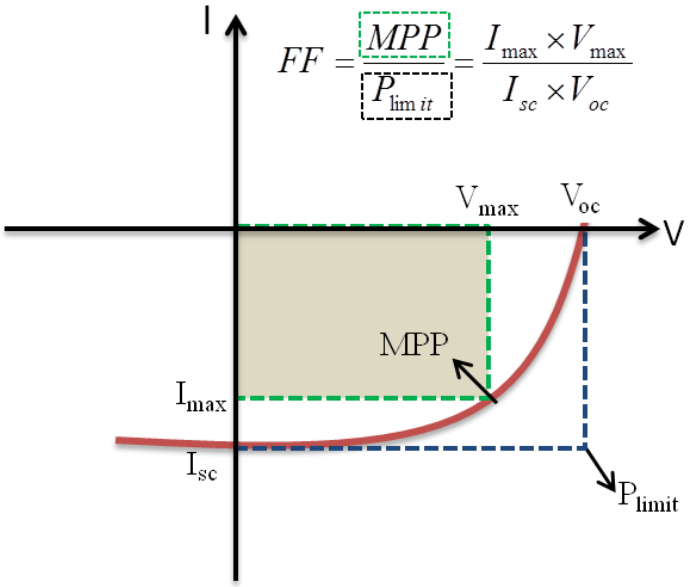

Figure 2.5 Definition of FF from the typical I-V curve of a PV cell.

The value of FF also indicates the sharpness of the curvature of the I-V curve. The higher FF is desired because it is a result of higher maximum power point. The value of FF is always less than 1 in OPV device due to the diode-like behavior of the device and the additional resistances. This value depends on charge dissociation and transportation, and recombination rate [81]. Also, the active layer morphology and thickness, and the polymer interface with the contacts can affect the value of FF. The series resistance (R_s) and the shunt resistance (R_{SH}) can reduce the FF value.

The main factor that can reduce FF value, by varying the series resistance, is the interfacial area between the active layer and the electrodes. For OPV devices made in vertical geometry, low FF has been reported as a result of the absence of injection layers at the electrode [82, 83, 84]. The main function of injection layers such as PEDOT:PSS or metal oxides is to decrease the injection barrier for the carriers at the electrode interface which leads to high R_{SH} and low R_s. Gupta et al. found that FF highly depends on the quality of polymer/cathode

interface, and can be reduced when charge accumulation due to defects at the interface occurs [85]. The high thickness of active layer increases R_s and decreases R_{SH} leading to a lower FF, this is due to larger distance that carriers must travel to be collected at the electrodes which increases the recombination and reduces the mobility of the carriers. M. Kim et al. have studied the ways to control FF and have shown that increasing the active layer thickness decreases the FF values [86]. Also, they have shown that R_{SH} and FF are reduced when increasing the light intensity due to the higher recombination rate in the active layer.

2.3.4 Power conversion efficiency

The most parameter discussed when describing the performance of an OPV device is the power conversion efficiency (PCE) which is defined as the ratio of the maximum output power to the incident irradiance (power per unit area). The overall power conversion efficiency (PCE) of an OPV device can be calculated by:

$$PCE = \frac{I_{max} \times V_{max}}{P_{in}} \times 100\% = \frac{I_{sc} \times V_{oc} \times FF}{P_{in}} \times 100\% \quad (2.5)$$

Where, P_{in} is the incident power per unit area. Typical values for PCE and OPV device performance are normally reported in AM1.5G conditions where P_{in} is 100 mW/cm^2 matches the irradiance of the sun when it is at angle of 48.2^o from the earth's surface. It is clear from the above equation that PCE depends mainly on the FF, I_{sc}, and V_{oc} values. Furthermore, the illuminated area used to calculate PCE can affect its value. Usually when calculating PCE, I_{sc} is presented by the short circuit current density (J_{sc}) which is the short circuit current divided by the illuminated area.

2.4 Organic photovoltaic materials

Two types of materials have been mainly used in OPV field: vacuum processed materials like small organic molecules and solution processed materials such as semiconducting polymers/molecules [87]. The variation of the polymers' properties made their discovery a turning point in the photovoltaic field. Optical and electrical properties are mainly important in addition to the ease of processing the polymers. Polymers in general are either saturated, with all valence electrons form covalent bonds making the polymer insulator, or conjugated polymers where for each carbon atom there is one unpaired electron called the π electron or bonding. This π bonding results in a delocalization along the back bone of the polymer chain leading to high charge mobility along the backbone. The conductivity level of conjugated polymers depends on the chain symmetry which determines the electronic structure of that polymer. Some polymers can even show metallic properties depending on the electronic structure [88]. Conjugated polymers have been a material of interest in photovoltaics [89], OLEDs [90,91,92], and OFETs [93,94] because they can absorb light and transfer the photo generated charge carriers due to the extended delocalized π electron on their structure. A good chemical stability and high visible light absorption are required for organics to be considered as an active material in an OPV device which makes conjugated polymers good candidate for an active layer [95]. However, using conjugated polymers only as an active material led to poor PV device performance [96]. This was changed and a better device performance was achieved by mixing conjugated polymers with electron acceptor materials such as fullerenes [97,98,99,100,101]. In such combination (polymer-fullerene) the polymer performs as an electron donor material and the fullerene performs as an acceptor. The soluble derivatives of Buckminsterfullerene, C60, are famous acceptor materials such as [6,6]-pheny1 C_{61}-butyric acid methy1 ester (PCBM) (Figure 2.6). PCBM was

synthesized by Wudl et al. [102] and commonly used in organic PV devices because of its solution processability. Some widely used hole conducting donor polymers because of their charge transport, low bandgap, and optical properties are: poly[2-methoxy-5-(3,7-dimethyloctyloxy)]-1,4-phenylenevinylene) (MDMO-PPV), poly(3-hexylthiophene) (P3HT) and (poly(9,90-dioctylfluorene-co-bis-N,N0-(4-butylphenyl-1,4 phenylenediamine) (PFB) and PCDTBT. MDMO-PPV has a bandgap of 2.2 while P3HT has a 2.1 eV and M3H-PPV has a ~2.4 eV bandgap. MEH-PPV has 3.0 eV bandgap while PCDTBT has a 1.8 eV. Different bandgaps varies the range of the wavelengths that these polymers can absorb and ability to transport charges.

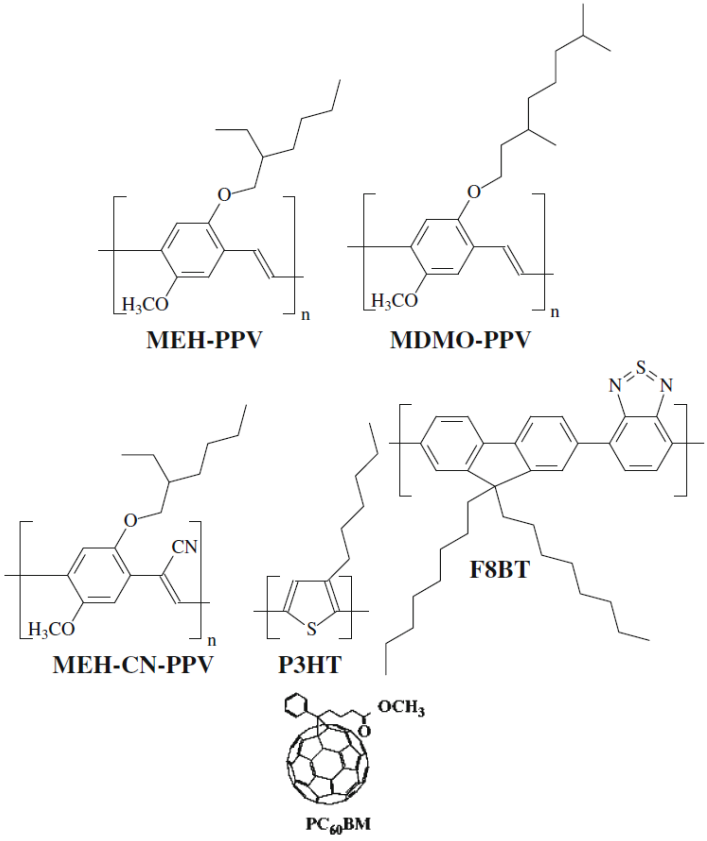

Figure 2.6 Examples of famous donor polymers and acceptor materials used in OPV device.

2.5 Organic photovoltaic device architecture

The common OPV device consists of transparent substrate (glass) covered with a transparent conducting material that form an electrode (mostly indium-tin-oxide (ITO)). ITO material is chosen because it allows light to be shinned through and reach the device, at the same time it is conducting so it collects the holes. However, using ITO as an electrode in the PV comes with different draw backs such as the low conductivity in comparison with metals, oxygen discharge into the organic layer, low transparency in the blue region, and large-scaling PV device using ITO will be expensive due to the price of Indium [103]. Mostly, the ITO electrode is coated with PEDOT:PSS, poly(ethylene-dioxythiophene). PEDOT:PSS is a conducting material that enhances the hole extraction at the surface of the ITO electrode and reduces the amount of shorts at the ITO surface [104, 105, 106]. The second major element in OPV device is the photo active layer (organic material blend) which coats the ITO/PEDOT:PSS electrode. The most famous methods of depositing this layer are: spin coating, doctor blading, screen printing, and ink jet printing.

The last element to be fabricated in the PV device is the top electrode which is, commonly, a metal with an under interfacial layer made of lithiumfluoride (LiF). The LiF layer has the same function as the PEDOT:PSS of enhancing the surface and reducing the metal work function, and other roles for this underlayer are still under debate in the literature [107, 108, 109, 110]. The use of two electrodes with two different work functions introduces a potential drop at the donor-acceptor interface to efficiently separate the electron-hole pair (exciton dissociation). In the following, the most common device configurations are discussed a long with their advantages and disadvantages. The main difference between these configurations is in the exciton dissociation process and the charge transportation.

2.5.1 Single layer OPV device

The single layer OPV device is constructed by sandwiching a p-type conjugated polymer between a transparent electrode (ITO) and a metallic one (Al) (Figure 2.7 (a)). polyacetylene [111] and polythiophene [112] were the main conjugated polymers used in the early work done on single layer OPV. Poly [2-methoxy-5-(20-ethyl-hexyloxy)-1,4-phenylene vinylene] (MEH-PPV) is a famous example of these polymars and considered a material of interest in single layer organic optoelectronics [113]. However, using this polymer with single layer OPV device architecture ITO/PPV/Al had resulted in a low efficiency 0.07% - 1% for light intensities of 1 mW/cm^2 [114, 115, 116]. The potential difference created by the asymmetry of the work function of electrodes was not enough to produce reasonable power efficiency. In addition, the main reason behind the low efficiency in the single layer OPV devices is the low carrier generation resulted from low exciton dissociation rate (electron and hole separation). Because of the short exciton diffusion length (10 nm), photoexcitations can only dissociate at the polymer/cathode interface where a depletion region of the Schottky contact exists. Therefore, only a small area contributes to free charge generation in single polymer-based OPV devices. It was later discovered that the exciton dissociation process is more efficient when an interface between donor and acceptor exists; this led to the development of bi-layer OPV device by introducing an acceptor layer between the donor (polymer) layer and the cathode. Single-layer conjugated polymer-based devices experienced a poor PV behavior. The device architecture affects the overall performance of OPV device.

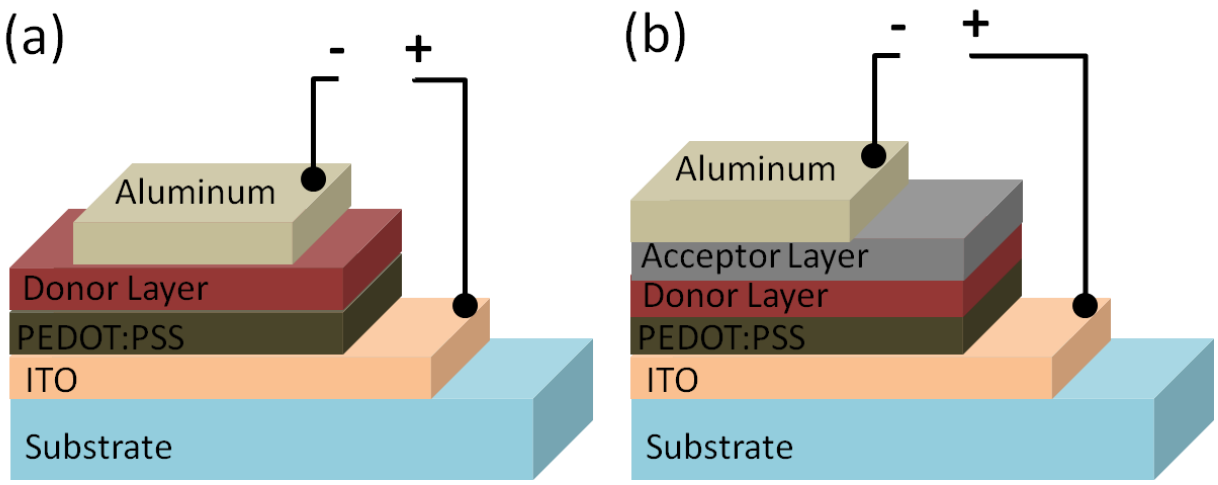

Figure 2.7 (a) Single layer OPV device architecture. The donor layer is a conjugated polymer. (b) Bilayer OPV device where the donor layer and the acceptor layer form the active material.

2.5.2 Bi-layer OPV device

The major drawback in single-layer OPV device is the low current generation because the only area that contributes to the generation is the polymers/electrode interface area. To overcome this problem, the bi-layer, donor and acceptor, OPV device was introduced [117]. The donor and the acceptor layers are stacked above each other in a bi-layer device, and then sandwiched between an ITO and Al electrodes (see Fig. 2.7 (b)). In bi-layer device, interaction and photogeneration occur at the geometric interface between the donor and the acceptor layers. Under photoexcitation, the conjugated polymers (electron donors) show ultrafast and stable electron transfer to Buckminster fullerenes (acceptor layer) in solid films [11, 118, 119, 120]. The interface between the two layers plays the main role in device performance and the outcome PV properties [121]. Research groups have used different methods to fabricate bi-layer OPV device like: (i) thermal deposition [122,123,124], (ii) solution casting of one material and evaporation of the other [125, 126, 127], and (iii) solution casting using polymer precursor [128]. Power conversion

efficiencies of 3.6% using bi-layer OPV device were achieved using vacuum-deposited copper phthalocyanine/C60 thin-film [129, 130, 131].

Comparing to single layer OPV device, large improvement was accomplished by using bi-layer OPV device. However, some limitations existed due to the bi-layer device architecture such as: (i) charge separation only happens close to the donor/acceptor interface (ii) device efficiency is limited by the amounts of absorbed photons at the layers interface [132].

2.5.3 Bulk hetrojunction OPV device

A blend of a conjugated polymer (donor) and a fullerene derivative (acceptor) makes a bulk hetrojunctions (BHJ) material which is considered to be the most promising combination for an active material. To make a BHJ OPV device, the active layer which consists of materials (donor and acceptor) is sandwiched between two contacts with different work functions (see Figure 2.8 (a)). The BHJ material is considered to be a major breakthrough in the OPV field because of the large amount of interfacial areas created between the donor and the acceptor resulted from mixing the two materials together [133]. The interfacial areas can be controlled by the processing parameters in order to form a donor-acceptor interface within a distance close or less than the exciton diffusion length ~ 10 nm. Each material type in the BHJ active layer creates an interpenetrating network in nanometer scale for a better charge transportation to the electrodes (see Fig. 2.8 (b)). Material wise, BHJ device is similar to bi-layer device except that more interfacial areas exist in BHJ device which increases the photon absorption and charge separation. For a BHJ device to perform, percolated pathways for the holes and electrons are required to transfer them to the contacts. This makes the BHJ device more affected by morphology of the film and the processing conditions.

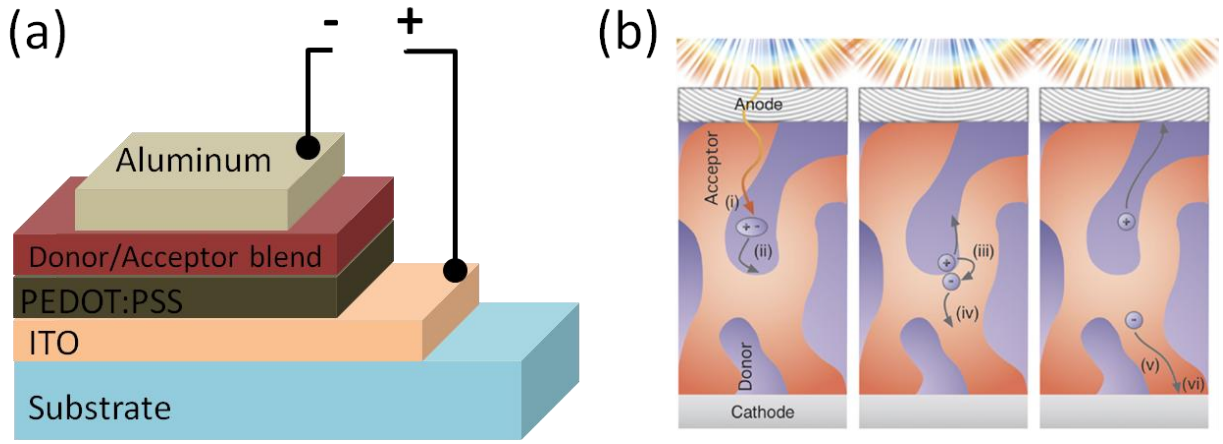

Figure 2.8 (a) BHJ OPV device architecture. The donor/acceptor blend is the BHJ blend that forms the active layer. (b) Schematic of BHJ OPV device [134].

An efficiency of 2.5% achieved by Shaheen et al. was a breakthrough on using MDMO-PPV/ PCBM BHJ material. MDMO-PPV/PCBM was then a main topic for research focusing on morphology, electronic structure, and charge transport of this BHJ material [135, 136, 137, 138, 139, 140]. Another donor material that competed with MDMO is P3HT that is usually blended with PCBM to create the BHJ material. The higher charge carrier mobility and lower band gap compared to MDMOPPV made P3HT more popular in OPV field. OPV device made with P3HT/PCBM blends has shown higher efficiency up to 5% [141, 142, 143, 144].

2.5.4 Tandem organic photovoltaic device

As mentioned before, different techniques are followed to enhance the OPV device performance. Some of those techniques focus on the device structure to enhance the light absorption or the charge transport. Tandem OPV device structure is one of those techniques that provides a way to increase the light absorption and hence the overall device efficiency. A tandem cell is fabricated by stacking more than one solar cell, usually two cells, on top of each other

with a transparent electrode in-between the cells (see Figure 2.9). The middle layer that separates the two cells plays an important role because it is considered as a foundation to fabricate the second cell, at the meantime it serves as an electron transport and collecting layer for the first cell. In the tandem cell, the light passes through the first cell and then reaches the second cell through the transparent layer. Since the tandem cell is considered as two solar cells in series then the produced voltages by both cells will add up and the current will be limited by the lowest current of both cells. The two cells can be made from the same BHJ material; in this case the tandem sell allows more light absorption for thicker overall active material thickness. The two cells can be also made from two different BHJ materials that have complementary absorption spectra to cover a broader portion of the solar spectrum. This leads a reduction in the energy lost due to the unabsorbed photons with energy slightly larger than the energy band gap of either BHJ material.

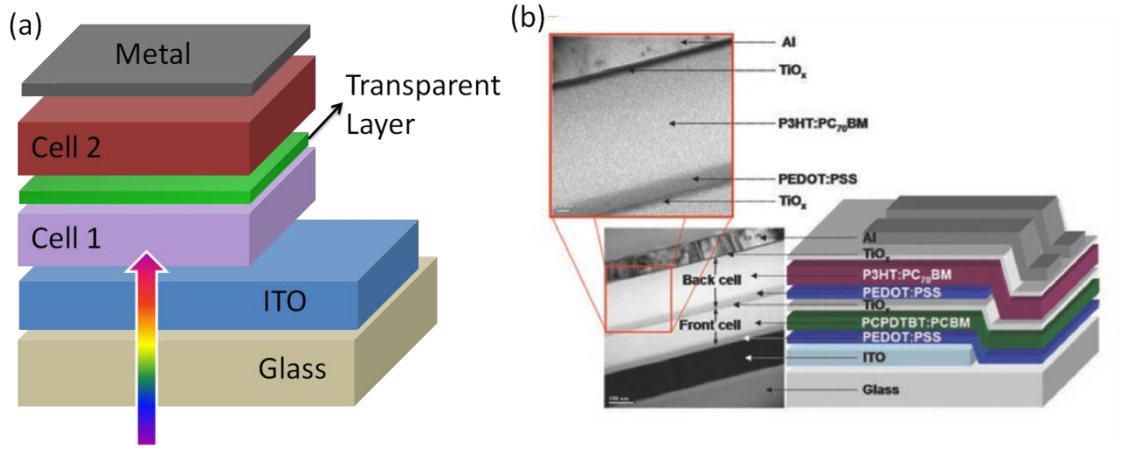

Figure 2.9 (a) Schematic diagram of tandem solar cell with two cells on top of each other with a transparent layer in between. (b) SEM images for a tandem cell made from P3HT/PCBM and PCPDTBT/PCBM solar cells from ref [145].

The first tandem solar cell was demonstrated by Hiramoto *et al.* where a thin layer of Au between two organic cells was fabricated by thermal evaporation [146]. They showed that the V_{oc} value was doubled when comparing to a single cell while photocurrent was reduced because of the reduction in the light intensity in the back cell. By additional interfacial layers and tuning the first cell for long wavelengths and the second cell for short ones, an efficiency of 5.7% was reported for vacuum-deposited tandem cell [147]. A high efficiency of 8.3% was reported by Heliatek where they fabricated tandem cells from small molecules [148]. Some of the famous BHJ materials that are used to fabricate tandem cells by vacuum deposition are CuPc /PTCBI [149], ZnPc / C60 [150,151], SnPc / C70 [152], and pentacene / C60 [153].The middle layer is normally made from Ag or Au enclosed by thin metal oxide or organic layers [154, 155], or from only doped organic layers [156]. One of the highest reported efficiency for solution-processed tandem cell is 6.5%; the device is made from PCPDTBT/PCBM as the first cell, and P3HT/ PC71BM as the second cell, and TiO_2 and PEDOT as the middle layer [157]. A higher PCE 8.3% was reported when the P3HT and PCBM material mixed with other polymers [158]. However, efficiencies produced by tandem have not exceeded the values produced by single cells due to many challenges facing the tandem cell fabrication. Some of those challenges are: (i) difficulties to match the photocurrent of the two cells, (2) damaging the first cell when depositing the second cell.

2.6 Reports on PCE in organic photovoltaics field

The research in organic photovoltaics field has been rapidly growing in the last few decades aiming to reach the commercial level that demands a stable device with efficiency higher than 10%. Determining a fair comparison between the devices efficiencies generated by the working groups in the OPV field became a crucial issue [159]. In order to compare between

different OPV devices from different groups, PCE value which represents the device performance should be accurately extracted and reported, also this value must be reproducible for a same device [160]. Specific conditions must be attained when PCE is reported for an OPV device; those conditions are temperature, spectral irradiance, and total irradiance, commonly known as the standard reporting conditions (SRC) [161, 162]. The SRC defines the irradiance to be 100 mW/cm^2, temperature to be 25 ^{o}C, and device should measure under AM 1.5 global spectrum. Shrotriya et al. have described the right experimental procedure that should be followed in order to report an accurate OPV device performance [163]. In their work, spectral responsively, light source calibration, spectral mismatch, and device area showed to have an effect on the reported PV device performance. Device area which is usually defined by the shadow mask used to deposit the upper electrode is an important factor because it is used to calculate the current density generated by the device.

Reported PCE values in literature has shown a range of variation from as low as 0.6% to 7.4% [164]. The variation is due to the different proceeding condition and device parameters applied by the different groups such as active layer thickness, materials ratio, power input, solvent, and annealing temperature. Under illumination of 100 mW/cm^2, 1:1 P3HT:PCBM ratio, and DCB solvent PCE values were PCE=4% for thickness of 60 nm [165], 2.7% for a film thickness 70 nm [166], PCE=4.4% for thickness of 175 nm [167], PCE=5% for a film thickness of 220 nm [168], and PCE of 3% for a thickness of 320 nm [169]. Increasing the thickness in the mentioned devices did not lead to an increase in the PCE, instead a jumping in the values are noticed. Several groups have studied the effect of increasing the P3HT/PCBM layer thickness on the device performance; for example, L Zeng et. al. have fabricated OPV devices with P3HT:PCBM with thickness ranges from 130 to 1200 nm; they extracted the higher PCE value

for the device with 830 nm and the lowest PCE values for the devices with the thickness 130 and 1200 nm [170]. S Lee et. al. have tried a different range of thicknesses between 170 nm to 100 nm and found the highest efficiency 3.7% for the device with thickness 520 nm and lowest PCE when the thickness is higher [171]. High PCE values for P3HT:PCBM devices about 4%–5% are normally reported for an active layer thickness in the range of 100–250 nm [172, 173]. Other studied have focused on different P3HT:PCBM ratios; when blending ratio 1:0.8 was used with the solvent to CB, reported PCE values were about 5% [174, 175]. Also, other groups have reported PCE values of 3.1% and 2.8 % for 1:2 and 1:3 ratio, respectively [176, 177]. Annealing temperatures were different between 75 and 150 ^{o}C for these reported works.

All of the above discussed PCE values from the literature were extracted from optimum OPV devices that utilize the interfacial layers (injection layers) in their structure to enhance the charges extraction at the active-layer/electrodes interface. On the other hand when no injection layers were used, OPV devices showed low V_{oc} and FF leading to low PCE values about 0.25-2% by using P3HT:PCBM BHJ material [178, 179, 180]. In the planar device geometry reported in this thesis, these injection layers are not present.

The efficiency of an OPV device can be also affected by the device design. Cravino et al. showed that the OPV device performance can be affected by using two different device designs: (i) cross layout where the Al electrode overlaps with the active and PEDOT:PSS layers outside the ITO area, and (ii) the active layer is in contact with PEDOT:PSS/ITO only [181]. Their conclusion from analyzing the photocurrent was that the overlapping area between the Al electrode and the active and PEDOT:PSS layers is the most contributing area to the generated current and hence the device performance while other overlapping areas contribute less. The same designs: (i) island and (ii) crossbar were also investigated by Kim et al. [182]. They have

shown that a significant error occurs in the efficiency value when using the cross design if the device area is less than the illuminated area (the incident beam light spot). This is because an extra current is generated in the overlapping area between the PEDOT:PSS and the active layer because PEDOT:PSS layer can act as an anode. Two solutions were suggested by Kim et al. to avoid this efficiency overestimation: (i) making device area equal to illuminated area (ii) making no overlapping area between PEDOT:PSS and the active material by using island device layout. Among other factors that affect the reported OPV device performance are: processing conditions [183, 184], used solvent [185], and the oxygen effect [186, 187].

CHAPTER 3: DEVICE FABRICATION AND EXPEREMENTAL METHODS

3.1 Introduction

All of the organic field effect transistor (OFET) and planar organic photovoltaic (P-OPV) devices described in this work are fabricated in a planar structure where the source and drain electrodes are in plane with each other. Figure 3.1(a) shows a general cartoon of the OFET device design used in this work and Figure 3.1(b) shows a cartoon of the P-OPV device. In chapter 4, the planar device structure will be fabricated with similar electrodes (same metallic material) to be only used as an OFET device to probe the output and transport characteristics. For the rest of the chapter the planar device structure is used as OPV device where two dissimilar electrodes are used. The light will be shinned on the device and the PV-behavior will be investigated. In chapter 6 and 8 the shape of the electrodes in the P-OPV device will be varied to serve the purpose of the study.

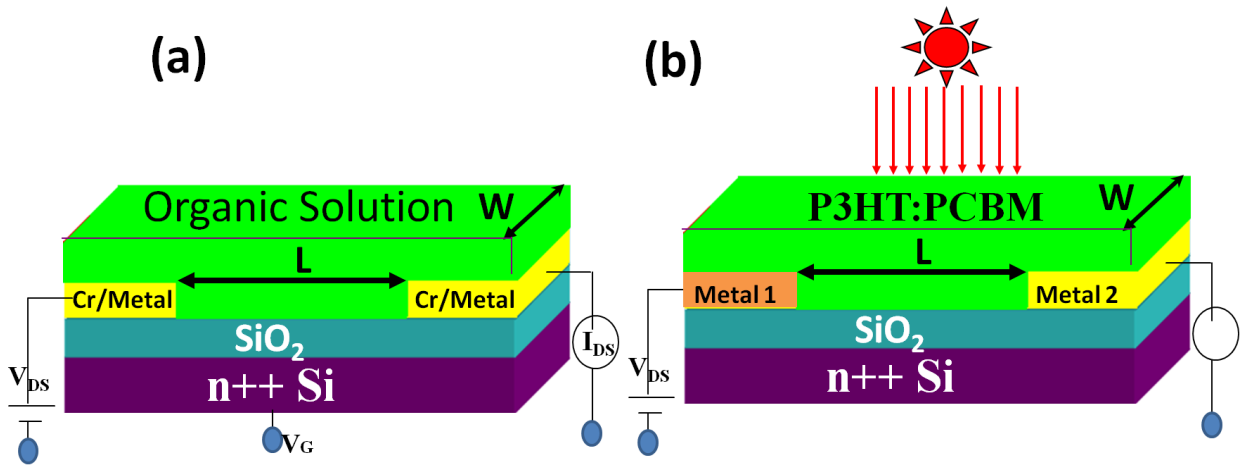

Figure 3.1 Device schematic of (a) OFET device with similar electrodes on Si/SiO_2 substrate, organic solution is P3HT, PCBM, or P3HT/PCBM blend. (b) P-OPV device with dissimilar electrodes.

In this chapter, firstly an overview about fabricating of electrode patterns using electron beam lithography (EBL) will be discussed and then the organic solution processing and the fabrication of P-OPV devices will be discussed. Finally the experimental setup and the characterization of the fabricated devices will be discussed.

3.2 Fabrication of electrodes (general techniques)

All devices in this work were fabricated on top of highly doped (<0.005 Ω cm) silicon substrates (~350 um thick from Silicon Quest International) with a 250 nm thick SiO_2 capped layer. The electrodes for OFET devices were fabricated by optical lithography which will not be discussed in the thesis. While for P-OPV devices, electron beam lithography (EBL) was used to draw the pattern of the electrodes. Optical lithography was used in OFET because of the large feature size ~ 20 μm, while the P-OPV devices were made with smaller feature size ~2 μm where EBL was needed.

3.2.1 Photo resist and electron beam lithography (EBL)

After cleansing the blank Si/SiO_2 wafer, the photo resist is spun coated on top of it. In the presented work, double-layer resist technique where two different resists are spun coated on top of each other was used. Figure 3.2 shows a diagram of the fabrication of metal structures on Si/SiO_2 substrate using double-layer resist by e-beam lithography.

In the double-layer technique, the photo resist forming the bottom layer is more sensitive to the e-beam than the photo resist forming the top layer. This creates an undercut in the exposed layers which results in easier lift-off. The photo resist in the bottom layer is MMA (MicroChem, EL9), spun coated at 4000 rpm (thickness ~ 300 nm) for 60 seconds and then baked on a hot

plate for 15 minutes at 180^0 C. Then, the second photo resist PMMA 950K (C2, MircoChem) is spun coated at 4000 rpm for 60 seconds and baked on hot plate for 15 minutes at 180^0 C. After coating the resist, the wafer is exposed in Zeiss ULTRA-55 FEG SEM (EBL process). The photo resist is exposed according to the electrodes patterns patterned by nano patterns generation system (NPGS) software and provided to the SEM system by Nabity system. We typically expose the resist with a dose of ~300 $\mu C/cm^2$ at 29 kV using the Nabity system. After lithography, the wafer is developed in Methyl isobutyl ketone (MIBK)/Isopropanol (IPA) (1:3) for 70 seconds, rinsed for 15 seconds with IPA, and then blown dry.

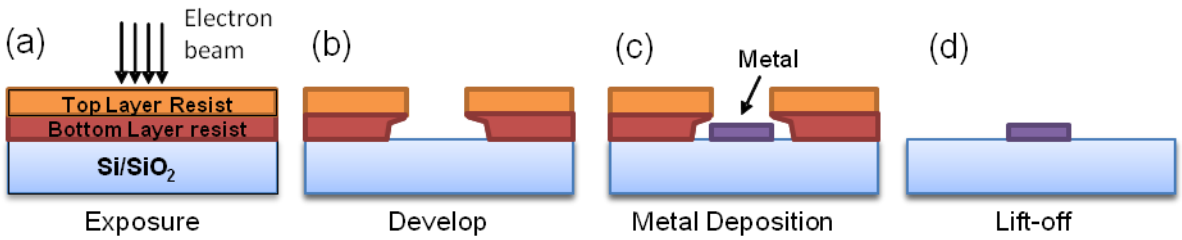

Figure 3.2 Schematic diagram of the e-beam lithography using double-layer resist technique.

3.2.2 Metallization

After the lithography and developing processes, the samples are then ready for metallization. Using the electron beam evaporation or thermal evaporation, 30 nm of the desired metal (evaporated at ~0.3 A/s) is deposited for P-OPV device. For OFET devices, typically 2 nm layer of Cr is evaporated as sticking layer followed by 30 nm of the desired metal. The thermal evaporation was only used to deposit Au metal.

3.2.3 Lift-off

Right after metallization, the wafer is dipped into Acetone for 2-4 hr's depending on the evaporated metal to lift off the metal deposited on the unexposed parts in the lithography

process. After lift-off, the wafer is rinsed gently in acetone, IPA, and water, and then blow dry with nitrogen gas. If the metal does not come off easily, the sample and the Acetone can be warmed for few minutes to help the lift-off process.

3.3 Fabrication of OFET devices

The organic field effect transistors (OFET) electrodes where fabricated by optical lithography followed by metalizing the desired metal. Figure 3.3 shows the large chip after gold metallization and lift-off. This chip contains 18 OFET devices.

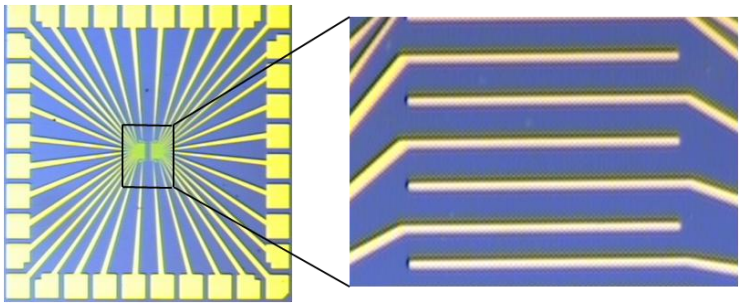

Figure 3.3 Optical image of 18 FET devices fabricated by optical lithography. Each pair on the right is on FET device.

3.3.1 OFET electrodes preparation

OFETs were fabricated on heavily doped n-type Si substrates with a 250 nm capped layer of SiO_2. Source and drain electrodes were defined using double layer photolithography (LOR 3A/Shipley 1813) developing in CD26, followed by thermal evaporation of chromium (Cr) (2 nm) and different metal electrode (30 nm) and finally standard lift-off. The channel length (L) and channel width (W) was 5µm and 200 µm, respectively. The lift off process was done with PG remover and then devices were cleaned with anhydrous acetone and IPA respectively for five minutes each.

3.3.2 Organic solutions processing

P3HT and PCBM were purchased from EMD chemicals Inc. and Sigma Aldrich Co. respectively and were used as purchased without any further purification. Three different solutions were prepared for the OFET purpose: 1) P3HT/PCBM blend, 2) pristine P3HT, and 3) pristine PCBM. One mL of 1,2 dichlorobenzene (DCB) solvent with 5 mg P3HT and 10 mg PCBM , were mixed together to make the desired P3HT/PCBM blend solution with 1:2 ratio and concentration 15 mg/mL. The solution was stirred in a vial with a magnetic stirrer for 12 hours at 40 ^{o}C for proper mixing of the solution. The solution was then filtered with 0.2µm syringe filter before fabricating the devices. After this cleaning process, the OFET devices were then fabricated by drop casting P3HT/PCBM blend on Si/SiO_2 substrate with the electrodes without any further surface treatment inside a N_2 glove box. For the pristine P3HT and pristine PCBM OFETs, solutions of P3HT with molecular weight concentration 5 mg/mL and PCBM 10 mg/mL were separately prepared in 1,2 dichlorobenzene and the devices were fabricated by drop casting individual solution on pre-cleaned Si/SiO_2 substrate with metal electrodes. All of the fabricated devices were then thermally annealed at 150 ^{o}C on a hotplate for 15 minutes to evaporate the solvent and better organic molecules alignment.

3.3.3 Device characterization and measurement set up

The current-voltage output and current-gate voltage transport characteristics of the OFET devices were extracted using Hewlett Packard (HP) 4145 B semiconductor parametric analyzer in an enclosed glove box system with N_2 flow.

3.4 Fabrication of P-OPV devices

Planar organic photovoltaic (P-OPV) device were fabricated in two steps EBL, each step was followed by metallization process. This is because two different metal electrodes should be deposited for the P-OPV operation.

3.4.1 Electrodes Fabrication

P-OPV devices were fabricated on doped Si substrates with a 250 nm capped layer of SiO_2. Dissimilar metal electrodes, Au and Cr, were designed using two steps of electron beam lithography (EBL). In the first step of EBL, Au electrode and markers were defined using double-layer MMA/PMMA resist, and then developed in (1 : 3) methyl isobutyl ketone : isopropyl alcohol (MIBK : IPA) followed by deposition of 30 nm Au. Finally, standard lift-off in acetone was performed and then subsequently cleaned with acetone and (IPA) respectively (see Figure 3.4).

Second step of EBL was then implemented to define the second electrode Al, Mg, Ag, In, Cr, or Ti following the same process as Au electrode. The markers drawn in the first layer were used to align the second electrode with the Au electrodes. The electrodes separation (channel length (L)) of the P-OPV devices was varied 0.24, 0.5, 0.8, 1, and 3 µm and the channel width (W) was fixed to 100 µm (see Figure 3.5).

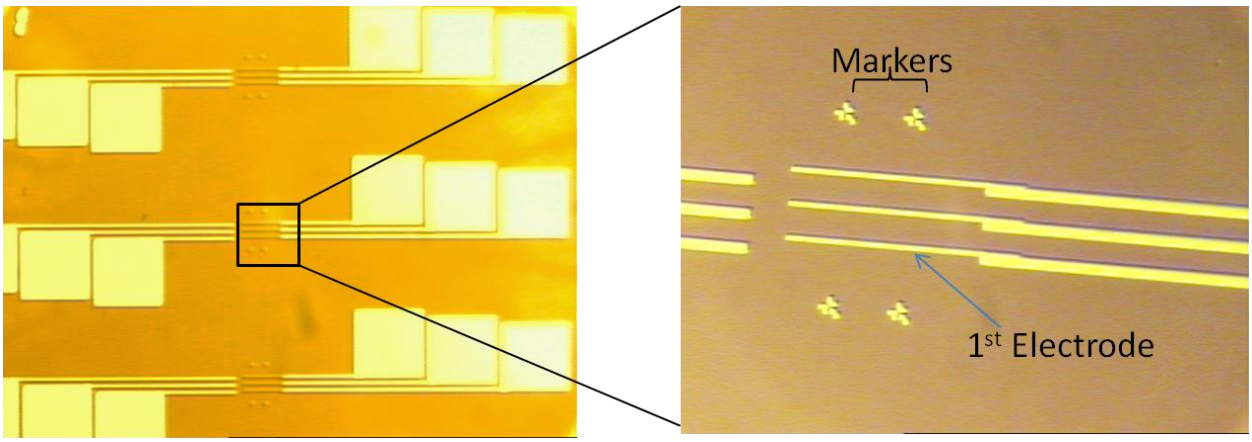

Figure 3.4 Optical image of the first EBL step where the 1st electrode (Au) is drawn followed by metallization and left-off. To the right, the markers will be used to draw the second electrode by EBL.

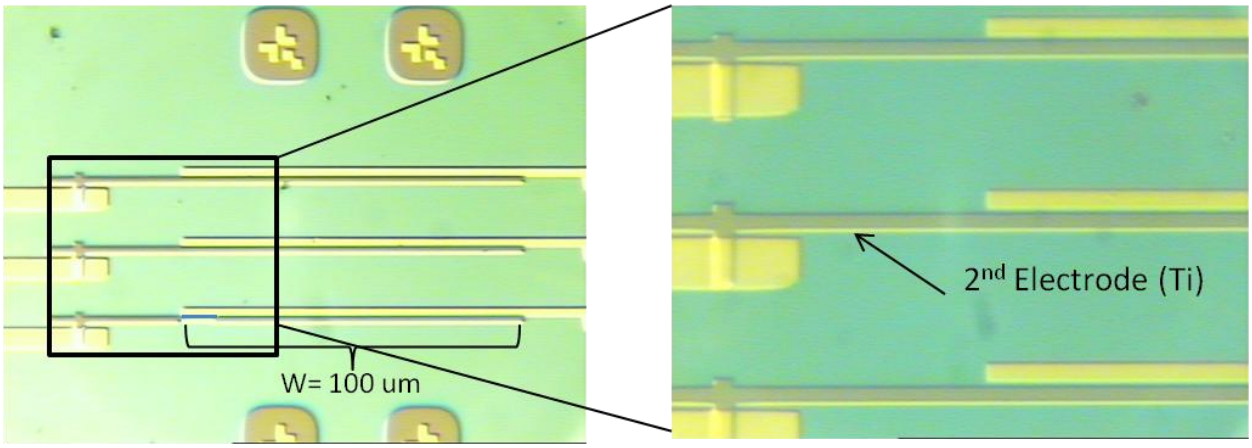

Figure 3.5 Optical images of three P-OPV devices showing the second electrode after the second EBL stage.

3.4.2 Organic blends preparation

The active materials used for fabricating P-OPV devices were made from a blend of P3HT (molecular weight 33.3 kD) and PCBM that were purchased from EMD chemicals Inc. and Sigma Aldrich Co. respectively and were used without any further purification. Three different solutions were prepared from P3HT/PCBM with weight three different ratios of 1:1, 1:2, and 1:3 in 1,2 dichlorobenzene solvent. The concentrations were (32 mg/ml) for 1:1 ratio,

(48 mg/ml) for 1:2 ratio, and (64 mg/ml) for 1:3 ratio. The solutions were stirred in vials with a magnetic stirrer for 12 hours at 40 ^{o}C for proper mixing of the materials. The solutions were then filtered with a 0.2 µm syringe filter. For ratio effect study in Chapter 7, the three solutions were individually spun-coated on the bare Si/SiO2 substrates for surface morphology imaging and on top of Si/SiO_2/electrodes to make P-OPV device. In the rest of the chapters, the P3HT/PCBM blend with 1:2 ratio was used when making the P-OPV devices because this ratio provides the best device performance according to this work. The surface morphologies of the blended films were examined by tapping mode atomic force microscope (AFM). AFM was also used to define the active layer thickness by examining the height profile of the film compared to the bare substrate. When performing the absorption measurement, the blended P3HT:PCBM films were spun-coated on top of glass substrate covered by 250 nm SiO_2. Then absorption was measured using UV-Vis 300-Bio spectrometer. All samples undergo a heat treatment of 150 ^{o}C for 10 min. The solution preparation and the film spin coating were executed inside a N_2 glove box.

3.4.3 P-OPV device characterization and Measurement set up

The P-OPV devices were characterized by current-voltage (I-V) measurements in dark and under simulated AM 1.5G solar irradiation at 100 mW/cm^2 Oriel 96000, 150 W solar simulator, instrument that was calibrated with a standard monocrystalline silicon reference solar cell (Newport, 91150V) with KG-5 visible color filter certificated by NIST (National Institute for Standards and Technology) to the ISO-17025 standard that is traceable to the National Renewable Energy Laboratory (NREL). The I-V characteristics of the devices were measured using Hewlett Packard (HP) 4145 B semiconductor parametric analyzer in an enclosed glove box system with N_2 flow (see Figure 3.6). Temperature inside the glove box was between 25-30 ^{o}C.

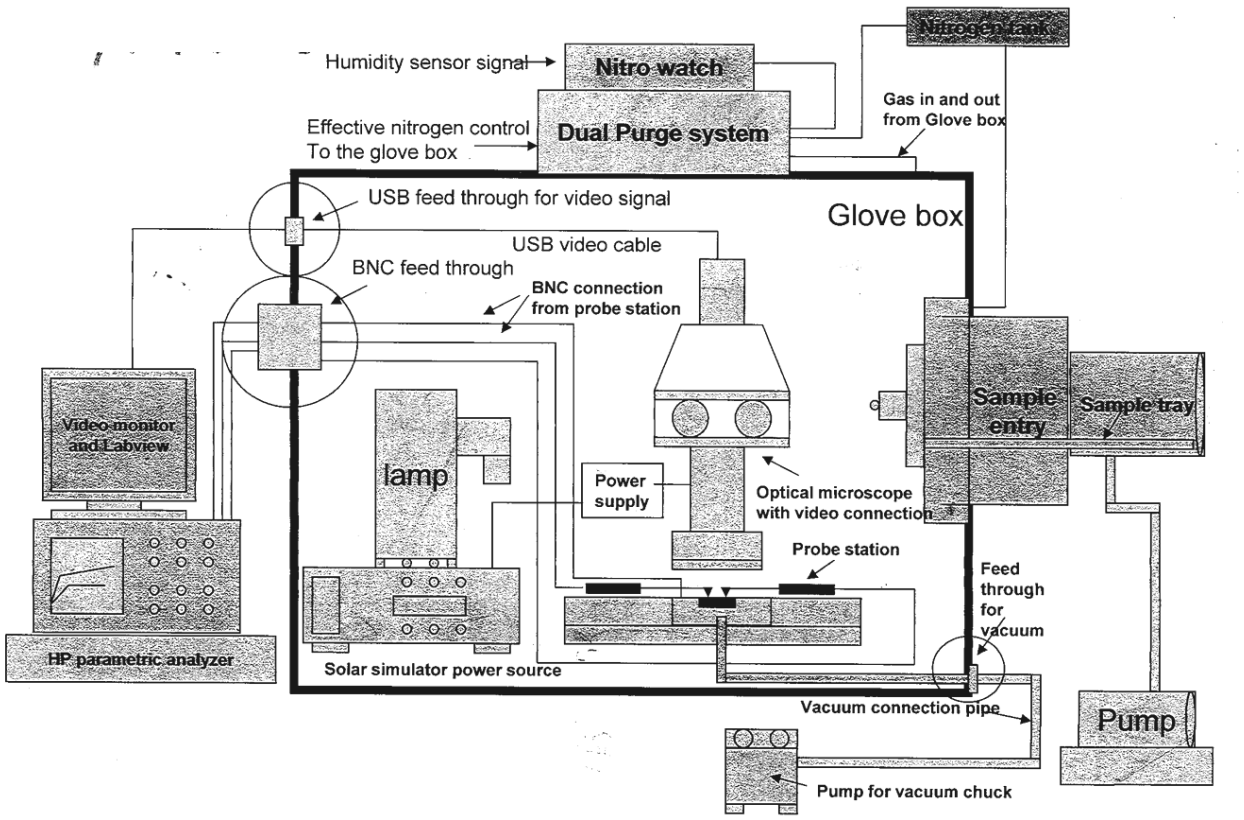

Figure 3.6 Measurement apparatus and set up for measuring PV behavior of P-OPV device. This apparatus without solar simulator is also used to measure the OFET devices.

CHAPTER 4: STUDY OF ORGANIC FIELD EFFECT TRANSISTOR (OFET) TOWARDS THE DESIGN OF PLANAR PHOTOVOLTAIC DEVICE

4.1 Introduction

Ambipolar charge transport with both n and p-type characteristics has shown to be promising interest for solution processed ambipolar field effect transistor, complementary logic circuits (CMOS inverters), light emitting field effect transistors, and organic photovoltaic (OPV) devices [188, 189]. P3HT and PCBM mixture as a bulk heterojunction (BHJ) material has shown to be successful candidate as an active material for OPV devices with efficiency ~ 5%. The most utilized OPV device structure is made in a vertical geometry; this structure is facing some challenges and limitations that prevent it from addressing the effect of some physical parameters on the OPV device performance as mentioned in CH.1. As a deviation from the vertical structure and its related limitations, the planar device structure (dissimilar source and drain are in plane with each other) using bulk heterojunction material has shown to be promising interest for organic photovoltaics [190, 191] and light emitting ambipolar field effect transistor [192, 193].

Since the use of the planar structure in OPV field still developing, the optimized active material, processing conditions, choice of electrodes still not reached; in some cases, study such as the proper choice of electrodes has not been established yet. Since the planar OPV devices are made in the same structure as OFET devices, then studying the relation of mobility in OFET with variety of electrodes metals provides a leading direction to choose the proper contacts for planar OPV devices. In addition, the proper set of contacts helps to develop planar OPV and OFETs devices with enhanced charge carrier transport for efficient and optimal charge injection/extraction process at the source/drain electrodes. Improper selection of metal contacts

creates inefficient charge injection/collection of holes and electrons from the HOMO and LUMO level of the donor and acceptor materials due to high injection/collection barrier at the interface which leads to lower device performance. For example when using P3HT/PCBM, the low work function metal such as Ca or Mg shows air sensitivity for efficient electron injection and high barrier for hole injection. Also the high work function metal such as Au, Pt, Pd shows high injection barrier for electron and hence make non ohmic contact.

What should be mentioned here is the difference in the charge transport mechanism in OFET and OPV devices. In BHJ OPV device under illumination, holes and electrons are created and transported through percolated donor and acceptor pathways at the same time. However in OFET, either electrons or holes are accumulated and transported in the film depending on the applied voltage and gate voltage. This charge transportation is affected by the difference between the contact's work function and the materials HOMO and LUMO levels [[194], [195], [196]]. In addition, the actual hole and electron mobility in OPV device depends on the film morphology and the recombination process.

In this chapter, we have systematically investigated the ambipolar charge transport with a controlled variation of a range of metal work function (from low to high) with symmetric source and drain contact to demonstrate ambipolar operation of P3HT and PCBM blend with a ratio of 1:2 from different metal contact without any surface treatment. The results show a clear evidence of metal injection barrier effects on the performance of the devices. Our observation of ambipolar FETs with different metal contact leads us with the conclusion that injection barrier for both holes and electrons lies ~ $0.3 < \varphi < 1$ eV range shows well balanced p and n channel characteristics. In addition, we have also studied the p-type and n-type behavior of pristine P3HT and PCBM separately with similar metal work function to validate the effect of injection barrier

on hole and electron mobility. Our results from these studies demonstrate the importance of contact metal effect on device performance and potential application of different metal electrode towards the design and development of planar photovoltaic and ambipolar FET devices.

4.2 Results and discussion

OFETs were fabricated according to the procedure discussed in Chapter 3. Figure 4.1 shows the schematic diagram and the actual OFET devices. The channel length (L) and channel width (W) was 5µm and 200 µm, respectively.

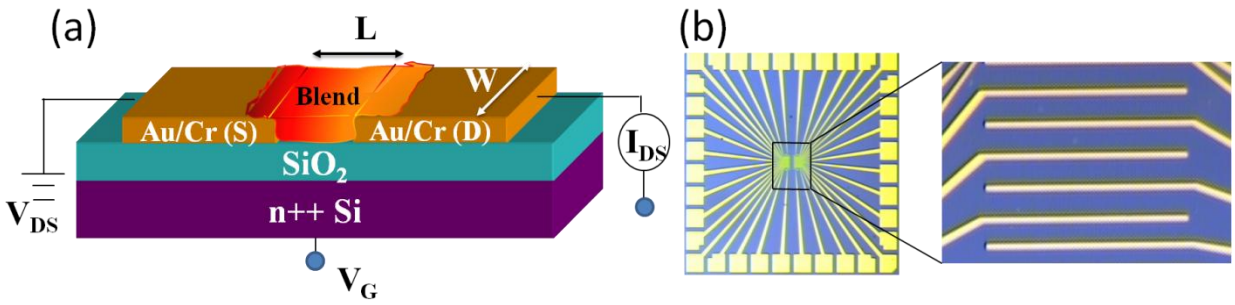

Figure 4.1 (a) schematically shows the device structure with transport measurement set up and (b) is the optical image of the FET devices.

4.2.1 OFET of pristine P3HT and PCBM with different electrodes metals

In this section we discuss the performance of OFET's made from pristine P3HT and pristine PCBM. Their electronic transport properties at room temperature such as the mobility and the I-V characteristics will be reported.

In order to achieve an efficient charges injection to P3HT or PCBM material, the work function of the electrode should allow efficient injection of holes in to the highest occupied molecular orbital (HOMO) level of P3HT and injection of electron into the lowest unoccupied molecular orbital LUMO level of PCBM. For this purpose we have selected a range of metal

work function (from low to high) for systematic investigation of P3HT, PCBM FET's performance and as well as ambipolar charge transport with symmetric source and drain contact. Figure 4.2 shows the schematic energy level diagrams of the (HOMO) and (LUMO) of P3HT and PCBM with respect to the different metal work function and their corresponding electron and hole injection barrier height (difference in energy level between HOMO or LUMO and metal work function). From the energy diagram with different metal contacts it is clearly evidenced that Au has the lowest hole injection barrier and Mg has the highest barrier for efficient injection of holes in to the LUMO level of P3HT for P type operation. On the other hand, low work function metal shows the lowest electron barrier in to the LUMO level of PCBM.

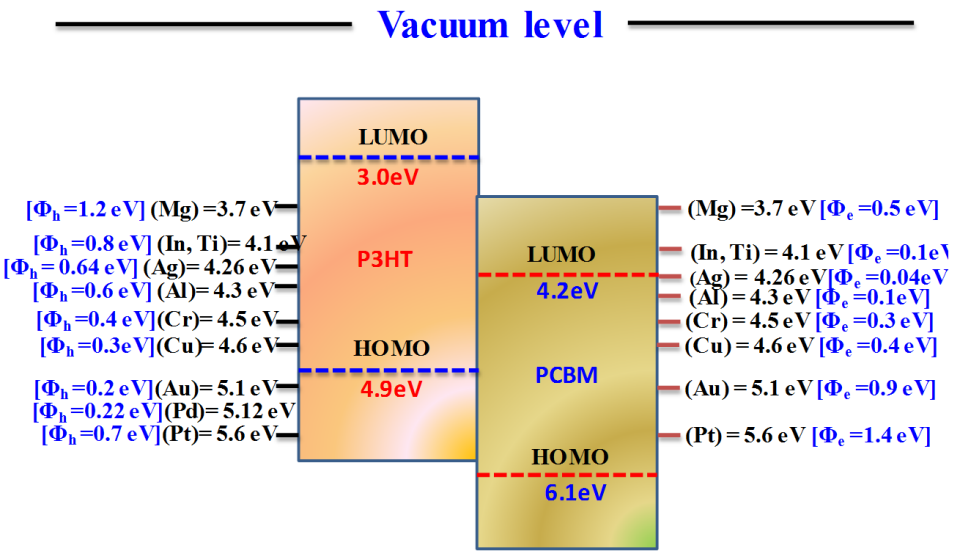

Figure 4.2 Schematic energy level diagram of P3HT and PCBM and different metal contact with their corresponding work function, electron and hole injection barrier height.

All the P3HT FETs with different metal contact were characterized from their output and transfer characteristics. For output characteristics source-drain current (I_{DS}) vs. source-drain voltage (V_{DS}) was measured at different gate voltage (V_G) from 0 to -80V (20V intervals). For P3HT OFET, all the device exhibits well defined p-type behavior in accumulation mode with

current saturation. For transfer characteristics, I_{DS}-V_G was measured from -80 to +60V at fixed V_{DS}= -60V. Figure 4.3 (a) shows I_{DS} vs. V_{DS} of P3HT FETs measured at gate voltage (V_G= -60V) for different metal contact. For comparison with different metal contact, the I_{DS} -V_{DS} for Au electrode is shown partially. The data shows a systematic variation of I_{DS} depending on different metal contacts. Au electrode that makes ohmic contact is showing the highest source-drain current. At V_{DS}=80 V Au electrode shows almost 10-15 times higher current than Al and Mg electrode which has the higher barrier (1.2eV) for hole injection. In addition, we speculate that Al and Mg OFETs show air sensitivity oxidation problem because the I_{DS} -V_{DS} plots for Al and Mg show higher threshold voltage compared to all other metals. Figure 4.3 (b) shows the transfer characteristics from P3HT OFETs where I_{DS} is plotted as function of V_G at fixed V_{DS}= -60V for all different metal contact. The current on/off ratio varies from 10^3 to 10^4.

The effect of barrier height for electron injection was investigated from the PCBM FETs. Figure 4.3(c) shows the I_{DS} vs. V_{DS} plot of PCBM OFETs measured at gate voltage (V_G = 60V) for all the different metal contacts that were used for P3HT OFETs. Low work function metals such as Mg, In, Ag make ohmic contact with PCBM because of the very low barrier with the LUMO level for electron injection. In contrast high work function metals such as Au, Pt make severely non ohmic contact due to very high electron injection barrier which is clearly indicated in the I_{DS}-V_{DS} plot. For V_G=60V, the Mg electrode shows almost 100 times higher current than Pt and Au electrode at V_{DS}=60V. The transfer characteristics of the same samples are shown in figure 4.3(d) where I_{DS} is plotted as function of V_G at fixed V_{DS}= 60V. The current on/off ratio varies from 10^4 to 10^5.

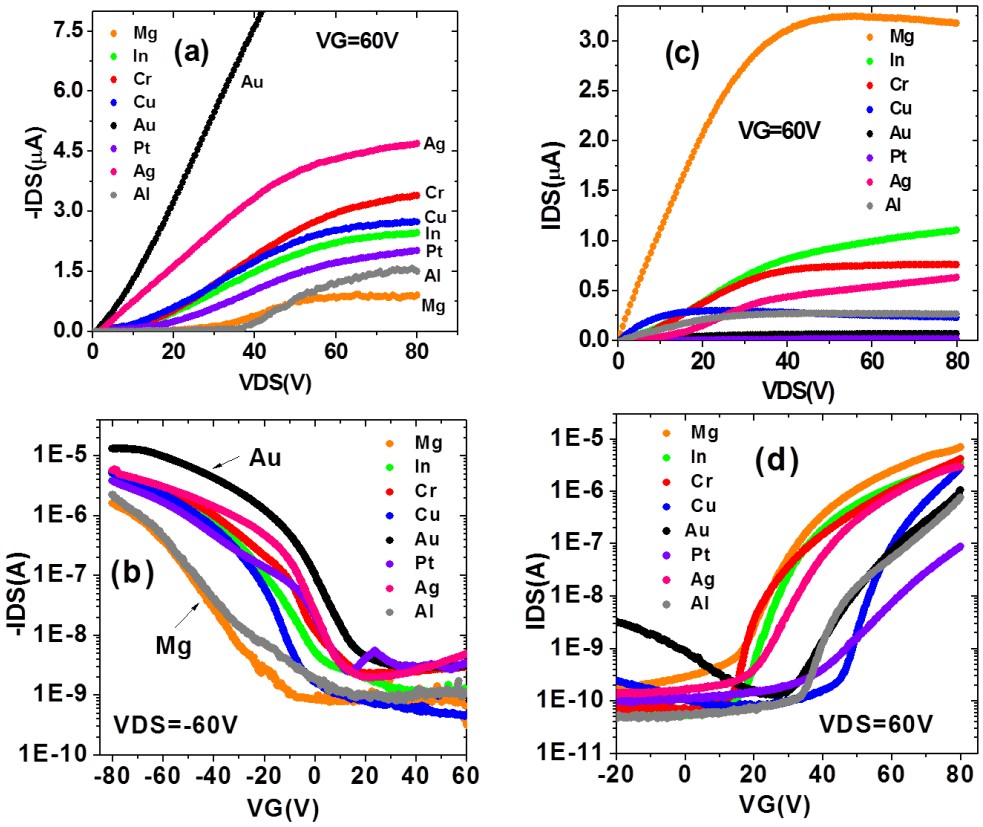

Figure 4.3 (a) I_{DS} vs. V_{DS} of P3HT FETs measured at gate voltage (V_G= - 60V) for different metal contact (b) transfer characteristics (I_{DS} vs. V_G) at V_{DS}=-60V for the same P3HT FETs (c) I_{DS} vs. V_{DS} of PCBM FETs measured at gate voltage (V_G= 60V) for different metal contact and (d) transfer characteristics (I_{DS} vs. V_G) at V_{DS}=-60V for the same PCBM FETs.

The field effect mobility μ is determined from the saturation regime using the relationship between I_{DS} and the V_G from the equation $I_{DS} = (WC_i/2L)\,\mu(V_{GS} - V_T)^2$ where V_T is the threshold voltage; C_i is the capacitance/unit area of the oxide layer (13.8nF/cm^2). The calculated saturation mobilities for all different metal contacts are summarized and shown in Figure 4.4 which shows the hole and electron mobility in P3HT and PCBM FETs as a function of different metal work functions. For P3HT, the hole mobility gradually increases with increasing metal work function up to 5.1 eV for Au which is the closest energy level that coincides with HOMO level of P3HT and shows the best mobility of 2×10^{-2} cm^2/Vs. With increasing metal work

function more; for example, Pt (5.65eV) creates large injection barrier for hole and hence low hole mobility. The lowest hole mobility for P3HT OFET was obtained for Mg and Pt electrode 5.5×10^{-3} cm^2/Vs which can be ascribed due to the large energy mismatch with HOMO level of P3HT.

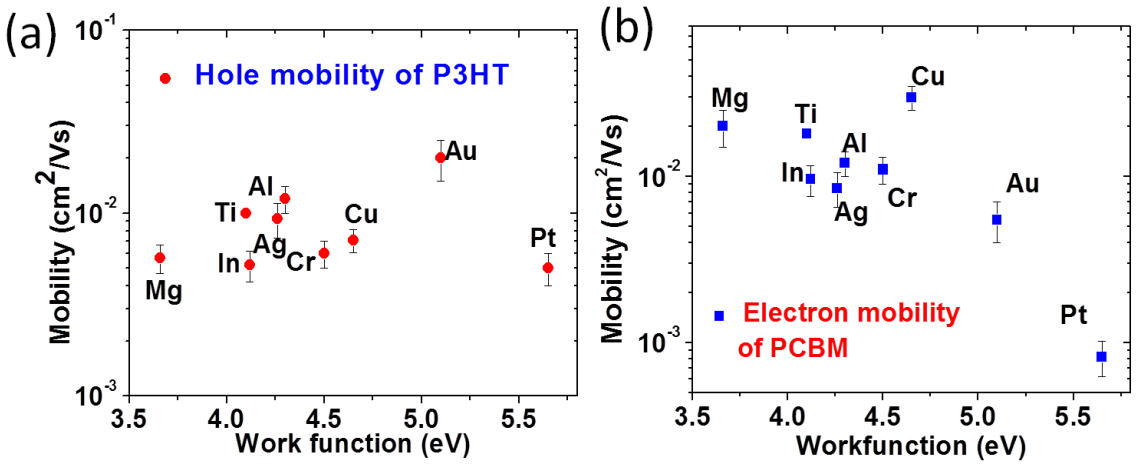

Figure 4.4 Mobility as a function of different metal work function of (a) Holes for pristine P3HT FETs and (b) Electrons for pristine PCBM FETs

In contrast, electron mobilities of n-type PCBM FETs fabricated from different metal contact shows reverse order and mobility decreases with increasing metal work function. Low work function metals shows higher mobility compared to high work function metal except Cu. PCBM FET with Pt electrode shows the lowest mobility of 8.2×10^{-4} cm^2/Vs due to the high barrier between the Pt work function and PCBM LUMO. We should mention that PCBM transistor with Cu and Cr electrodes shows almost three times change in mobility despite Cu and Cr having very similar work function. This is most probably due to the variation of contact resistance which can arise by the formation of interfacial dipole layers altering the energy barrier by a small amount.

We should mention here that the measured mobilities in the pristine P3HT and PCBM using OFET with different metals describe the best case scenario in the BHJ OPV devices and not the real case. This because the effective mobility in the P3HT/PCBM blend is less than the one in the pristine P3HT and PCBM due to the existence of another component that creates number of scattering sights and dead ends leading to a deviation in the carriers path; as a result, lower mobility and more recombination. However, calculating the mobilities for pristine P3HT and PCBM becomes useful when choosing the right set of electrodes for the planar OPV device because the metals with balanced mobilities can be good candidates to fabricate a P-OPV device.

4.2.2 OFET of P3HT/PCBM blend with different metal electrodes

One of the important requirements for proper operation of ambipolar OFETs is efficient and optimal charge injection of both carriers from respective contacts. The main drawback for ambipolar transport in typical OFET structure is its limitation to symmetrical source and drain contact which leads to a high injection barrier for one type of charge carrier. To eliminate the injection problem for proper ambipolar OFET operation, one need to develop asymmetrical source and drain contacts or the design of device structure where electrodes need to have a work function that allows injection of holes in the HOMO of the semiconductor and the injection of electrons in the LUMO level. In our study of ambipolar OFETs with different metal electrodes, we have chosen a fixed ratio (1:2) of P3HT to PCBM without any further optimization of the device parameter because our main focus is to understand the effect of metal work function and injection barrier on the ambipolar operation, and subsequently designing of P-OPV devices from P3HT:PCBM blend and dissimilar metal contacts. Figure 4.5 exhibits the output and transfer characteristics of ambipolar OFETs with Mg, In and Cr electrode.

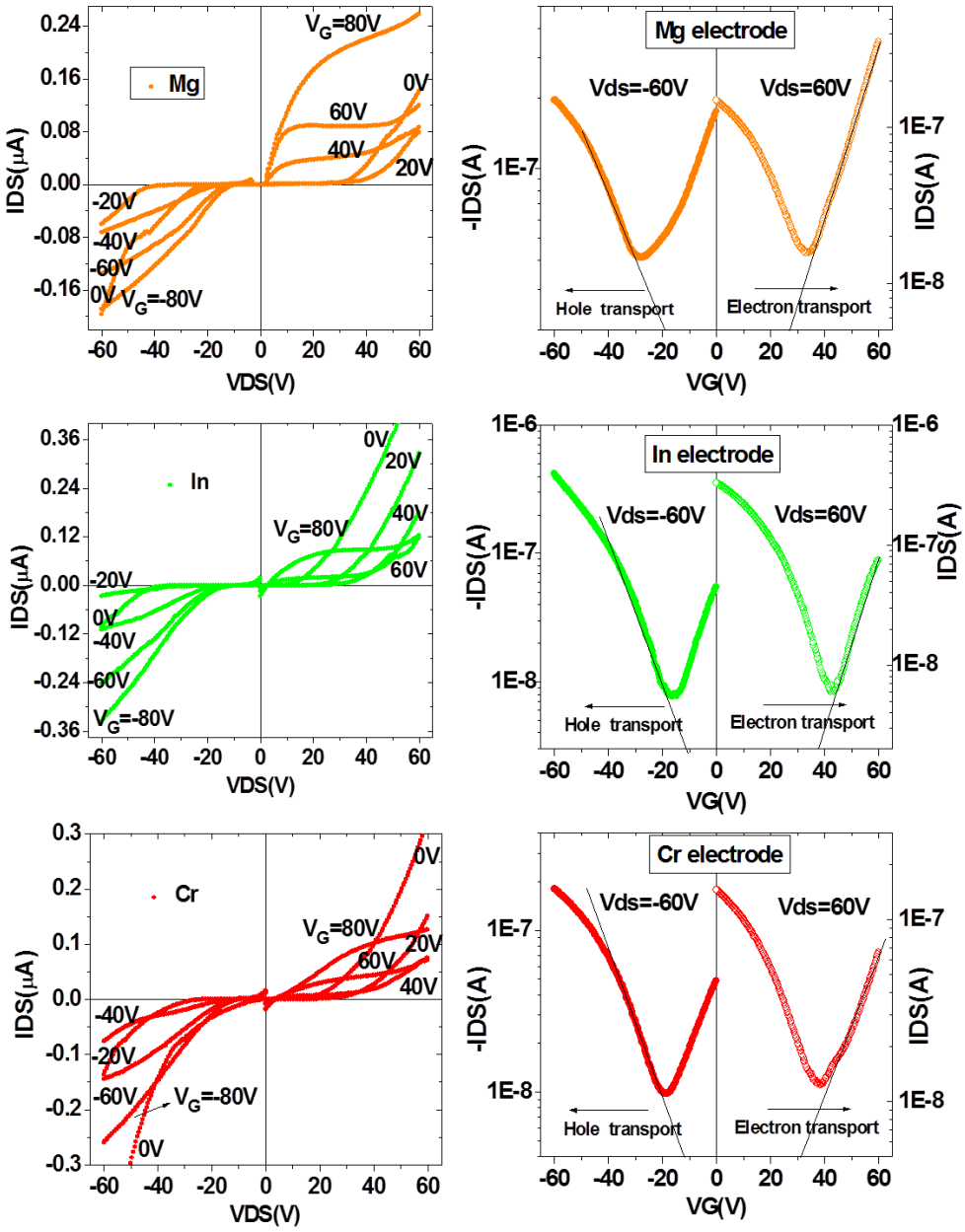

Figure 4.5 Output (I-V) and transfer (I-V_G) characteristics of ambipolar OFETs with Mg, In and Cr electrodes.

In the left column of Figure 4.5, for p-channel operation the device was negatively biased up to -60V with V_G varies from 0 to -80V with -20V increments. For the n-channel operation the device was positively biased up to 60V with positive V_G. Device fabricated from low work function metal Mg shows n and p-channel characteristics with better n-channel operation than p-

channel. For low V_G and at high V_{DS} the devices show nonlinear diode like behavior which is typical for ambipolar transistor operation due to the presence of both carriers (holes and electrons) indicating the formation of a p-n junction in the channel region. The p-channel enhancement and n-channel enhancement mode occur above V_G=-20V and +40V, respectively. Below these voltages the other charge carries in the channel dominates.

The transfer characteristics of the same device is shown in right column in Figure 4.5 which indicates the positive and negative carrier accumulation at voltages -20V and +40V. Device fabricated from In electrode shows well balanced n and p-channel characteristics though there are some non-ohmic contact resistance features at low V_{DS} for both p and n-channel. This current behavior is similar for both carriers and symmetrical around the V_{DS}=0 V point. Although energy barrier between work function of Mg and In with HOMO level of P3HT (1.2 eV and 0.8 eV) is greater than that for electron injection (0.5 eV and 0.1 eV), the hole currents are still sufficiently large to support ambipolar performance. Device fabricated with Cr electrode makes almost similar energy difference (0.4 eV and 0.3eV) with HOMO level of P3HT and LUMO level of PCBM and hence shows symmetrical output characteristics in the electron and hole enhancement mode. In contrast, device made with Al electrodes represented in figure 4.6 shows better n-channel performance with current saturation than p-channel because the work function of Al is much closer to the LUMO level of PCBM than HOMO level of P3HT.

Figure 4.6 represents the ambipolar operation of the devices fabricated from Al, Cu, and Ag electrodes. Although the work function of Ag electrode is much closer to the LUMO level (0.06 eV) of PCBM compared to that that of HOMO level of P3HT (0.64 eV) but it does not show good n-type operation and current behavior is asymmetrical around V_{DS} = 0V with much higher current in p-channel mode than n channel. This might be due to the formation of interface

dipole at the Ag surface which increases the injection barrier for electron due to the rapid oxidation of Ag. For Cu electrode the injection barriers are about the same (0.3eV and 0.4 eV) for both carriers and hence it shows symmetrical p and n-channel characteristics.

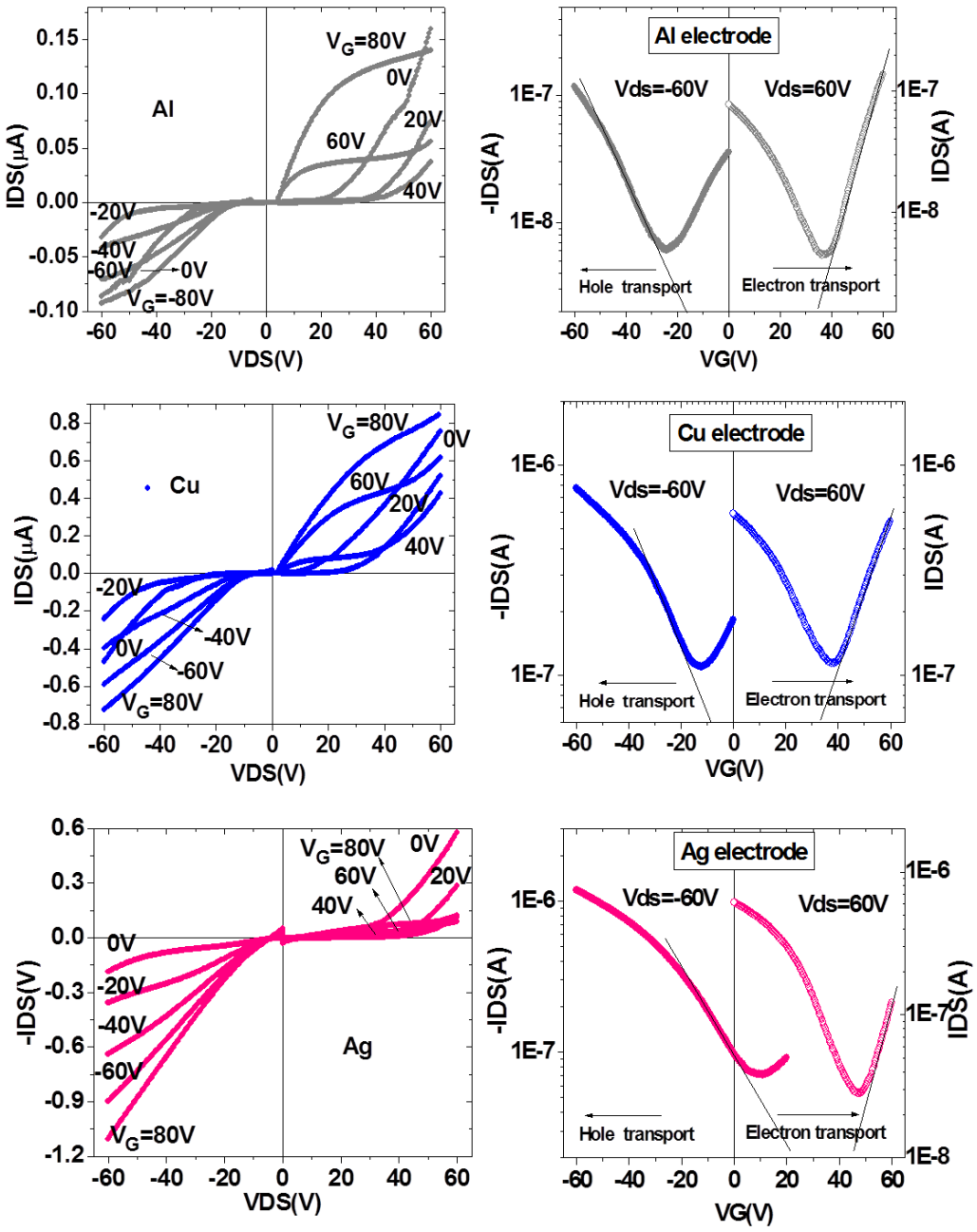

Figure 4.6 Output (I-V) in left column and transfer (I-V_G) characteristics in right column of ambipolar OFETs with Al, Cu and Ag electrodes.

In order to investigate the effect of high injection barrier on the performance of ambipolar OFETs we have also fabricated P3HT/PCBM OFETs from Au and Pt electrode where both metal have very large injection barrier (0.9 and 1.2 eV) with PCBM. It has been reported previously that on clean gold surfaces, PCBM can form a strong interface dipole layer and can significantly reduce the injection barrier for electron and shows good n type characteristics. But in blend solution the PCBM shows a huge injection barrier for electron in to LUMO level of PCBM and shows nonlinear behavior. Figure 4.7(a) and (b) show the output characteristics of ambipolar OFETs with Au and Pt electrodes, the Figure also shows the transfer characteristics measured from the same device. Since the injection barrier of holes is much lower than that of electron for both Au and Pt devices, the FET behavior shows dominantly p-channel characteristics and the n-channel shows severely non-ohmic behavior due to the formation of shottky barrier for electron injection into the P3HT/PCBM blend. Such non-ohmic behavior is consistent with the metal organic contact when the injection barrier is higher than 0.3-0.5eV.

Although it is not straight forward to directly measure the injection barrier from the performance of ambipolar OFETs but one can indirectly estimate this information from the ohmic and non-ohmic behavior of the transistor output and transfer characteristics with enhanced electron or hole transport. Our observation of ambipolar OFETs with different metal contacts leads us to the conclusion that injection barrier for both holes and electrons lies ~ $0.3 < \varphi < 1$ eV range shows balanced p and n channel characteristics with current behavior similar for both carriers and is symmetrical around V_{DS}=0V. In addition, the injection barrier of ~1 eV or more shows severe contact resistance which leads to highly nonlinearity in the OFET output characteristics.

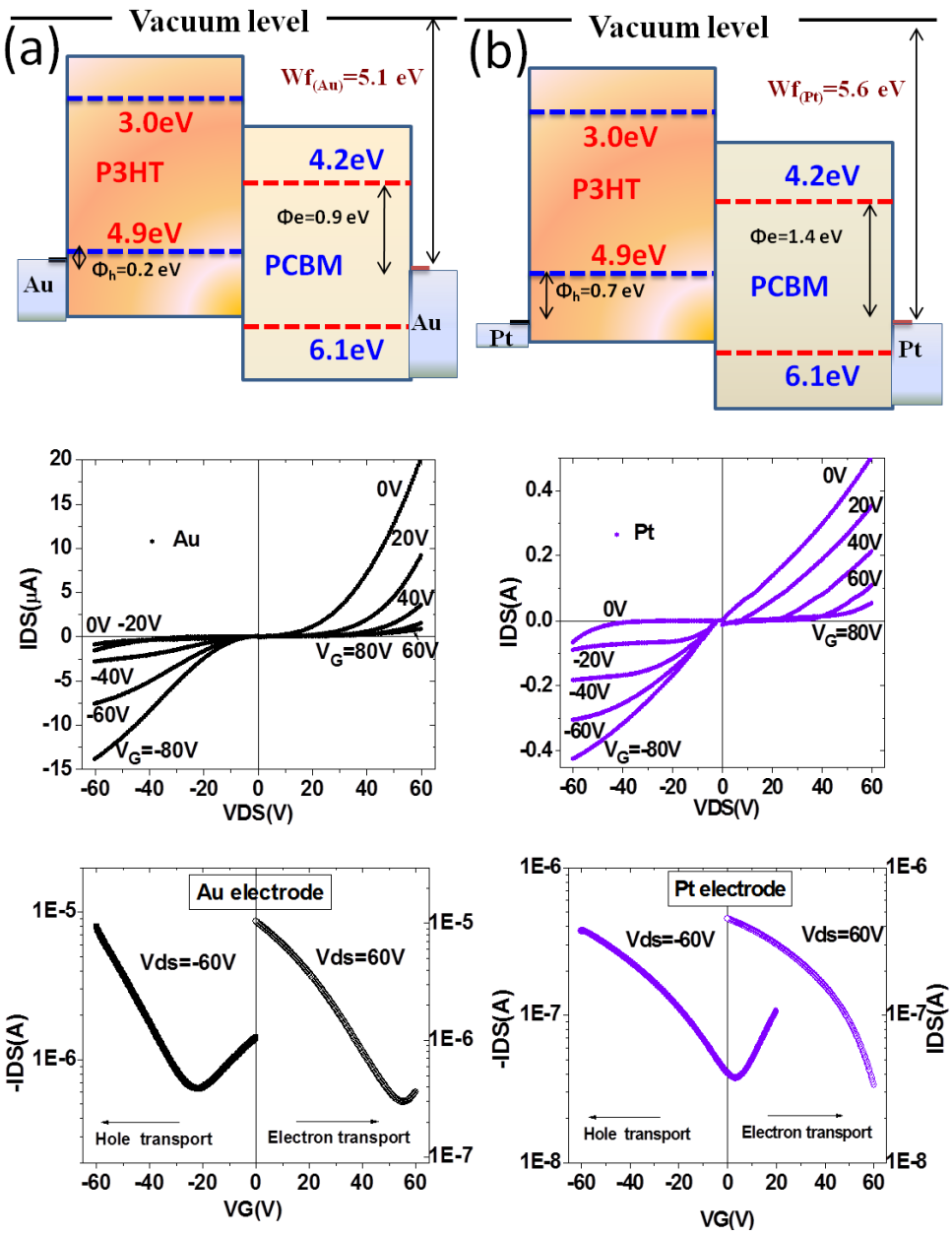

Figure 4.7 Output (I-V) and transfer (I-V_G) characteristics of ambipolar OFETs with Au and Pt that have high barrier injection with PCBM.

The calculated saturation electron and hole mobilities for OFET with P3HT:PCBM blend with different metal contacts are summarized in Figure 4.8. We observe no trend for the hole mobilities with increasing the work function; however, electron mobilities decreasing when increasing the work function. The examined OFET devices exhibit electron mobilities in the rage

of $8x10^{-3}$ to $4x10^{-4}$ cm^2/Vs and hole mobilities in the range of $1.2x10^{-2}$ to $2x10^{-4}$ cm^2/Vs depending on the metal work function. Au with lowest barrier height with HOMO level of P3HT has shown the highest hole mobility of $1.2x10^{-2}$ cm^2/Vs. On the other hand, electron mobility of ~ 1×10^{-3} cm^2/Vs was calculated for the metals with almost matching work function to LUMO level of PCBM: Al, Ag, Ti. On the other hand, Au, Pt, and Pd showed the lowest electron mobility because of their high injection barrier with LUMO level of PCBM.

The values of electron and hole mobilities for P3HT/PCBM blend are lower than the values extracted from pristine P3HT and PCBM due to the charge screening effect from either component which affects the charge transport. Those values however give a closer picture to the expected values in the P-OPV device made from P3HT/PCBM blend. Because of the recombination process in the P-OPV device, the mobility is expected to decrease from the values of OFET devices.

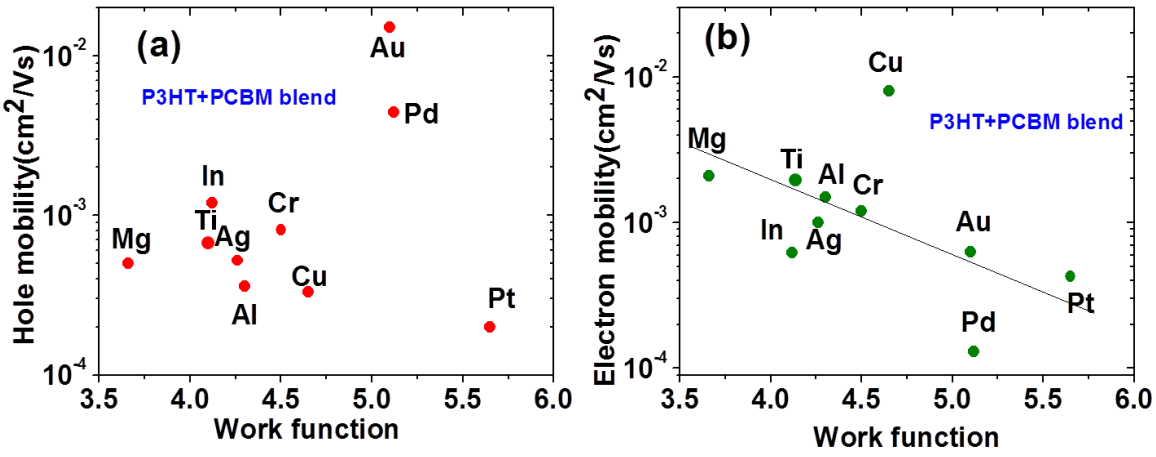

Figure 4.8 Mobility as a function of different metal work function of (a) Holes and (b) Electrons for P3HT/PCBM (1:2) OFETs.

4.3 Conclusions

In conclusion, we have reported on the fabrication of OFETs using pristine P3HT and PCBM and a 1:2 ratio blend of both materials from different metal contacts. A range of metal from low work function to high work function was selected to find out the ambipolar FET properties. The results show a clear evidence of injection barrier effects on the performance of the devices. All the resulting OFET devices with P3HT/PCBM blend exhibit electron mobilities in the range of $8x10^{-3}$ to $6x10^{-4}$ cm^2/Vs and hole mobilities of $1x10^{-2}$ to $3.3x10^{-4}$ cm^2/Vs depending on the various metal contact. This makes these metals possible candidates to be used as electrodes in a P-OPV because they show balanced hole and electron mobilities. Au with high on current and hole mobility can be used as anode (hole extractor) in the planar organic photovoltaic device while metals such as In, Cr, and Ti with a reasonable electron mobility can be used as a cathode (electron extractor). We have also found that Al, Mg, Ag have shown a threshold voltage which can be a result of the rapid oxidation of these materials which make them undesired electrode materials in the planar organic photovoltaic device. Our results from this study demonstrate the importance of contact metal effect on device performance and potential application of different metal electrode towards the design of planar photovoltaic devices.

CHAPTER 5: INFLUENCE OF CATHODE MATERIAL, CHANNEL LENGTH, AND ACTIVE LAYER THICKNESS ON THE PERFORMANCE OF PLANAR ORGANIC PHOTOVOLTAIC DEVICE

5.1 Introduction

Since organic photovoltaics is considered as a relatively new technology [[197], [198]], the understanding of the OPV device operation is still developing and rapidly improving. Developing an understanding of the physics of the OPV device including its parameters is crucial to improve engineering and performance of the devices. One of the goals of this work is to help establish this understanding. While the current vertical OPV device structure is limited by the need of a transparent metal oxide electrode, mostly ITO, and the inseparable relation between the active material thickness and the electrodes separation, the utilize of planar organic photovoltaic device (P-OPV) opens up the opportunity to choose verity of metallic materials as electrodes and the light can be directly shinned on the active material with no need to pass through a transparent electrode (ITO). In addition, active layer thickness and the electrodes separation (channel length) can be independently varied to investigate the effect of the absorption and the charge transport on the P-OPV device performance. The recent studies that utilized the P-OPV device have shown a low device performance [[199], [200], [201]]; and so far the role of the electrodes work-functions, electrodes separation, and the film thickness in planar structure have not been investigated. The reasons for poor device performance of planar devices in these studies can be the use of 1) improper electrodes combination, 2) non optimized channel length, 3) non optimized film thickness, and 4) non optimized blending ratio.

In this chapter, we focus on studying the P-OPV device using BHJ active material poly (3-hexylthiophene) and [6,6]-phenyl C61-butyric acid methylester (P3HT:PCBM). We fix Au as

the anode and alternate the cathode to Al, Mg, Ag, In, Cr or Ti metal to study the effect of the contacts work-function on the device performance. For the optimized set of electrodes Au/Cr and Au/Ti we report the effect of independently varying the active layer thickness and channel length on the device characteristic parameters (I_{sc}, V_{oc}, FF, and PCE).

5.2 Results and Discussions

All of the devices discussed in this chapter are fabricated as described in chapter 3 using the two steps e-beam lithography technique. The P3HT/PCBM (1:2 ratio) spun coated with different thicknesses (50, 100, 150, and 200 nm). Thicknesses were determined by AFM. The channel length was varied as L= 0.24, 0.3, 0.5, 0.8, 1, and 3 µm. I-V curves for all P-OPV devices were extracted under illumination of 100 mW/cm^2.

In this chapter we investigate the PV behavior in three main sections. In the first section we measure the photovoltaic behavior for P-OPV devices with Au anode and (Mg, Ag, or Al) as cathode. Then, the PV behavior of Au/In, Au/Cr, and Au/Ti P-OPV devices will be discussed, and finally the effect of varying the active layer thickness and the channel length independently on the P-OPV with Au/Cr and Au/Ti electrodes will be discussed.

Figure 5.1 (a) shows the schematic diagram of the (P-OPV), where cathode and anode are in-plane with a P3HT/PCBM BHJ blend active material. Figure 5.1 (b) shows optical image of the P-OPV devices fabricated by two steps electron beam lithography with clear gap (channel length) between two electrodes. One of the advantages of utilizing P-OPV device structure is flexibility of choosing the electrodes with no constrain to be transparent. However, in order to achieve a better OPV device performance and less energy loss at the metal/organic contact, the work function of the chosen electrodes should allow efficient charge extraction of holes from the

highest occupied molecular orbital (HOMO) level of P3HT and of electron from the lowest unoccupied molecular orbital (LUMO) level of PCBM. Therefore, the work function of the hole extractor electrode should match the HOMO level of the P3HT and for the electron extractor electrode the work function should match the LUMO level of the PCBM.

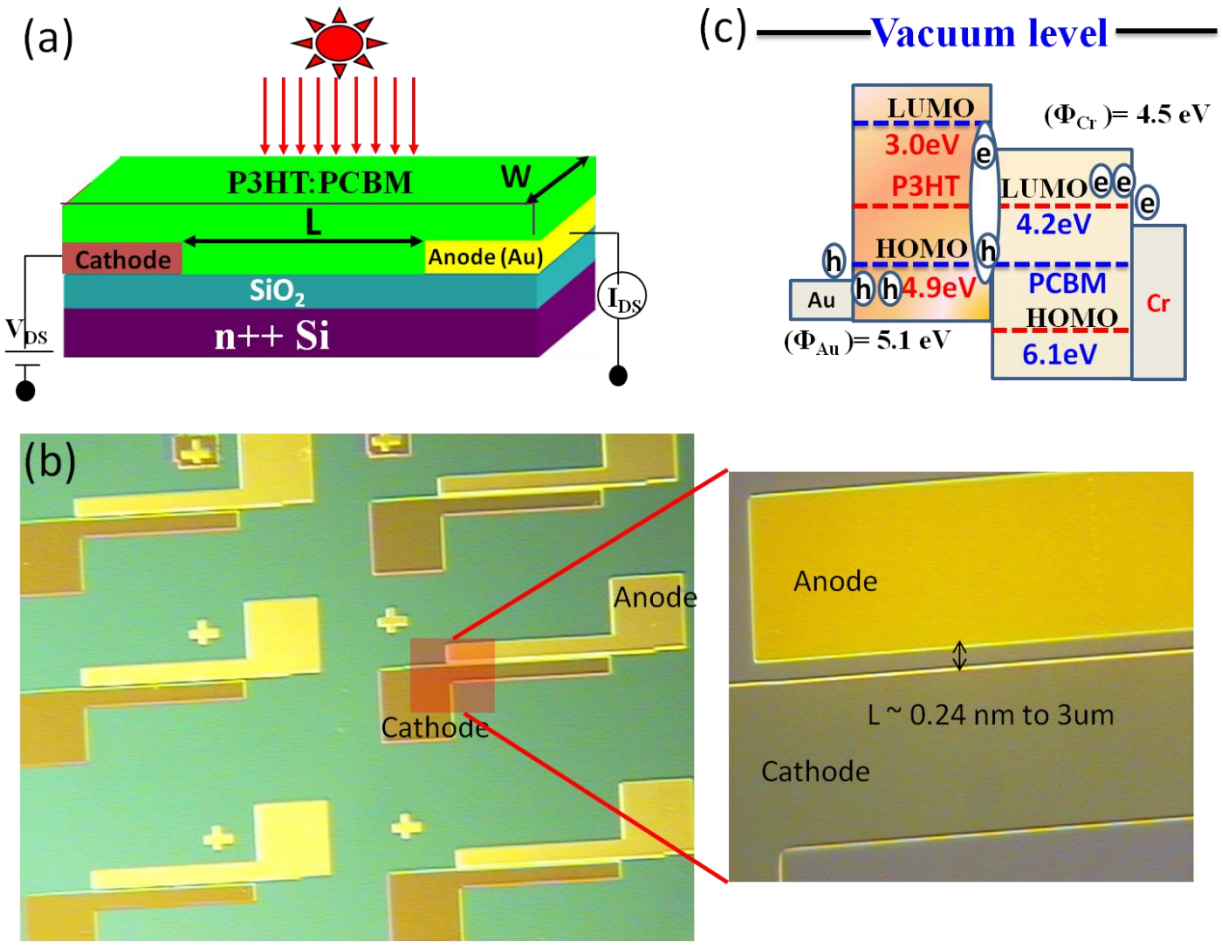

Figure 5.1 (a) Schematic diagram of the P-OPV device with fixed anode (Au). (b) The optical image of 6 P-OPV devices fabricated by standard electron beam lithography with clear separation between two electrodes showed in zoomed in image. (c) Simplified energy level diagram of P3HT/PCBM blend with Au-Cr electrodes.

Figure 5.1 (c) shows the schematic energy level diagram of the P3HT/PCBM blend with the work function of Au and Cr for solar cell operation as an example to explain how the OPV

device works. Au has a small energy difference (0.2 eV) with the HOMO of P3HT for collection of holes and Cr has 0.3 eV energy difference with LUMO of PCBM for collection of electrons. In organic solar cell operation, the generated photoexcitons dissociate at the interface of the P3HT and PCBM and followed immediately by electron transfer to PCBM and holes to P3HT [202]. Because of the internal electric field created by asymmetric Au and Cr electrode in the active layer under short circuit condition the separated holes and electrons move toward the respective electrodes through the potential drop without any bias voltage. As a result, a current passes in the device and photovoltaic behavior is observed.

5.2.1 PV characteristics for Al, Mg, and Ag cathode materials

Figure 5.2 shows the schematic energy level diagrams of the HOMO and LUMO of P3HT and PCBM with respect to the different metal work functions to show the corresponding electron and hole injection barrier height. Based on this, Au (φ=5.1eV) was selected and fixed to be efficient contact for hole extraction electrode because of the low barrier height with HOMO level of P3HT. In addition, Au has shown a high current and hole mobility in the p-channel in OFET device (Chapter 4). On the other hand, Mg, Ag, Al, In, Cr and Ti were chosen to be candidates for electron extraction electrode because the values of their work functions lie around the LUMO level of PCBM and showed reasonable electron mobility values in the OFET study.

The experimental results on varying the electrodes work function by varying the cathode material between Al, Mg, and Ag are presented in Figure 5.3. The PV behavior investigations were carried out for twenty of devices for each set of electrodes. Figure 5.3 (a) shows the I-V characteristics for P-OPV device with Au/Al set of electrodes and P3HT/PCBM active material. For this device, neither diode-like behavior under dark nor photovoltaic behavior under

illumination was exhibited. As can be seen in Figure 5.3 (b) and (c) no PV behavior was found under illumination for P-OPV devices with Au/Mg and Au/Ag set of electrodes as well.

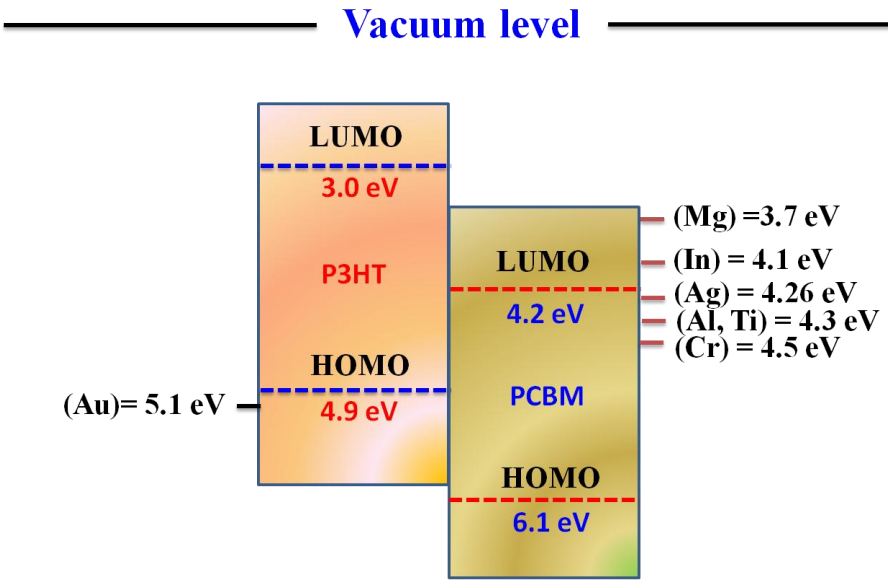

Figure 5.2 Energy levels of cathode contact metals to the right with respect to the LUMO level of PCBM where the electron injection will be from. To the left is the work function of the gold with respect to HOMO level of P3HT where the hole injection will be from.

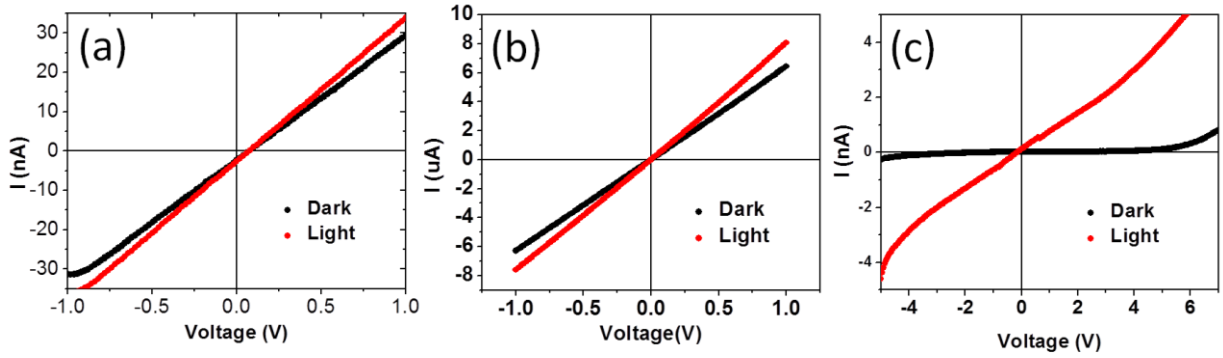

Figure 5.3 Output characteristics for planar device with structure (a) Au/P3HT:PCBM/Al (b) Au/P3HT:PCBM/Ag and (c) Au/P3HT:PCBM/Mg. Light is 100 mW/cm^2.

The reason for not showing PV behavior by the P-OPV device with the structure Au/P3HTPCBM/Al even though Al has a low barrier height with LUMO of PCBM and has shown a reasonable value of hole and electron mobilities might be the rapid oxidation of the Al at the interface with P3HT:PCBM. The oxidation of the Al creates an oxide layer that acts as insulator at the interface with the active material blocking the charges from being extracted. In order to understand this behavior we should examine in depth the OFET device with structure Al/P3HT:PCBM/Al that was fabricated and measured in Chapter 4. The output measurement for this device that is presented in Figure 5.4 shows high threshold voltage (voltage where current starts passing in the device) around 25 V in both P-type and n-type behavior supporting the creation of large barrier at the interface with P3HT:PCBM. This behavior is usually seen in metal/insulator/semiconductor (MIS) system which supports the creation of AlO_2 layer that acts as an insulator layer.

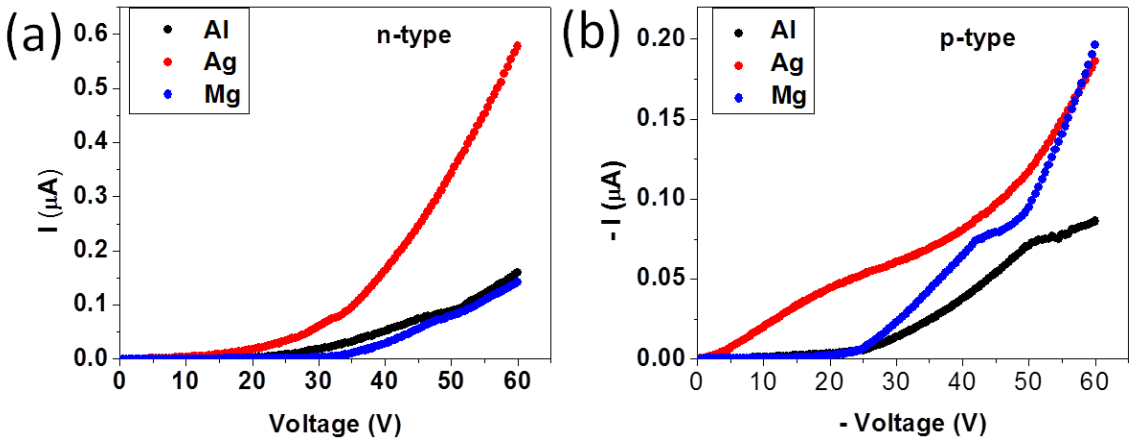

Figure 5.4 Output characteristics for OFET devices made from Al/P3HT:PCBM/Al, Ag/P3HT:PCBM/Ag, and Mg/P3HT:PCBM/Mg in (a) n-type channel and (b) p-type channel.

The same explanation for not showing PV behavior is also applicable for the P-OPV devices with the structures Au/P3HT:PCBM/Ag and Au/P3HT:PCBM/Mg because Ag and Mg share the rapid oxidation property with Al. The output measurements for Ag/P3HT:PCBM/Ag and Mg/P3HT:PCBM/Mg FET devices shown in Figure 5.4 indicate a formation of oxide interfacial layer that prevented the extraction of the charges leading to no PV behavior for these P-OPV devices. As we can see, a threshold voltage about ~ 20 V is observed for the Ag electrodes in the n-channel while a ~ 35 V threshold voltage is observed for the Mg electrodes in the n-channel. In addition, both contacts show threshold voltage in p-type behavior which prevents holes from being extracted in the PV device.

5.2.2 P-OPV devices with In, Cr, Ti cathode materials: Effect of varying contact work function

Planar organic photovoltaic (P-OPV) devices discussed in this subsection were fabricated with Au as an anode and In, Cr, or Ti as cathode. Before going any further in the discussion, I should mention here the difference in calculating PCE value between the Planar and vertical OPV devices. The standard equation of calculating PCE is given by:

$$PCE(\%) = \frac{FF \times V_{oc} \times (J_{sc} \times A_{cross-section})}{power_{input} \times A_{illuminated}} \times 100\% \tag{5.1}$$

Where the power input is in mW/cm^2 and the short circuit current density is:

$$J_{sc} = \frac{I_{sc}}{A_{cross-section}} \tag{5.2}$$

In vertical OPV device where $A_{illuminated} = A_{cross\text{-}section}$ (see Figure 5.5 (a)), the PCE standard equation 5.1 becomes:

$$PCE(\%) = \frac{FF \times V_{oc} \times J_{sc}}{power_{input}} \times 100\% \tag{5.3}$$

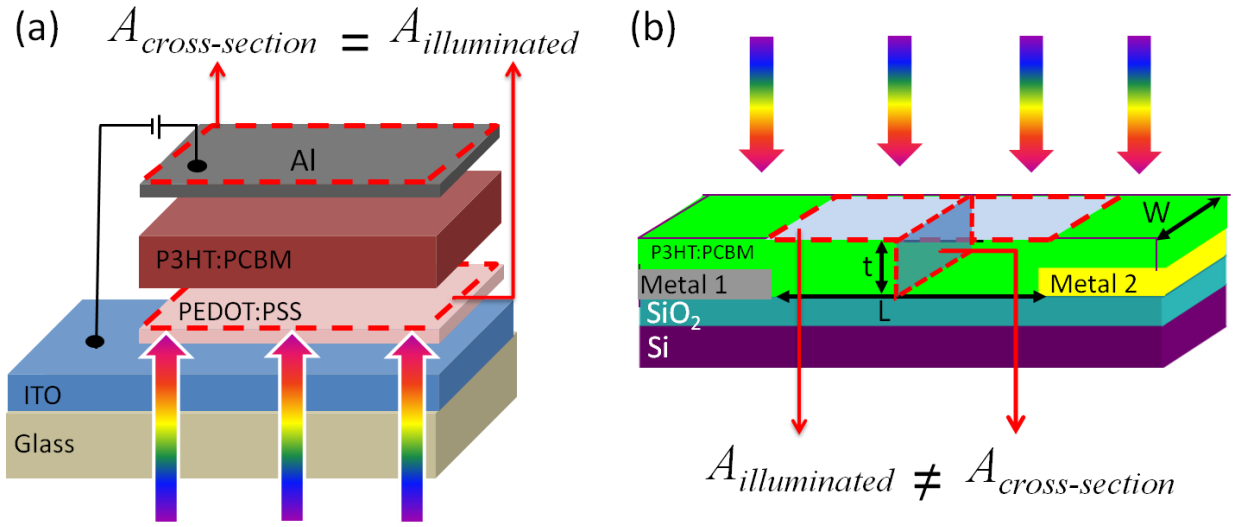

Figure 5.5 Definition of the illuminated and cross-section areas in (a) vertical OPV device, and (b) P-OPV device. "t" is the film thickness.

In the P-OPV device, $A_{illuminated} \neq A_{cross\text{-}section}$ as shown in Figure 5.5 (b),

$$A_{illuminated} = l \times w \tag{5.4}$$

$$A_{cross-section} = t \times w \tag{5.5}$$

Where, l is the channel length, W is the channel width, and t is the film thickness (height).

Because the two areas are different in the planar device, then the standard PCE equation 5.1 becomes:

$$PCE(\%) = \frac{FF \times V_{oc} \times I_{sc}}{power_{input} \times L \times W} \times 100\% \quad (5.6)$$

The difference in calculating PCE in the two device structures is that in vertical structure J_{sc} value is needed while in planar the I_{sc} value is used.

Figure 5.6 (a), (b), and (c) show the I-V characteristics in the dark condition for the P-OPV devices with Au/In, Au/Cr, and Au/Ti electrodes, respectively. The devices with Cr and Ti cathodes show rectifying I-V characteristics and exhibits diode like I-V behavior which can be attributed to the formation of Schottky barriers (SB) at the metal/polymer contact. The dark current or the diode-like behavior for these devices can be characterized by two parameters: (i) current rectification which is the ratio between the maximum forward bias current (on-current) to the maximum reverse bias current, (ii) the ideality factor "n" that can be extracted from the slope of the exponential curve in the forward bias by rearranging Equation 2.1 to be:

$$n = \frac{e}{KT}\left[\frac{dV}{d\ln I}\right] \quad (5.7)$$

The importance of these parameters is that they reflect the rectification behavior of the donor-acceptor heterojunctions. Low rectification is related to ideality factor value greater than one. In addition, the value of large "n" indicates high recombination and charge traps in the active material.

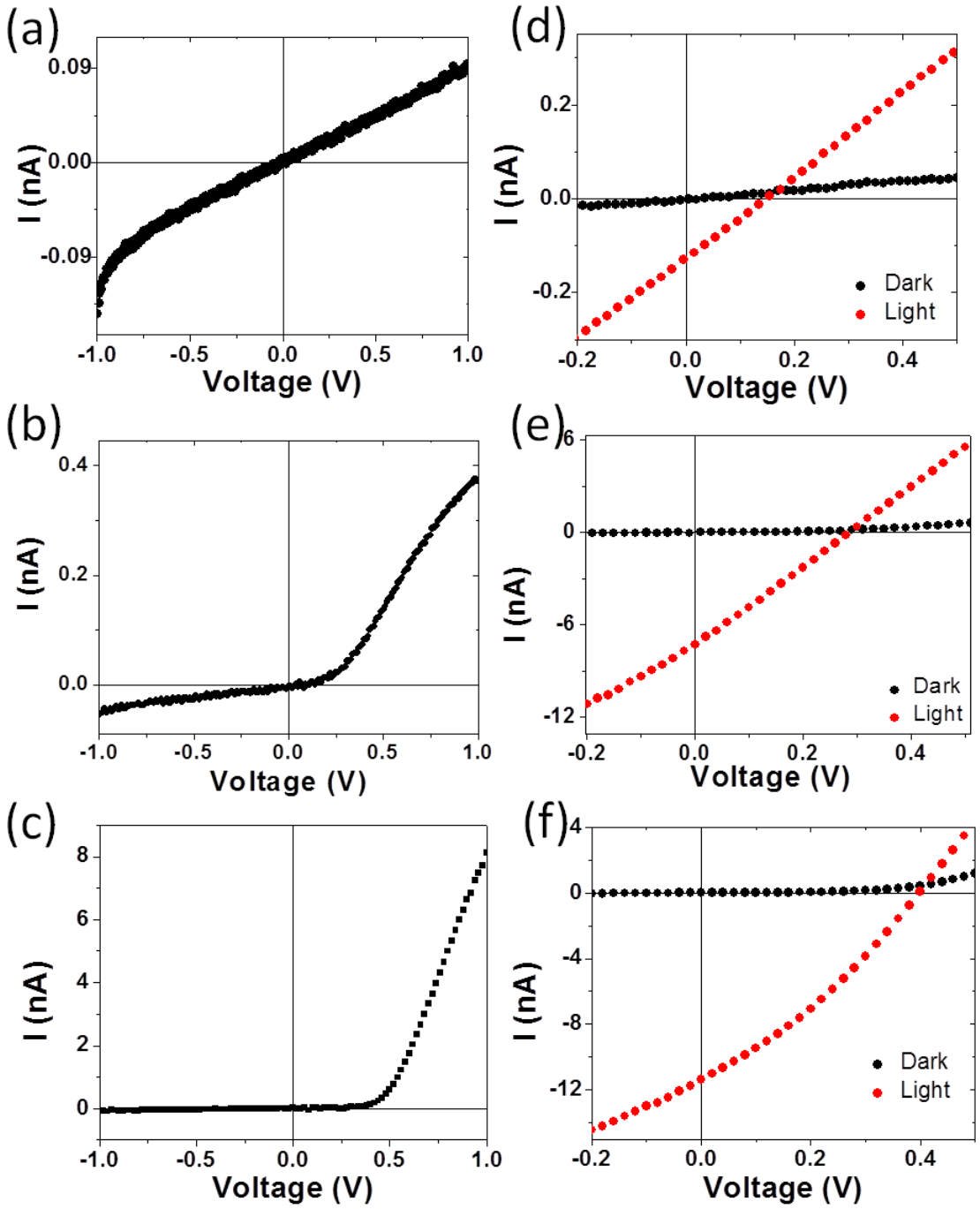

Figure 5.6 I-V characteristics under dark condition for of P-OPV device with structure (a) Au/P3HT:PCBM/In, (b) Au/P3HT:PCBM/Cr and (c) Au/P3HT:PCBM/Ti. I-V cherctristics under light for P-OPV device with structure (d) Au/P3HT:PCBM/In, (e) Au/P3HT:PCBM/Cr and (f) Au/P3HT:PCBM/Ti. Light is 100 mW/cm^2 and active material thickness=200 nm and channel width W= 100 µm.

P-OPV devices started to exhibit photovoltaic behavior when In was used as cathode material. Figure 5.6 (d) shows the I-V characteristics for the Au/P3HT:PCBM/In P-OPV device under 100 mW/cm^2 illumination. As can be seen, a small short circuit current ~ 0.12 nA and V_{oc} value ~ 0.15 V were measured which led to a small FF ~ 0.25 and PCE value ~ 0.04% using Equations 5.6:

$$PCE = \frac{0.25 \times 0.15V \times 0.12nA}{100mW/cm^2 \times (240nm \times 100\mu m)} \times 100\%$$

$$PCE = \frac{0.0045nA.V}{100mW/cm^2 \times (240nm \times 100\mu m)} \times 100\% = 0.04\%$$

Due to this low device performance, no further study conducted using In material. Figure 5.6 (e) shows the I-V characteristics of the best device performance using Cr as cathode with L = 0.24 µm and W = 100 µm under 100 mW/cm^2 illumination. The device shows PV effect with short circuit current of I_{sc} = 7.3 nA and V_{oc} = 0.27 V. The fill factor of this device is estimated to be about 0.27 which leads to a PCE value of 2.25%. In comparison with device performance with In and Cr cathode materials, a better PV behavior was observed when Ti metal was used as a cathode electrode. Figures 5.6 (f) shows output characteristics under illumination for P-OPV device with Au/P3HT:PCBM/Ti structure with L= 300 nm. The Figure shows the best PV behavior in this work with V_{oc}= 0.4 V, I_{sc}= 11.4 nA, and FF= 0.34 leading to PCE value 4.75%. The performance of Au/Cr or Au/Ti devices is better than reported for planar OPV device that were fabricated with large channel length up to 1 mm, Au/Al or Ca electrodes, and 1:1 ratio with a maximum PCE value of 0.6% [[203], [204]]. Here, we consider the better device performance is due to using different set of electrodes Au/Cr and Au/Ti with P3HT/PCBM 1:2 ratio in addition to a

smaller channel lengths 0.24 and 0.3 µm. Furthermore, the PCE values of 2.25% and 4.75% are comparable to the reported values for vertical OPV devices structured without using any injection (buffer) layers between the electrodes and the P3HT:PCBM layer PCE ~ 0.9 – 4 % [205, 206, 207, 208, 209, 210, 211, 212]. The P-OPV devices in this work were fabricated without using any buffer layers that are usually used in the vertical structure to enhance the injection of the carriers at the respective electrodes [213, 214, 215, 216]. For the common vertical OPV device fabricated from P3HT:PCBM and injection layers, higher PCE values were reported about 5% [217, 218, 219].

Table 5.1 below summarizes the extracted values of current rectification, n, the series (R_s), shunt (R_{SH}) resistances, and the characteristic parameters for the three P-OPV devices with In, Cr, and Ti cathode materials. (R_s) and (R_{SH}) were calculated by Equations 2.2 and 2.3.

Table 1 The effect of cathode material in P-OPV device on the device parameters

Parameter	Au/P3HT:PCBM/In	Au/P3HT:PCBM/Cr	Au/P3HT:PCBM/Ti
Current rectification	0.9	6.89	101
Ideality factor (n)	7.74	3.87	2.76
R_s ($\Omega.cm^2$)	200	100	33.3
R_{SH} ($\Omega.cm^2$)	180	220	689.7
I_{sc} (nA)	0.12	7.3	11.4
V_{oc} (V)	0.15	0.27	0.4
FF	0.25	0.27	0.34
PCE (%)	0.04	2.25	4.75

The reported V_{oc} values for the three P-OPV devices 0.15, 0.26, and 0.4 V are substantially lower than the ideal V_{oc} values which is the difference between the HOMO and

LUMO levels of P3HT:PCBM ~ 0.7 V. This low V_{oc} value can be attributed to the large interfacial energy barrier between In, Cr, Ti electrodes and P3HT:PCBM. The interfacial energy barrier can be attributed to the low resistance of In and Cr to corrosion which creates an oxide layer at the cathode/P3HT:PCBM interface [220]. In addition, large energy barrier can be as a result of not using any injection layers that lowers this barrier and enhances the charge injection at the interface. The effect of the interfacial energy barrier is evident from large series resistance values (R_s) ~ 200 $\Omega.cm^2$ and 100 $\Omega.cm^2$ for P-OPV device with In and Cr as cathode, respectively. This value decreased to 33 $\Omega.cm^2$ when Ti used as cathode which is known for its strong corrosion resistance. Studies have shown that increasing recombination rate and charge traps in the active layer can decrease V_{oc} value [221]. In addition, the low value of R_{SH} ~ 180 $\Omega.cm^2$ for In cathode indicates a large lost current due to the recombination. This value of R_{SH} increased to ~ 690 $\Omega.cm^2$ when the cathode was changed to Ti reflecting a less recombination in the device. Moreover, the high value of "n" about ~ 7 for the P-OPV device with In cathode also supports the high recombination rate in the device while this value was less for Cr and Ti cathodes. Furthermore, the fill factor values 0.25, 0.26, and 0.34 for In, Cr, and Ti, respectively are lower than those typical reported values for vertical OPV devices between 0.48-0.69 [222]. For vertical PV devices low FF has been reported as a result of the absence of injection layers at the electrode which results in lower R_{SH} and higher R_s values. In the planar device geometry reported in this work, the low FF can be attributed to higher injection barriers due to the absence of injection layers, resulting in higher R_s ~ 200 $\Omega.cm^2$ for In cathode. When comparing with reported values for vertical structure less than 100 $\Omega.\ cm^2$ [223, 224], R_s values for In and Cr cathodes are higher and for Ti cathode it is falling in the same range.

It clear from the data summarized in table 1 that the variation of the cathode material affects the characteristic parameters because the work-function value of the cathode determines the barrier at the interface with the active layer which leads to a variation in the device parameters. Ti metal with work function of 4.3 eV makes the energy difference between the work function and LUMO of PCBM lower when comparing with Cr metal which leads to a less energy lost and contributes to increasing V_{oc} from 0.27 for Cr to 0.4 for Ti. Also, 4.3 eV value of work-function for Ti matches the LUMO level of PCBM which creates an ohmic contact thus less energy lost at the interface and more charges extraction. In addition, Ti is more stable metal comparing to Al, Ag, Mg, In, and Cr because of its excellent resistance to corrosion which enhances the interface with P3HT:PCBM material. Hence, Au with Ti electrodes combination showed better photovoltaic behavior. The presented results in this section have shown that when the work function of the cathode electrode is varied the characteristic parameters of the device change depending on the barrier hight difference between the work function and LUMO of PCBM.

5.2.3 Bimolecular recombination in Au/Cr P-OPV device

An important issue that can limit the and affect the values of OPV cell's parameters (I_{sc}, V_{oc}, and FF) is the amount and the type of the carrier's recombination in the active material. Two types of recombination that can occur in the P3HT:PCBM active layer: (i) the monomolecular recombination resulted from defect or charge traps in the layer, and (ii) bimolecular recombination as a result of unbalanced hole and electron mobilities. It has been shown previously that for polymer based solar cell because of a large difference in electron and hole

mobilities a space-charge limited (SCL) photocurrent occurs at high input light intensity due to an unbalanced charge transport which can be described by:

$$J_{ph} \leq (qG)^{0.75} \left(\frac{9}{8}\epsilon_0 \epsilon_r \mu_h\right)^{0.25} \sqrt{V} \tag{5.8}$$

Where G is the generation rate of the free carriers and μ is the mobility of the slowest carrier which is hole in this organic BHJ materials. This SCL current results in a bimolecular recombination because of the unbalanced holes and electrons mobilities that leads to a low FF and V_{oc}. Several authors have reported that I_{sc} is proportional to P_{in}^{s} where P_{in} is the power input and the power "s" is ranging from 0.75 in case of SCL current (bimolecular recombination) to 1.0 for SC free current (monomolecular recombination). In order to determine the exponent s for our P-OPV we measured the values for I_{sc} at different light intensities (25, 50, 75, and 100 mW/cm^2) for the P-OPV device with structure Au/P3HT:PCBM/Cr with L=0.24 μm (see figure 5.7).

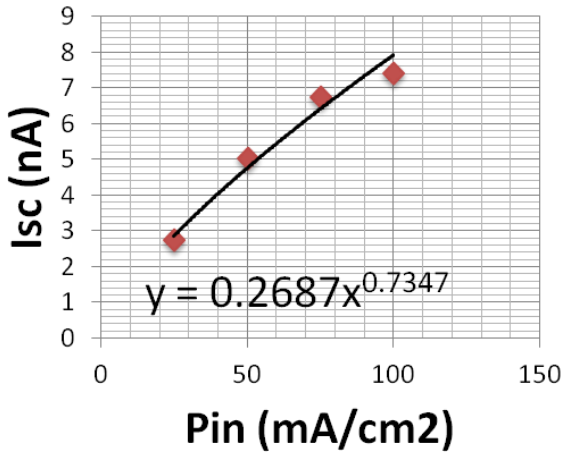

Figure 5.7 Short circuit current as a function of the power input. The fitting equation is used to extract the exponent s that defines the type of recombination in the P-OPV device.

We found that with increasing light intensity the short circuit current increases due to the generation of large number of excitons. When fitting theses data (I_{SC} vs. P_{in}) to the best power trend curve, we found the exponent s to be ~0.73. This is a clear indication of a bimolecular recombination in the P-OPV devices resulted from a SCL current which explains the low V_{oc} and FF achieved in this work. In order to reduce the amount of this recombination to insure an increase in the FF and Voc values, an injection layer at the organic/metal interface should be introduce. Here, in this work we didn't use any injection layer; however, this will be considered in future work.

5.2.4 The effect of channel length on the P-OPV device performance

By utilizing the planar structure, P-OPV devices with structures Au/P3HT:PCBM/Cr and Au/P3HT:PCBM/Ti with five different channel lengths, L = 0.24, 0.5, 0.8, 1, and 3 µm were fabricated with 20 devices for each L with a different active material thicknesses 50, 100, 150, and 200 nm in order to address the effect of the separation between the electrodes (channel length) on the device performance. Figure 5.8 (a) shows the I-V characteristics of five individual P-OPV devices with the different channel lengths for devices with Cr as cathode and a film thickness = 200 nm; all the devices showed PV behavior and the measured devices resulted in efficiencies ranging from lowest 0.08 % for L= 3 µm to a maximum value 2.25 % for L=0.24 µm. The variation of I_{sc} and PCE values as a function of the channel length at the four different film thicknesses are summarized in figure 3(b) and 3(c), respectively. As shown in the figures, highest I_{sc} and PCE values are observed for the high thickness 200 nm. At that thickness, with the decrease of L from 3 µm to 0.24 µm the average value of PCE increases from 0.1 % to 2 %

and the I_{sc} values followed the same behavior of increasing. V_{oc} and FF values were the same for all the devices with different channel lengths about 0.27 V and 0.26, respectively.

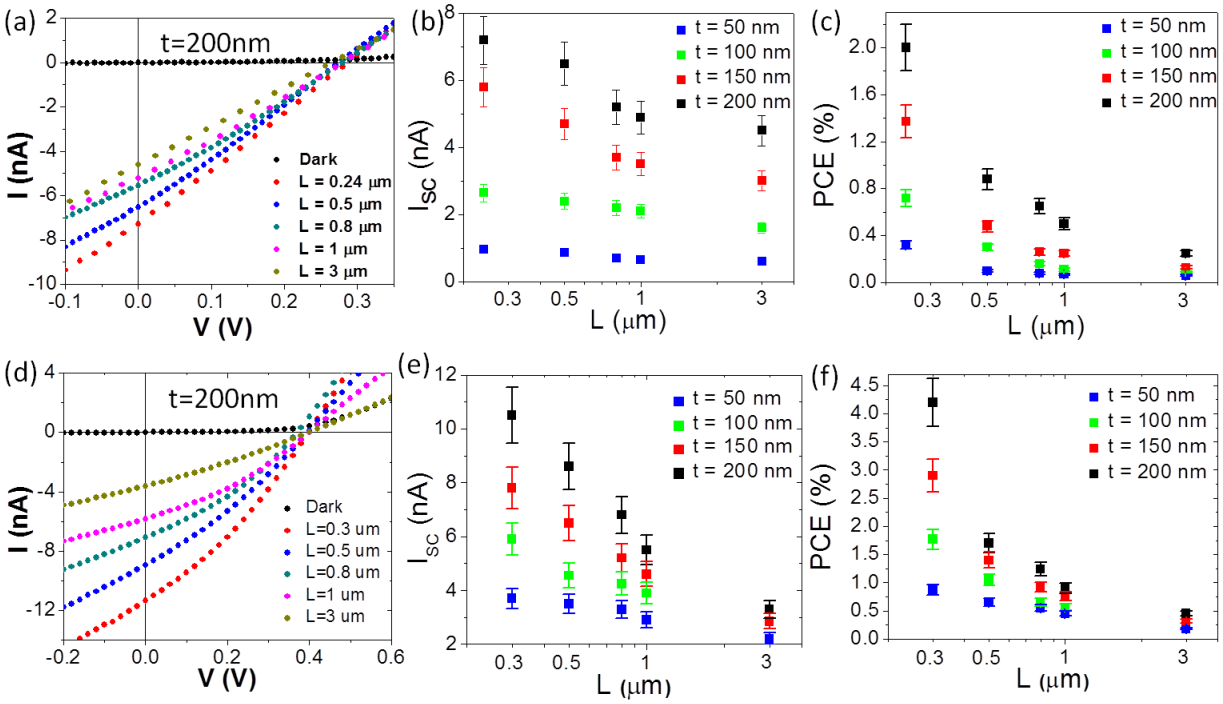

Figure 5.8 The devices structures are Au/P3HT:PCBM/Cr in (a, b, c) and Au/P3HT:PCBM/Ti in (d, e, f). (a) an (d) I-V characteristics for different channel length obtained from P3HT:PCBM solar cell under incident intensity of 1 Sun at thickness t= 200 nm. (b) and (e) Average values of I_{sc} as function of channel length for the four film thickness of 50, 100, 150, and 200 nm. (c) and (f) Variation of average PCE values as a function of channel length for the four film thickness of 50, 100, 150, and 200 nm.

For Au/P3HT:PCBM/Ti P-OPV device, a better device performance was achieved. Figure 5.8 (d) displays the I-V curves for the P-OPV devices with the different channel lengths at a fixed film thickness 200 nm. V_{oc} about 0.4 V didn't change with varying the channel length and I_{sc} increased from 3.8 nA to 11.2 nA with decreasing the channel length from 3 µm to 0.3 µm. The comprehensive results of I_{sc} and PCE values as a function of the channel length (L) at the four different film thicknesses are summarized in figure 5.8 (e) and (f), respectively. As

shown in the figures, average PCE value increases from about 0.3% to 3.75% with the decrease of L from 3 µm to 0.3 µm for the film thickness 200 nm. The I_{sc} and PCE values also exhibited the same behavior at other film thicknesses.

As the channel length decreases the carrier's diffusion length ($L_{n,p}$) increases as given in the equation [225]:

$$L_{n,p} = \mu \frac{\tau(V - V_{bi})}{L} \tag{5.9}$$

Where, µ is the mobility, τ is the recombination life time, V is the applied voltage, and V_{bi} is the build in potential between the two electrodes. Typically, µ is in order of 10^{-3} cm^2/V.S for P3HT:PCBM system and τ is microsecond range [226]. Considering these values, the $L_{n,p} \simeq \frac{10^{-9}(cm^2)}{L}$. Decreasing L from 3 µm to 0.24 µm (almost one order of magnitude) increases the diffusion length by an order of magnitude to approximately 10^{-5} cm. This increase of the diffusion length reduces the recombination rate at the short channel lengths, and it increases (I_{sc}) as given in [227]:

$$J_{sc} = qGL_{n,p} \tag{5.10}$$

As a result, we consider that the short circuit current increases for the short channel lengths because of the greater chance for the electron and hole to reach the cathode and anode before they recombine and hence improves the charge collection and increases PCE. The results in both P-OPV device structures with Cr or Ti as cathode material clearly illustrate that short channel length provides better PV device performance with higher PCE value. In addition, V_{oc} and FF didn't change for the different channel lengths.

5.2.5 The effect of active layer thickness on the P-OPV device performance

Another advantage of utilizing the planar structure is the ability to increase the active material thickness while keeping the channel length fixed which cannot be achieved in the vertical structure. In order to address only the importance of the active layer thickness on the P-OPV device performance, more than 100 devices were fabricated with four different thicknesses, 50, 100, 150 and 200 nm of P-OPV device with Cr and Ti as cathode materials. Figure 5.9 (a) represents the I-V characteristics of the Au/P3HT:PCBM/Cr devices with channel length L = 0.24 µm under dark and illuminated condition of 100 mW/cm^2 with varying the film thickness. Figures 5.9 (b) shows the average values of the measured I_{sc} as a function of film thickness for the five different channel lengths under an illumination of 100 mW/cm^2. I_{sc} values of the devices increases linearly with increasing the film thickness. For the fixed L= 0.24 µm Average I_{sc} increases from as low as 1 nA for the device with active layer thickness ~ 50 nm to 7.2 nA for the thickness ~ 200 nm. The same linear behavior is exhibited at the other channel lengths. The averaged data for PCE as a function of film thickness for the five channel lengths are shown in Figure 5.9 (c). PCE follows the same behavior as for I_{sc}, when increasing the film thickness the average efficiency increases up to 2% for the film thickness 200 nm and L= 0.24 µm.

For the P-OPV device with Au/P3HT:PCBM/Ti structure, the PV behaviors over a range of film thicknesses (50, 100, 150, and 200 nm) for a the five different channel lengths were depicted. Figure 5.9 (d) shows the I-V characteristics for the four film thicknesses at a fixed L= 0.3 µm. V_{oc} of 0.4 and FF of 0.34 didn't change with thickness variation. However, I_{sc} increased for higher film thicknesses because of the fact that absorption path is higher for higher thicknesses which increases the charge generation and hence the current. Figures 5.9 (e) and (f) present the I_{sc} values PCE values with varying the film thickness for the five different channel

lengths, respectively. A linear relation between PCE and increasing the thickness can be seen for all channel lengths. The highest PCE for L=300 nm is about 4.75% was achieved at the highest thickness= 200nm. For all channel lengths studied in this work, I_{sc} and PCE values are linearly dependant on the thickness. We also notice for the different channel lengths, a smaller variation in the value of I_{sc} and PCE for the film thickness 50 nm in comparison with wide variation of these values at the large film thickness 200 nm. We attribute the small variation at the low film thickness to the low carriers' generation at that thickness which results in a small value of I_{sc} which reduces the effect of the channel length.

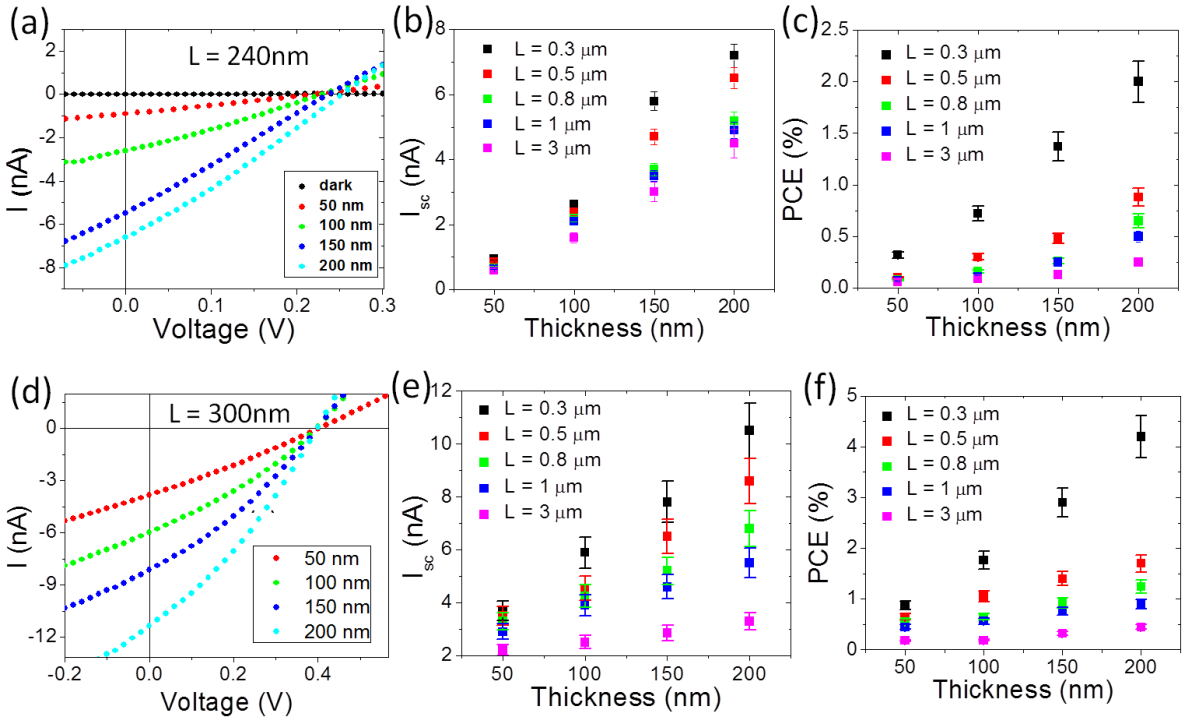

Figure 5.9 I-V characteristics for 4 different thicknesses, 50, 100, 150, and 200 nm under intensity of 1 Sun for (a) Cr cathode L= 240 nm and (d) for Ti cathode L= 300 nm. Average values of I_{sc} as function of active layer thickness for different channel lengths for (b) Cr cathode and (e) Ti cathode. Variation of average PCE values as a function of active layer thickness for (c) Cr cathode and (f) Ti cathode.

It is clearly shown from the above results that with increasing thickness I_{sc} increases. The increase of I_{sc} can be attributed due to the increased in absorption path length in thicker P3HT/PCBM films which is related to the photon absorption [228]. As a result of higher photon absorption, the carriers' generation is increased resulting in an increase in I_{sc} value. It is reported that based on the band-gap energy of P3HT ~1.85 ev, P3HT/PCBM blended material can absorb at the best 27% of the photon flux available in the solar spectrum ($4.31 \times 10^{21}\ s^{-1}m^{-2}$). This leads to $1.16 \times 10^{21}\ s^{-1}m^{-2}$ photons absorbed in the P3HT/PCBM layer if the entire incident light is absorbed in the active layer. However, an attenuation of the incident light occurs in the P3HT/PCM layer depending on the thickness of the layer. For a P3HT/PCBM active layer with a thickness (t= 200 nm), the attenuation factor or the transmittance (T) can be calculated by Beer's Law: $T = \frac{I}{I_0} = e^{-\alpha t}$ where I and I_0 is the emergent and incedent intensities, respectively, and α is the absorption coefficient about $10^5\ cm^{-1}$for P3HT/PCBM. The calculated T was 13.5%, meaning that 86.5% of the incident intensity is absorbed in the 200 nm P3HT:PCBM layer. Therefore, the estimated number of photons absorbed is $\sim 1 \times 10^{21}\ s^{-1}m^{-2}$ which also can be considered as the surface generation rate, assuming the best case scenario of charge generation where each photon creates one exciton. For the 200 nm P3HT/PCBM layer the volume generation rate G is $\frac{1\times10^{21}\ s^{-1}m^{-2}}{200\ nm} = 0.5 \times 10^{28} s^{-1}m^{-3}$. This estimated generation value is falling in the reported values [229]. Considering this amount of charge generation, the current density value can be estimated by using $J_{sc} = qGL_{n,p}$ with $L_{n,p} \cong 4 \times 10^{-7}m$ for the channel length L=0.24 µm. The calculated current density was $J_{sc} = 330\ A/m^2$. Finally, the estimated I_{sc} value considering the best case scenario of charge generation and for thickness ~200 nm and L=0.24 µm was calculated to be 16.6 nA using:

$$I_{sc} = J_{sc} \times Cross\ sectional\ Area = 330\ A/m^2 \times (100 \times 10^{-6} \times 0.2 \times 10^{-6})m^2$$

This estimated I_{sc} value is falling in the same range of I_{sc} value of the P-OPV device with Au/Cr electrodes ~7.2 nA and Au/Ti electrodes ~ 12 nA. The estimated value is higher because we assumed the best case scenario of charge generations and we did not take in consideration the space charge limited current effect which usually reduces the value of the current. In general, the presented linear behavior of I_{sc} as a function of film thickness in this work does not follow the same relation as for vertical devices were an oscillatory dependence on the thickness was reported with optimum thickness values around 60 nm and 160 nm [230, 231, 232].

5.3 Conclusion

In conclusion, in this chapter we have studied planer organic photovoltaic device which allows the freedom of electrodes choice and independent control over the active layer thickness and the channel length which allows us to study the effect of varying those parameters. Al, Mg, and Ag cathode materials showed no photovoltaic behavior. On the other hand, when varying the work function of the cathode material by varying the contact material to In, Cr, or Ti, P-OPV devices showed PV behavior. Low characteristic parameters were observed for In cathode while a better device performance achieved for Cr and Ti cathodes because of their matching work-function to the LUMO of PCBM. Furthermore, we were able to study the effect of independently varying the channel length and the film thickness. We showed that the average value of PCE increases from 0.1 % to 2 % for PV device with Au/Cr electrodes, and from 0.28 % to 3.75 % for PV device with Au/Ti electrodes with decreasing channel length from 3 µm to 0.24 µm at a fixed film thickness 200 nm. On the other hand with increasing film thickness from 50 nm to 200 nm for a fixed channel length of 0.24 µm, average PCE linearly increases from 0.3% to 2 % and from 0.78% to 3.75 % for Au/Cr and Au/Ti respectively. V_{oc} and FF values were not affected by

varying the channel length or the thickness; however, their values were different for different cathode materials. The results indicate that work function of the contact materials can affect the characteristic parameters of the PV device. In addition, a control of the active layer thickness and electrode separation can improve the device performance by absorbing maximum photons as well as optimization of electrode separation for optimum charge carrier mobility which is not possible in present sandwich based design. Further device improvement can be achieved by reducing the channel length and increasing thickness as well as choosing different sets of metal electrodes and by engineering the polymer-electrodes interfaces through adding injection layers. In addition, the results provide a step forward to help design an ITO free PV device by the use of planar structure.

CHAPTER 6: VALIDATION OF THE AREA CALCULATION IN THE PLANAR PHOTOVOLTAIC STRUCTURE

6.1 Introduction

As the performance of photovoltaic device is evaluated by the value of power conversion efficiency, the accuracy of the measurement of this value must be tested and maintained [[233]]. One essential parameter that affects the accuracy of measuring and calculating PCE is the active device area or the illuminated area. The illuminated area defines the amount of power received by the active material and hence the amount of generated carriers. In the common vertical OPV device, usually the illuminated area is defined as the area of the top contact [[234]]. The accurate determination of the illuminated area is very crucial when calculating the short circuit current density (J_{sc}) which is an important quantity that affects the final value of PCE in addition to the open circuit voltage (V_{oc}). To insure an accurate measurement of PCE, it is important to correctly determine (J_{sc}) value.

In the planar organic photovoltaic device (P-OPV) where the two electrodes are fabricated in plan with each other and the active material is deposited in between, there is no upper electrode. In addition, the channel lengths used in this work are comparable or less than maximum absorption length of P3HT:PCBM about 500 nm. This makes the definition of the illuminated different from the current vertical PV device. Some studies that utilized the planar structure have reported the PV device performance using the short circuit current value, and made their calculation for the current density using the optical penetration depth ~ 100 nm [[235]]. Other group defined the illuminated area as the area of the whole organic film even though it covers more area than the device area in between the two electrodes [[236]].

In this chapter we present a simple two experimental approaches to proof that the active device area in planar photovoltaic structure can be defined as the area enclosed between the two electrodes. The first approach is based on the comparison between the I_{sc} and PCE values deduced from top light shining on the active material and the back light shining. The second approach is about investigating the effect of the electric field parasitic paths and the shinned areas that lie outside the channel on the final PCE value. Based on the results of those two approaches we propose that the illuminated area in the planar photovoltaic device is the area enclosed between the two electrodes.

6.2 Electrodes patterning and device fabrication

In the first approach, we fabricated P-OPV with (Au, Cr) or (Au, Ti) electrodes as described in Ch.3. The difference here is that the electrodes were fabricated on top of SiO_2 (100 nm) /ITO (150 nm) coated substrate; this allows the light to be shinned from the back. An ITO layer was needed as a conducting layer for electron beam lithography uses. A cartoon of the device design is shown in Figure 6.1. This structure allows us to compare the PCE deduced from top illumination versus the one deduced from bottom illumination through the SiO_2/ITO substrate. Channel length (L) was varied from 0.24 µm to 3 µm and channel width (W) is fixed at 100 µm. In the second approach, we patterned the electrodes in two different comb-like shapes as shown in Figure 6.2 in addition to the original parallel patterned electrodes. The fabrication process is the same as described in Ch.3 on Si/SiO_2 substrates. L was fixed to 0.24 µm and W for the three patterns was kept at 50 µm. The P3HT/PCBM solution of (1:2) ratio was spun coated on top of the fabricated electrodes in both approaches with a thickness of 200 nm. The illumination intensity was 100mW/cm^2 (AM 1.5G). Finally, I-V characteristics were extracted.

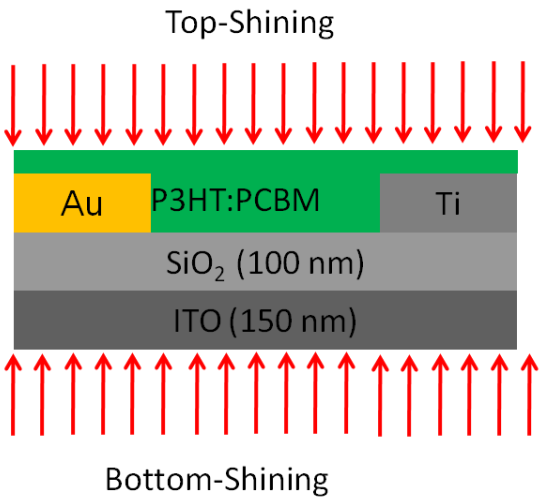

Figure 6.1 Schematic diagram of the bottom light shining experiment set up. Light can be shinned from the top as usual for comparison purpose. Incident light was 100mW/cm^2

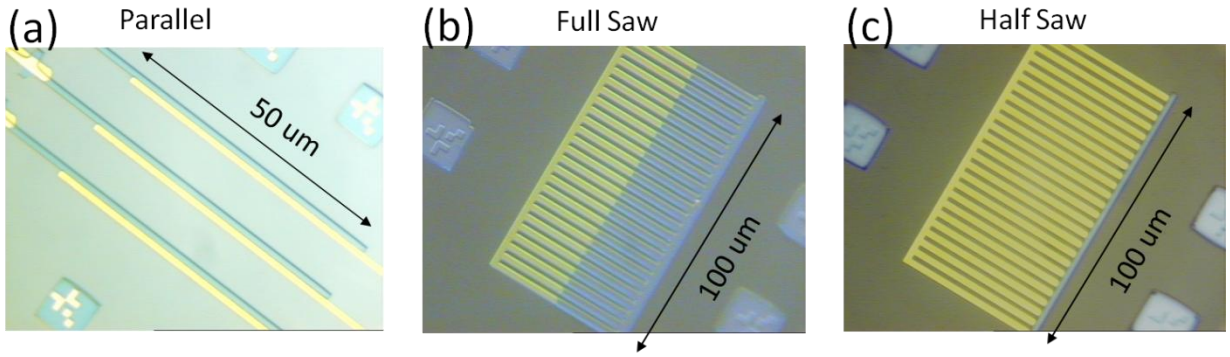

Figure 6.2 Parallel (original) electrodes for P-OPV device. (b) Full comb-shape electrodes for P-OPV device. (c) Half comb-shape electrodes for P-OPV device. Two different colors are for the two different electrodes Au and Cr electrodes. Channel length L=0.24 µm and W=50 µm for the three devices.

6.3 Defining illuminated area by bottom light shining technique

The first approach is based on the comparison between the I_{sc} and PCE values deduced from top light shining on the active material and the back light shining. The top light shining is the usual method used to measure the I-V characteristics of the P-OPV device in this work where the device is directly exposed to the light source. Back light shining is where the light from the

back of the P-OPV device through SiO_2 and ITO layers as in Figure 6.1 above. This way, the light only reaches the active layer area between the electrodes and doesn't reach the active material above the electrodes because the electrodes are blocking it. In the top light shining when the light is shinned, the charges are generated in the channel and on the top of the electrodes and everywhere in the active layer. Those charges can contribute to the current in the channel. On the other hand in the back light shining, the electrodes work as light shields preventing the generation on top of the electrodes to occur. By comparing between the two methods, we test if there is any contribution of the generated charges on top of the electrodes to the channel between the electrodes. We should mention that when investigating I_{sc} and PCE values in the two methods we take into consideration that the light is attenuated in the back light shining due to the non-fully transparent SiO_2 and ITO layers. This was shown by measuring the transparency of the ITO/SiO2 layers by UV-Vis experiment.

6.3.1 P-OPV devices with Au/Cr electrodes

Figure 6.3 (a) shows the schematic of P-OPV device with Au/Cr electrodes on top of ITO/SiO_2 with L=0.24, 0.5, 0.8, 1, and 3 µm. By studying Figure 6.3 (b) that shows the I-V characteristics of the device at different channel lengths for up and bottom light shining, it is obvious that I_{sc} decreased when the light was shinned from the bottom of the device. Figure 3 (c) and (d) displays the values for the PCE and I_{sc} for both methodes with varying the channel length. The highest PCE for this 200nm film thickness was 2.25% for the up light shining, and then it decreased to 1.8% for bottom light shining.

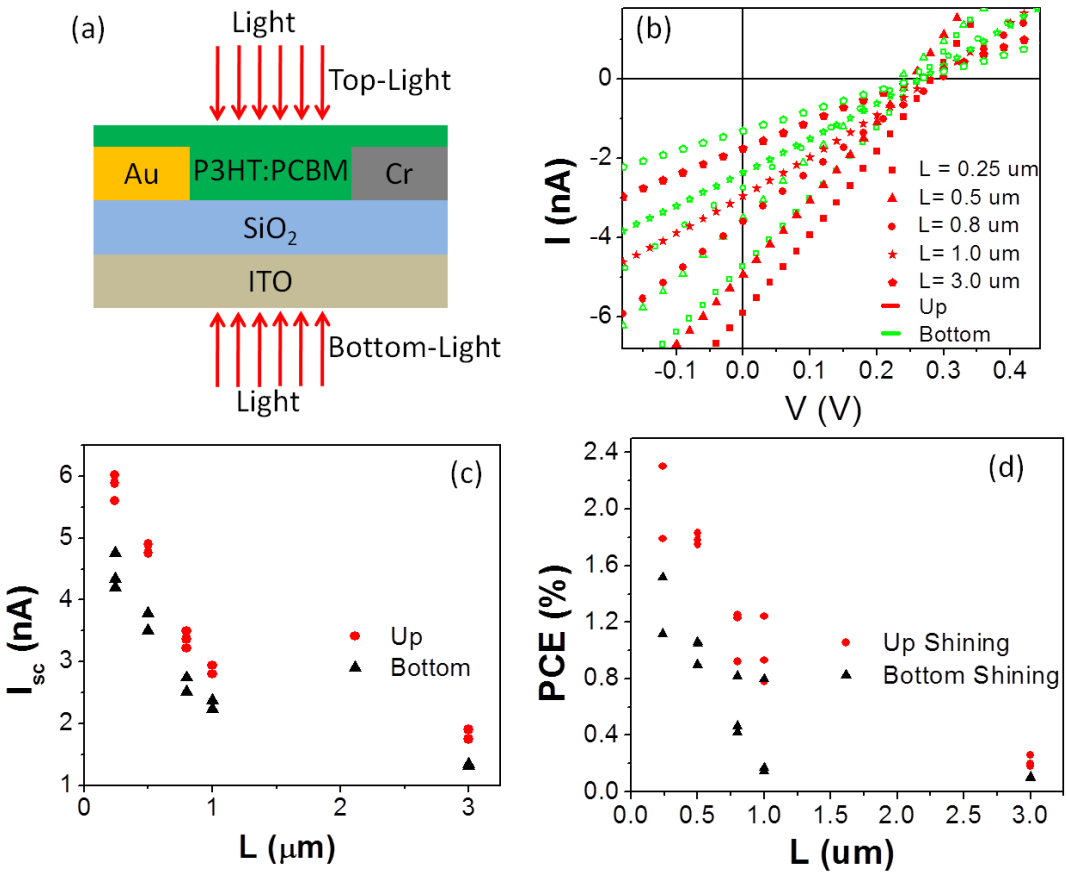

Figure 6.3 (a) schematic of the P-OPV device with Au/P3HT:PCBM(1:2)/Cr structure for the up and bottom light shining experiment. (b) I-V characteristics for up and bottom light shining for five different channel lengths (c) I_{sc} and (d) PCE behavior with varying channel length for up and bottom light shining at 200 nm thickness under 100 mW/cm^2.

I_{sc} was decreased from a maximum value of 6.2 nA to 4.8 nA when the active material was not directly exposed to the light with a reduction of ~ 22%. Basically, PCE and I_{sc} values for all the devices were decreased by ~ 20 to 30% of their original values for all the devices when the measurements were taking by shining the light from the bottom of the device through the ITO and SiO_2 layers. We focus more on the I_{sc} values because of the direct relation with light absorption and charge generation and because PCE values were reduced due to the reduction in the I_{sc} values.

6.3.2 P-OPV devices with Au/Ti electrodes

We have also fabricated P-OPV devices on top of ITO/SiO_2 with Au/Ti electrodes to reproduce the achieved results using Au/Cr electrodes. Figure 6.4 (a) shows the I-V characteristics of devices with L= 0.3 - 3 µm for up and bottom light shining. A reduction in I_{sc} occurred for bottom shining where V_{oc} did not change about 0.4 V. Figure 6.4 (b) and (c) compares the I_{sc} and PCE values between up and bottom measurement for the different channel lengths.

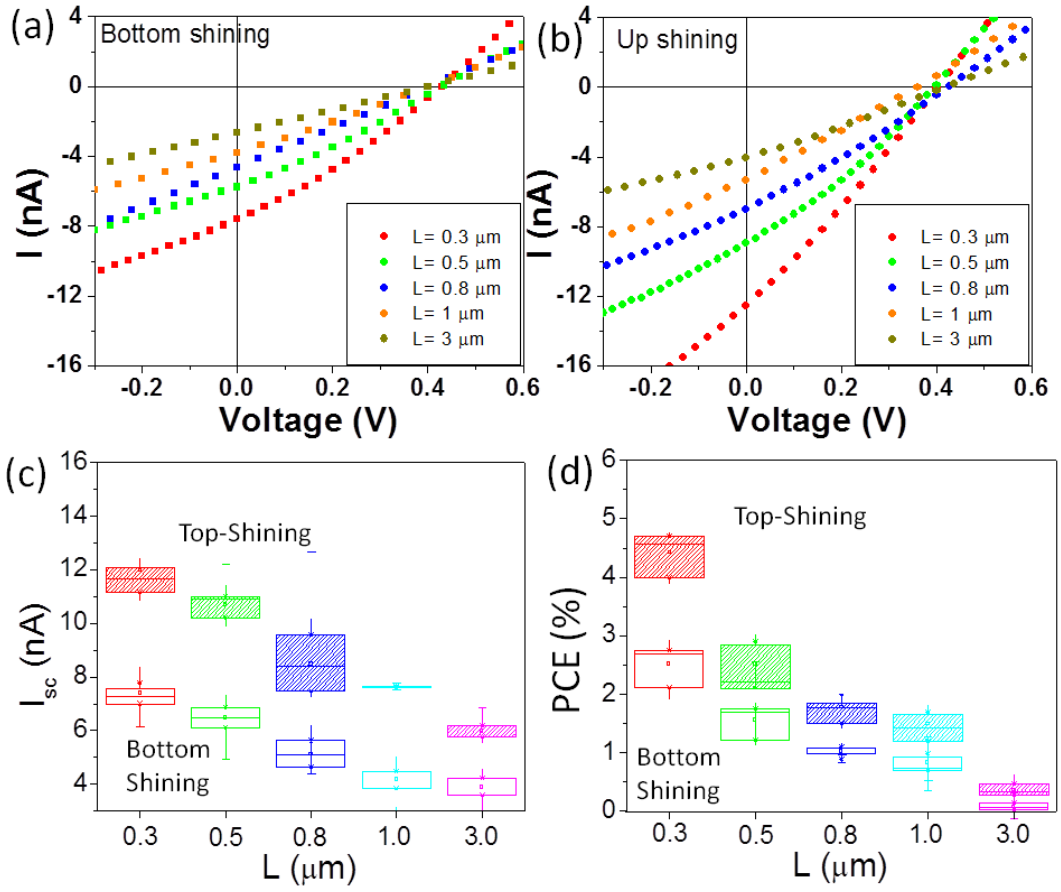

Figure 6.4 (a) I-V characteristics for up and bottom light shining (b) I-V characteristics for top light shining (c) PCE and (d) Isc behavior with varying channel length compared between up and bottom light shining at 200 nm thickness under 100 mW/cm^2 incident light for Au/P3HT:PCBM(1:2)/Ti devices.

A reduction of I_{sc} and PCE values of 30-40% was observed for all the channel lengths when the light was shinned from the bottom through ITO/SiO_2 layers. For L=0.3 μm I_{sc} decreased from 12.7 nA for up light shining to 8 nA for bottom light shining and PCE decreased from 4.7% to 3% accordingly. This reduction in I_{sc} and PCE values proves that part of the energy and photons are lost when shining the light through the bottom of the P-OPV device. We will prove next that part of lost energy is due to the attenuation of the light through the SiO_2 and ITO layer in the bottom light shining case.

6.3.3 Light attenuation effect

We have noticed that I_{sc} and PCE value are higher for top light shining comparing to the bottom light shining where the light travels through SiO_2 and ITO layers before it reaches the active layer. Figure 6.5 proves that ~ 20% of the reduction in the current values which leads to a reduction in the PCE values is due to the light attenuation due to the stacked layers of SiO_2 and ITO when the light is shined from the bottom. The UV-Vis experiment was carried out to extract the transmittance spectra for two samples: ITO 150 nm layer and ITO/SiO_2 150 nm and 100 nm layers, respectively. The transmittance spectra over the wavelengths 300-800 nm show 82% transmittance at wave length 480 nm for ITO/SiO_2 sample. This means about ~ 20% of the light attenuated in ITO/SiO_2 layers. This proves that the 20% of the lost energy that leads to a reduction in the I_{sc} values in the Au/Cr and Au/Ti devices in the bottom light shining is due to the stacked layers of ITO/SiO_2 layers.

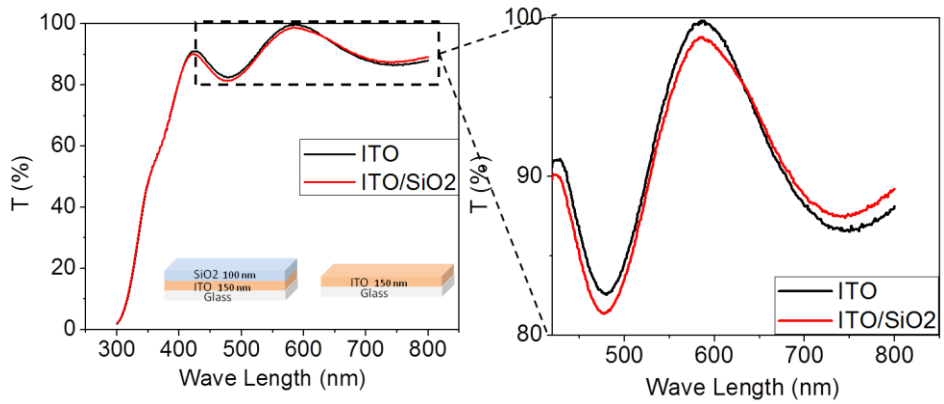

Figure 6.5 UV-Vis transmittance spectra for only 150 nm ITO layer and for ITO (150 nm)/ SiO_2 (100 nm) stacked layers. To the right is zooming in if the area of interest. The insets show the tested samples' schematics.

This study also introduces another advantage of using P-OPV over the current vertical structure. One of the main objectives of establishing ITO free PV devices is to avoid the loss caused by the fact that ITO is not fully transparent which attenuates part of the incident light before reaching the active material. We should mention here that in vertical PV device another layer on top of the ITO is used as an injection layer such as PEDOT:PSS which contributes in attenuating more light resulting in less absorption if we compare it with P-OPV device where the active material is directly exposed to the light. The uses of P-OPV results in more light absorption because the active material is directly exposed to the light source where in vertical PV device photon absorption will never be 100% because the active layer is embedded in a multilayer's structure with different refractive indices [[237]].

In order to confirm that the illuminated area in the P-OPV device is the area enclosed between the two electrodes then the whole amount of lost energy in the bottom light shining ~ 30% should be explained. So far, we explained that 20% of this lost energy is a result of light attenuation. Next we will show that the other 10% of lost energy is due to the fact that the used channel length in the P-OPV device is less than the incident wavelength.

6.3.4 Near field effect

In the fabricated P-OPV device in this work, the channel lengths are about or less than the maximum absorption wavelength of P3HT:PCBM about 500 nm. This increases the chance that the peak of the incident wave length can be absorbed outside the channel where excitons can be generated as a result. Figure 6.6 shows the schematic of the device compared to the incident wavelength.

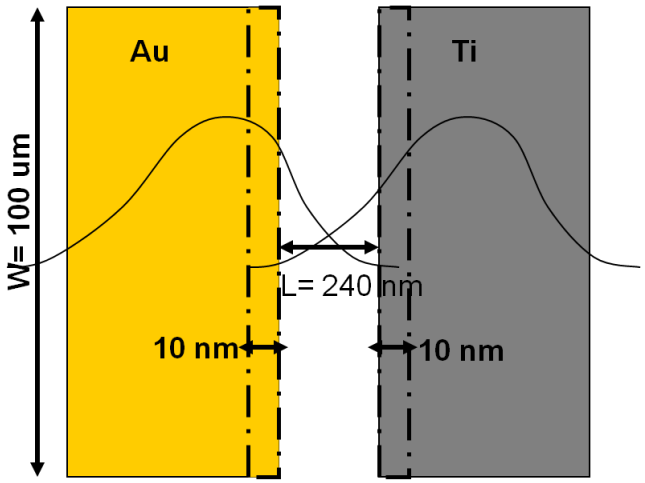

Figure 6.6 schematic of the P-OPV device with a channel length compared to the incident wave length. Dashed area is the area outside the channel that can contribute to the current .

It is known that the exciton diffusion length is about 10 nm, this means that the generated charges within the 10 nm on the surface of each electrode outside the channel can contribute to the current in the channel and to the overall device efficiency which is called the near field effect (see Figure 6.6). In order to take into account for this effect then the illuminated area, when calculating PCE values, should include the area created by this 10 nm from each side which is about $20nm \times 100\mu m = 0.02 \times 10^{-6} cm^2$. This area is about 10% of the area in between the electrodes which is used as the illuminated area when calculating PCE. In our calculation we did not include the outside area which means our values of PCE are overestimated by about 10% in

the up shining. However, in the bottom light shining this outside area has no effect since it is blocked by the electrodes. This means that in addition to the 20% lost by the light attenuation in the back light shining, the other 10% reduction is due to absence of the near field effect in the back light shining. These observations confirm that the illuminated area in the P-OPV device is the area enclosed between the two electrodes in addition to the areas with 10 nm outside the channel.

6.4 The effect of the parasitic paths in planar OPV device using comb shape electrodes

The second approach is about investigating the effect of the electric field parasitic paths and the shinned areas that lie outside the channel on the final PCE value. This was achieved by engineering three electrodes patterns with three different parasitic paths. I-V measurements for three different electrodes patterns result in PCE values falling in the same range. We show that parasitic paths in our electrodes geometry don't contribute to the final OPV device performance. In this section we present photovoltaic behavior measurements of P-OPV devices with 1) full comb-shape 2) half comb shape 3) parallel electrodes. P3HT:PCBM with 1:2 ratio is spun coated with thickness of 200 nm on top of the fabricated Au/Ti electrodes. Figure 6.7 presents the SEM images of the three electrodes patterns. By comparing between the three devices, we introduce different areas outside the channel between the electrodes where the main electric field lines are. If those areas with parasitic electric field lines contribute to the current in the channel then we should see a difference in the current values when extracting the PV behavior for the three devices.

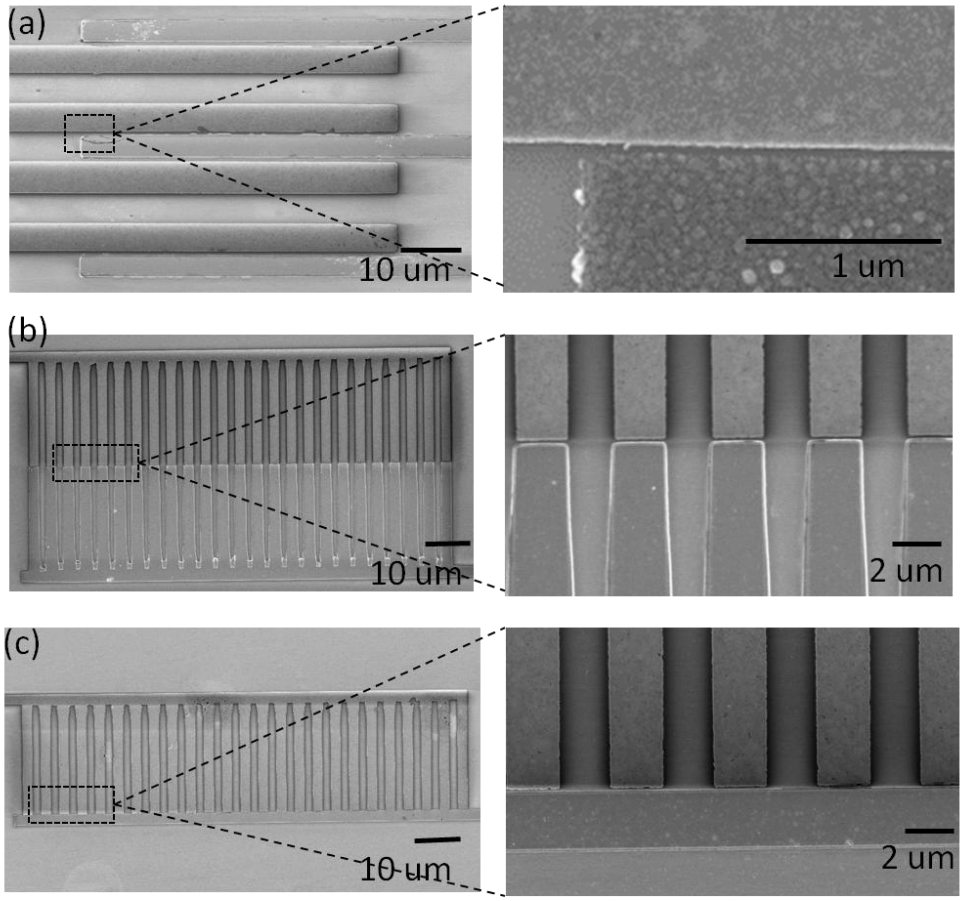

Figure 6.7 SEM images P-OPV devices with the three engineered electrodes: (a) parallel, (b) full comb, and (c) half comb shape. Different contrast colors are the two different electrodes Au and Ti

Figure 6.8 shows the three different electrodes with schematic for each one that shows the three different areas: (1) area in between the electrodes, (2) area outside the device, and (3) area between the same electrode fingers in comb and half comb electrodes. By introducing the area (3) in the full comb shape, we insure that the deep part of the electrode does not contribute in driving the generated charges in this area to the channel in between the electrodes. In addition, in full and half comb electrodes we are introducing more parasitic paths in comparison with the parallel electrodes where the parasitic paths are only at the tips of the electrodes (area (2)). We have measured the PV behavior for the three electrodes to test the effect of these parasitic paths.

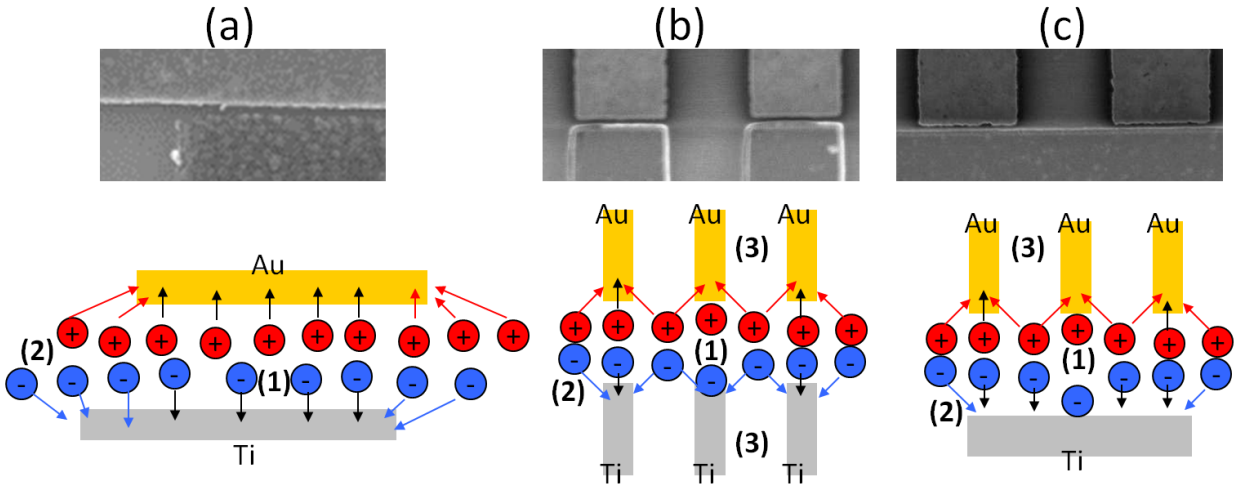

Figure 6.8 P-OPV devices with (a) parallel electrodes (b) full comb electrodes (c) half comb electrodes. Schematic diagrams show the three different areas created in the three designs.

Figure 6.9 presents the extracted I-V plots of the three P-OPV devices measured under 100 mW/cm^2 illumination. We found that I_{sc} values are in the same range averaging around 8 nA for the three patterns indicating a small contribution, not significant, from the parasitic paths. This again supports that the illuminated area in the P-OPV device should be defined as the area enclosed between the electrodes.

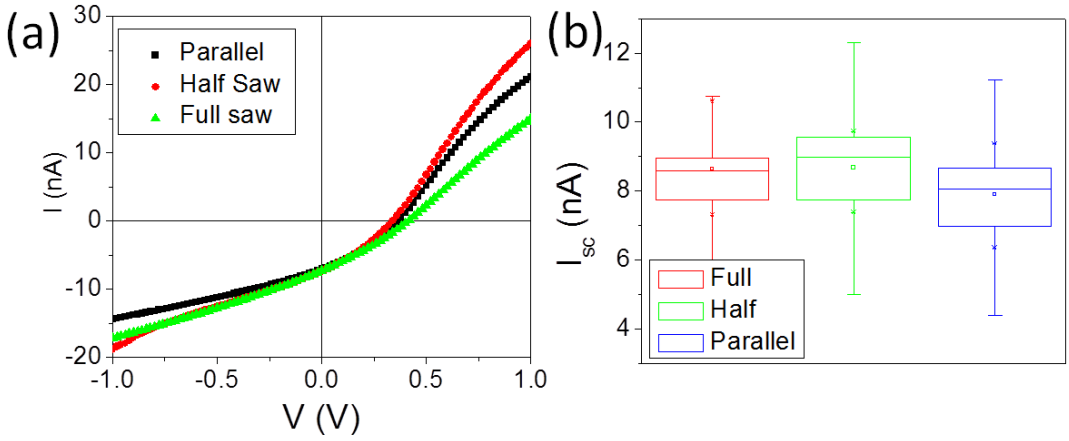

Figure 6.9 (a) I-V characteristics and (b) I_{sc} values of P-OPV devices with the three different electrodes patterns made with Au and Ti electrodes under illumination 100 mW/cm^2. Channel length was 300 nm and channel width 50 µm with P3HT/PCBM thickness= 200 nm.

6.5 Conclusions

In conclusion to this chapter, we have investigated the PV behavior for P-OPV device when the light is shinned directly on the active layer and from the back of the device through SiO_2 and ITO layers to test our proposal of defining the illuminated area to be only the area in between the electrodes. We show that the I_{sc} and PCE values reduced by 20-40% for Au/Cr and Au/Ti devices when the light was shined from the back. We proved that 20% of reduction is due to the attenuation of the light in the ITO/SiO_2 by UV-Vis measurement and 10% is due to the near field effect. In addition, in P-OPV device direct light shining increases the chance for the photons to be absorbed and decreases the energy lose due to the stacking layers as in vertical geometry. We have also shown that the parasitic paths and the areas outside the channel in between the electrodes don't contribute to the extracted PV current. This was shown by introducing different electrodes patterns that introduce more parasitic paths.

CHAPTER 7: PLANAR ORGANIC PHOTOVOLTAIC DEVICE: EFFECT OF P3HT/PCBM RATIO ON DEVICE PERFORMANCE

7.1 Introduction

Despite the potential that planar organic photovoltaic devices (P-OPV) offer, the investigation of planar organic solar cell is still at its infancy. Recent study by Heeger's group showed power conversion efficiency (PCE) of 0.6% on a planar device [[238]]. They used P3HT:PCBM BHJ film with a blending ratio of 1:1 deposited on SiO_2 substrate. In general, to achieve a high PCE, the BHJ active material system need to be blended in such a way that a network of phase separated donor and acceptor domain is created with a size of 20 nm because the exciton diffusion length for P3HT:PCBM is ~10 nm so that a maximum exciton dissociation and charge transport can occur [[239], [240]]. Achieving such phase separated nano-scale morphology depends on several processing factors such as type of solvent [[241], [242]], thermal annealing [[243]], the blending ratio of active material [[244], [245]], and type of substrate [[246]]. The 1:0.8 and 1:1 ratios are known to be optimized blending ratios commonly used for vertical OPV devices on ITO/PEDOT:PSS substrate [[247]] and it is not known whether the same blending ratio is also the optimum for planar structure where the substrate is different (SiO_2) since the effect of the surface energy of the substrate and its surface roughness may have a strong influence on the morphology of P3HT:PCBM [[248]]. In addition, the charge transport in planar structure is fundamentally different than vertical structure due to the anisotropic charge transport of P3HT [[249]].

In this chapter, we investigate the morphology of P3HT:PCBM films with blending ratio of 1:1, 1:2, and 1:3 in a planar OPV structure where SiO_2 was used as a substrate and examine the PCE of the fabricated OPV devices. The absorption measurements show that the films with 1:1 and 1:2 ratios have wider and well structured absorption spectra compared to 1:3 film.

Atomic force microscope (AFM) images of the films show that the surface morphology of 1:2 blend provides well separated P3HT and PCBM domain size of about 20 nm close to the diffusion length of the exciton, whereas for the 1:1 ratio the domain sizes were as large as 300 nm and 1:3 showed amorphous morphology and molecular level dispersion. The PCE value of the measured devices illustrate that the solar cell with 1:2 film shows higher PCE value of ~2% which is almost twice the value for the 1:1 ratio and four times the value for 1:3 ratio. The 1:2 optimized ratio in P-OPV on Si/SiO_2 substrate is different than the vertical OPV (1:0.8 and 1:1) on ITO/PEDOT:PSS substrate and can be explained due to the surface tension differences of the substrates.

7.2 Experimental

The active materials used for fabricating P-OPV devices were made from a blend of P3HT and PCBM. Three different solutions were prepared with P3HT:PCBM weight ratio of 1:1, 1:2, and 1:3 in 1,2 dichlorobenzene solvent. The concentrations were (32 mg/ml) for 1:1 ratio, (48 mg/ml) for 1:2 ratio, and (64 mg/ml) for 1:3 ratio. The solutions were stirred in vials with a magnetic stirrer for 12 hours at 40 ^{o}C for proper mixing of the materials. The solutions were then filtered with a 0.2 µm syringe filter and spun-coated on the bare Si/SiO2 substrates for surface morphology imaging. The surface morphologies of the blended films were examined by tapping mode atomic force microscope (AFM). For the absorption measurement the blended P3HT:PCBM films were spun-coated on top of glass substrate covered by 250 nm SiO_2. Then absorption was measured using UV-Vis 300-Bio spectrometer. All samples undergo a heat treatment of 150 ^{o}C for 10 min. The solution preparation and the film spin coating were executed inside a N_2 glove box.

P-OPV devices were fabricated with metal electrodes: Au as an anode and Cr as cathode. Devices were designed using two steps of electron beam lithography (EBL) described in Chapter 3. The channel length (L) of the P-OPV devices was 0.24 µm and the channel width (W) was 100 µm. The P-OPV devices were characterized by current-voltage (I-V) measurements in dark and under simulated AM 1.5G solar irradiation at 100 mW/cm^2. The I-V characteristics of the devices were measured using Hewlett Packard (HP) 4145 B semiconductor parametric analyzer in an enclosed glove box system with N_2 flow.

7.3 Results and discussions

Figure 7.1 shows the absorption spectra of the 1:1, 1:2, and 1:3 ratio films of the P3HT:PCBM deposited on SiO_2 substrates. Higher absorption in the range of 300 – 500 nm for the 1:2 and 1:3 blending ratios is expected due to the higher amount of PCBM molecules since PCBM contributes to the total photon absorption in that range [[250]]. In the range of 500 – 650 nm, where solar spectrum is more dominant than 300 - 500 nm, both 1:1 and 1:2 ratio films show better absorption profile compared to 1:3 along with several well structured shoulders which is an indication of crystalline P3HT chains. This is different than what has been reported for PEDOT:PSS substrate, where only 1:1 ratio film showed better absorption profile compared to 1:2 and 1:3 ratio film [[251], [252]]. This shows that the absorption profile is strongly influenced by the choice of substrate and that unlike PEDOT:PSS, both 1:1 and 1:2 ratio film can provide good photon absorption on SiO_2 substrate.

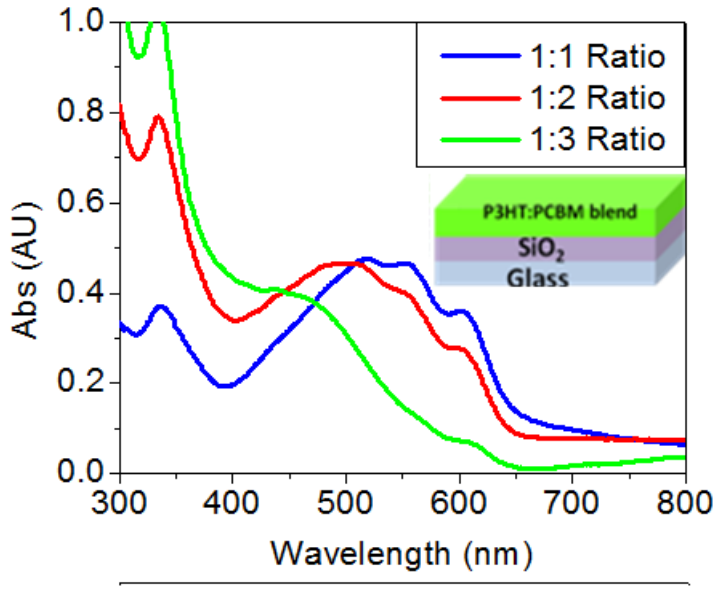

Figure 7.1 UV-Vis absorption spectra for P3HT:PCBM films with blending ratios 1:1 (blue), 1:2 (red), and 1:3 (green). The inset shows a schematic diagram of the SiO2 substrate and the P3HT:PCBM films for absorption measurement.

In order to understand the effects of SiO_2 substrate on active layer morphology, films of 1:1, 1:2, and 1:3 (P3HT:PCBM) ratios were deposited on SiO_2 and characterized with AFM. A critical indicator for active layer morphology in relation to PV device performance is the phase separation between the acceptor and the donor materials and the associated formation of percolated pathways throughout the active material, which can be observed by use of AFM in phase imaging mode. Figure 7.2 (a), (b), and (c) show the phase images for 1:1, 1:2, and 1:3 ratio respectively. As shown here, the domain size of 1:1 ratio (~300 nm) is significantly larger than that observed for the 1:2 ratio (~ 20 nm) P3HT:PCBM films on SiO_2 substrates. The 1:3 ratio appears to have an amorphous morphology with phase separation on a length scale below 5 nm, potentially indicating a molecular dispersion of P3HT and PCBM. The trend is different from that observed for vertical geometry OPVs, where 1:1 was found to provide the best active layer morphology. Because the exciton diffusion length is much smaller than the domain size in the

case of the 1:1 ratio films deposited on SiO_2 substrates, the generated excitons will mostly recombine before they reach the P3HT:PCBM interface. Thus, this may reduce the charge generation and ultimately decreases the photocurrent in the OPV device. On the other hand, the active layer with 1:2 blending ratio deposited on SiO_2 substrates leads to phase-separation and formation of domains with dimensions close to the exciton diffusion length (~20 nm). This active layer composition generates well developed networks with connected percolated paths for each phase separated component (P3HT and PCBM) is expected to result in higher short circuit current [253].

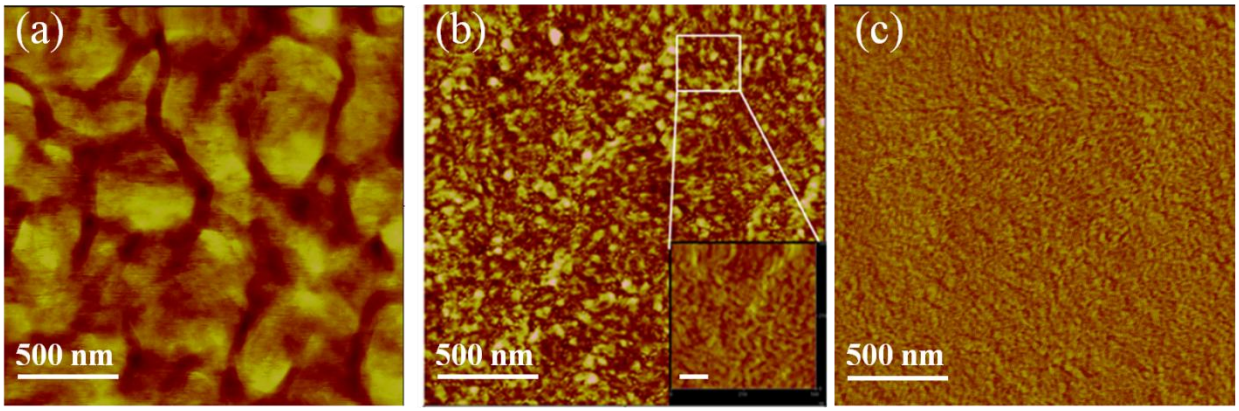

Figure 7.2 AFM phase images for P3HT:PCBM with (a) 1:1 blending ratio (b) 1:2 blending ratio and (c) 1:3 blending ratio. Inset (b) shows magnified phase image of 1:2 ratio, the scale bar in the inset is 100 nm

The P3HT self-organization crystals in of P3HT:PCBM blended films have been assigned in other reported studies as a cause to the surface roughness [254]. The AFM topography images of the films with 1:1, 1:2, and 1:3 blending ratio are illustrated in Figure 7.3 (a), (b), and (c) with the line profiles for each film illustrating changes in the surface roughness between the films shown in Figure 7.3 (d), (e), and (f). The average rms roughness for 1:1 blended films is about 5.27 nm, while for the 1:2 ratio it is about 2.26 nm and it is 1.1 nm for 1:3 ratio. Here, we

observe that by increasing the amount of PCBM in the active layer in the case of 1:2 and 1:3 ratios the film surface becomes smoother. By the addition of PCBM, the P3HT crystals are likely disturbed leading to small grains dispersion of PCBM in P3HT chains and reduction in the P3HT crystals size which is clearly seen in the phase images. Thus, AFM data shows 1:2 blended active layer on the SiO_2 substrate provides nanoscale morphology which makes it the optimum ratio on SiO_2 substrate, which strongly resembles the morphology of the optimal morphology for vertical geometry OPVs.

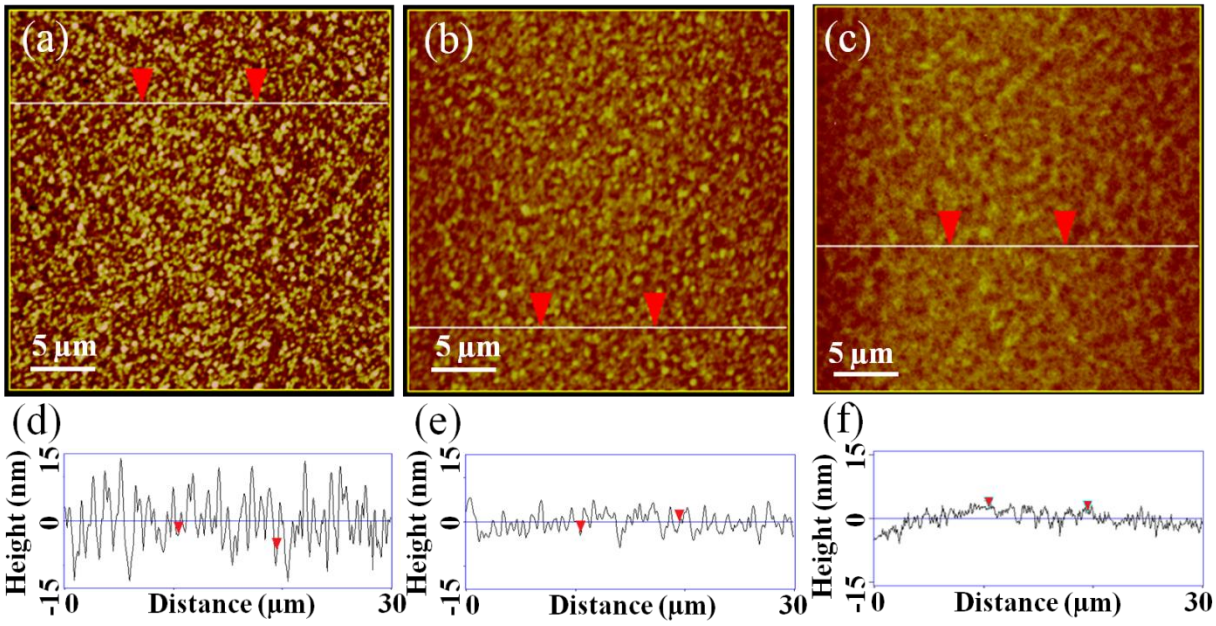

Figure 7.3 AFM height profile images for P3HT:PCBM with (a) 1:1 blending ratio (b) 1:2 blending ratio and (c) 1:3 ratio. And AFM line scans showing the change in the surface roughness for (d) 1:1 blending ratio (e) 1:2 blending ratio and for (f) 1:3 blending ratio.

The main reason that 1:2 ratio provides better morphology in planar structure and not 1:1 ratio as in the vertical structure can be attributed to the different substrate used in the planar structure (SiO_2) in comparison with substrate used in the vertical structure (PEDOT:PSS). It is known that the surface energy for SiO_2 (77.4 mN/m) is higher than the surface energy of PEDOT:PSS (45.7 mN/m) [255]. Because the SiO_2 substrate has higher surface energy than

PEDOT:PSS, more PCBM (surface energy 37.8 mN/m) molecules adsorb to reduce the free energy of the SiO_2 surface [256, 257]. This leaves the P3HT:PCBM blended active layers in planar devices with less PCBM molecules in the bulk of the film in comparison with the corresponding active layer in the vertical device structure on PEDOT:PSS [258].

In order to further investigate the effect of P3HT:PCBM blending ratio using SiO_2 substrate, we measured the photovoltaic behavior for three P-OPV devices with three different ratios. Figure 7.4 (a) shows a schematic diagram of the P-OPV device structure where the dissimilar electrodes Au and Cr are in-plane with P3HT:PCBM deposited in between. Active layers consisting of 1:1, 1:2, and 1:3 P3HT:PCBM blends were deposited with thickness of 200 nm on these planar devices. Figure 7.4 (b) presents the I-V characteristics of the P-OPV devices in dark and under 100 mW/cm^2 illumination. All devices show the same open circuit voltage V_{oc} ~ 0.26 V. For classical thin film PV devices, V_{oc} is determined by the energy gap between the HOMO of the donor and the LUMO of the acceptor in the active material as well as the difference in work functions between the electrodes [259, 260]. The energy gap is about 0.7 V for P3HT:PCBM while the work function difference between Au and Cr is ~ 0.6 eV. However, our reported V_{oc} value ~ 0.26 V is substantially lower than these values. The fill factor (FF) remained consistent at ~0.27 for the active layer compositions studied herein. These values are again lower than those typical reported value for vertical OPV devices between 0.48-0.69 [261]. For vertical PV devices low V_{oc} and FF have been reported as a result of the absence of injection layers at the electrode [262, 263, 264]. The main function of injection layers such as PEDOT:PSS or metal oxides is to decreases the injection barrier for the carriers at the electrode interface which leads to low series resistance (R_s). In the planar device geometry reported in this paper, these injection layers are not present. Thus the low V_{oc} and FF observed for our planar devices can be attributed to

higher injection barriers due to the absence of injection layers, resulting in higher series resistance evident from the I-V curve. R_s was found to be ~ $34x10^6$ Ω for 1:1 ratio, and $62x10^6$ Ω and $170x10^6$ Ω for 1:2 and 1:3 ratio, respectively. R_s values for the three planar devices are falling in the same order of magnitude, and are higher than reported value for vertical structure less than 100 Ω [265, 266]. Furthermore, a large interfacial barrier that lowers V_{oc} and FF can be attributed to the low resistance of Chromium to corrosion. A layer of Chromium oxide is most likely created at the Cr/active-material interface, which introduces an injection barrier for the electrons leads to lowering V_{oc} and FF values.

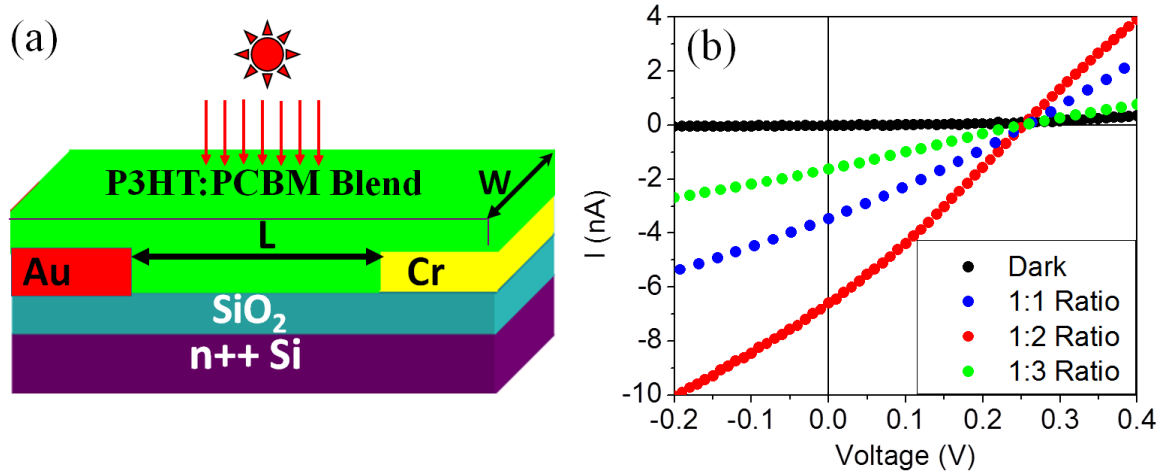

Figure 7.4 (a) The schematic diagram of the PV device structure using two different electrodes Au and Cr with a separation in between L=240 nm and W=100 µm. (b) I-V characteristics under dark and under 100 mW/cm^2 illumination condition for 1:1, 1:2, and 1:3 P3HT:PCBM blending ratios.

The most important observation in Figure 7.4 (b) is that the short circuit current (I_{sc}) was 3.5 nA, 6.6 nA, and 1.6 nA for P3HT:PCBM active layers with 1:1, 1:2, and 1:3 blending ratios, respectively. This leads to PCE values of 1.01 % for 1:1 ratio, 1.95 % for 1:2 ratio, and 0.44% for 1:3 ratio. These PCE values were calculated using standard equation 2.5. The PCE data

indicate that the 1:2 blending ratio affords the most efficient devices different from the finding made for vertical geometry OPVs where 1:0.8 and 1:1 blending ratios are considered optimum. For the 1:3 blending ratio, presumably an excess of PCBM molecules adsorbed on the SiO_2 surface creates a blocking layer at the hole-extraction electrode, which leads to the observed poor device performance. In addition, previously reported studies have shown that the large number of PCBM molecules in the active material for 1:3 ratio can create a mechanical stress break in the active material and poor PV device performance as a result [267]. Thus, because of the surface energy of the SiO_2 substrate the planar devices show optimum efficiency for the 1:2 blended active layer, as discussed above, which is different from the vertical PV structure.

The observed P-OPV device characteristics, the morphology and absorption properties of the active layers investigated here give a clear indication of the effect of the SiO_2 substrate on the active layer morphology and function of planar OPV devices built on this substrate. Different from vertical geometry OPVs on PEDOT:PSS, a 1:2 P3HT:PCBM is optimal for planar geometry devices. In this study, it has been shown that due to the different surface energy of SiO_2 substrate compared to PEDOT:PSS optimal active layer morphology is achieved for the 1:2 blended active layer, which exhibits phase separation with domains on the order of ~20nm. It should be also considered that the observation of high I_{sc} in 1:2 ratio film may be the result of higher electron mobility. For P3HT:PCBM field effect transistors with 1:2 blended active layers, it has been reported that the increase of PCBM blending compared to 1:1 films can result in more possible electron percolating pathways. In addition, hole mobilities in both 1:1 and 1:2 films showed almost constant values, and more balanced electron-hole mobilities in the 1:2 blended films [268]. The more balanced mobilities can provide improved I_{sc} and PV device performance

[269]. Therefore, we consider the better charge transport and the balanced mobilities of 1:2 ratio as another reason for this ratio to be optimal for the P-OPV devices.

7.4 Conclusion

In summary, we investigated the morphology of P3HT:PCBM with blending ratio of 1:1, 1:2, and 1:3 in a planar OPV structure where SiO_2 was used as a substrate and examine the PCE of the fabricated OPV devices. Both 1:2 and 1:1 ratio films show well structured absorption bands implying that both ratios can provide an optimum absorption in the OPV device. However, the morphology study using AFM shows that 1:2 ratio provides well developed P3HT-PCBM networks with a domain size of ~20 nm which led to a better absorption, charge transportation, and enhanced PV behaviors. As a result, a PCE of ~2% was exhibited by the device with blending ratio 1:2 higher than the values shown by devices with 1:1 and 1:3 ratios. These observations are discussed in relation to surface energies of substrates used for the fabrication of planar and vertical geometry devices. This study, in combination with further optimization of planar device geometry, may provide promising paths to achieve high efficiency OPV devices.

CHAPTER 8: CONCLUSIONS AND FUTURE DIRECTIONS

8.1 Summary

In this thesis, planar organic photovoltaic (P-OPV) device structure was utilized to address some of the issues that can help understand the OPV device operation improve the device performance. Chapters 1-3 provided a scope of history for the photovoltaic in general and organic photovoltaic in specific. In addition to the evolution of the PV field, the basic concepts of the PV device operation was discussed in addition to the different device architectures. We also discussed in details the experimental techniques and the device fabrication process that were followed in this work.

In chapter 4, we have studied organic field effect transistors (OFETs) using pristine (P3HT) and (PCBM) and a 1:2 ratio blend of both materials from different metal contacts. This study was established because of the need to properly choose contact metals to design P-OPV devices. We have studied the influence of injection barrier on the performance of the devices. All the resulting devices with different metal electrodes exhibit electron mobilities in the range of $8x10^{-3}$ to $6x10^{-4}$ cm^2/Vs and hole mobilities of $1x10^{-3}$ to $3.3x10^{-4}$ cm^2/Vs. This makes these metals possible candidates to be used as electrodes in a P-OPV because they show balanced hole and electron mobilities. However, Au has shown high on current and hole mobility in the p-channel which makes it a good candidate for an anode in the P-OPV device. On the other hand, In, Cr, and Ti have shown reasonable electron mobility values which make them suitable materials as cathode in the P-OPV device. Furthermore, Al, Mg, Ag have shown a threshold voltage which is probably due to the rapid oxidation of these materials making them undesired materials for P-OPV devices.

In chapter 5, after measuring the fabricated P-OPV device with different cathodes we have found that the characteristic parameters varies with varying the cathode material and for some such as Al, Ag, and Mg no PV behavior was observed. On the other hand, the P-OPV devices with Au/In, Au/Cr, and Au/Ti electrodes combinations show PV behavior. For Au/Cr and Au/Ti combinations we have studied the effect of independently vary the active layer thickness and the electrodes separation. Our results showed that by increasing the thickness up to 200 nm PCE values increase up to 2.25% and 4.75% for Au/Cr and Au/Ti P-OPV devices, respectively as a result of affecting the absorption path. Also, decreasing the channel length increases the PCE as a result of affecting the charge transportation and recombination in the device.

The study in chapter 6 was established because of the need to define the illuminated area when calculating the efficiency in P-OPV device. Two approaches were followed: i) comparing between up and bottom light shining, and ii) different electrodes patterns with different electric field parasitic paths. Results have proved that the illuminated area in the P-OPV device is the area enclosed between the two electrodes. We have also observed the near field effect where the areas outside the channel region can contribute to the created current in this region by ~ 10%.

In chapter 7, we studied the effect of P3HT/PCBM ratio on the P-OPV device performance. AFM images along with I-V measurement have shown that P3HT/PCBM active layer with 1:2 ratio provides the optimum device performance.

8.2 Future directions

Since the P-OPV device still in its infancy, more device controlling and parameters optimization is required in addition to what we have studied and presented in this work. More device improvement and physical insight can take the planar device structure to the level where it competes with the current vertical structure.

8.2.1 Organic photovoltaic devices with different metal electrodes

The described work in this thesis has discussed the photovoltaic behavior using Au/In, Au/Cr and Au/Ti as electrodes in the planar device structure. Next step in this path is to fabricate P-OPV device with other anode/cathode electrodes combinations such as Pd/Ti and Pt/Ti. Initial results have been extracted for the P-OPV device with Pd/Ti. Figure 8.1 (a) shows I-V characteristics for Pd/Ti with L= 0.25 μm and film thickness= 200 nm. Measurement was done under 100 mW/cm^2. A good PV behavior is observed with V_{oc}=0.45 V and I_{sc} of 11 nA. The calculated PCE value for this device was 3.5%. V_{oc} value of 0.45 V is higher than for Au/Ti P-OPV device; however, the overall PCE is less due to the lower I_{sc} value for Pd/Ti P-OPV device. Figure 8.1 (b) shows the PCE values for different channel length for the P-OPV device with Pd/Ti electrodes. As we can see the same behavior exhibited in the previous studied P-OPV device is exhibited here where PCE value increases with decreasing the channel length. For this study more device have to be tested and various electrodes combination.

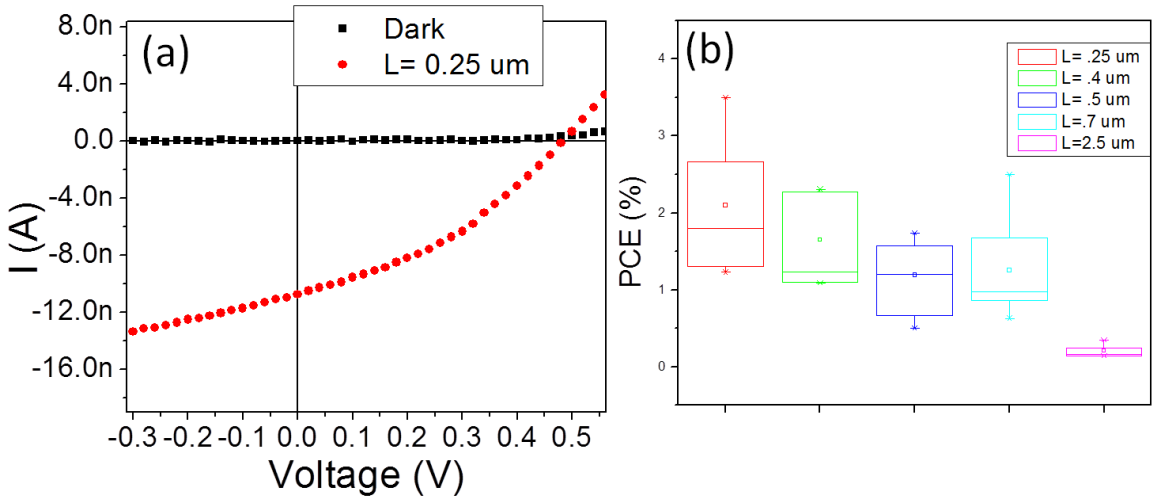

Figure 8.1 (a) I-V characteristics for Pd/P3HT:PCBM/Ti P-OPV device with film thickness=200 nm and channel length 0.25 µm under 100 mW/cm^2. (b) PCE values for various channel lengths for the same device structure.

8.2.2 Multi hole-collector electrodes

For a good OPV device performance, the generated charges in the device must be quickly harvested after dissociation process which depends on the mobility of those charges. It has been reported that the hole mobility is usually lower than the electron mobility in a PV device which can decrease the rate of the harvested charges at the electrodes i.e the current. Using the P-OPV device structure, we can enhance the hole collection at the electrodes by introducing more anode electrodes (where holes are collected) than the cathode electrodes. Figure 8.2 shows the optical images of the fabricated P-OPV devices with three different hole-collector to electron-collector electrodes ratio: i) one hole-collector to one electron collector, ii) two hole-collector to one electron collector, and iii) four hole-collector to two electron collector. By introducing more electrodes to the device we add more illuminated area. In order to keep the illuminated area the same as in the parallel design "one to one" in Figure 8.2 (a), we reduced the channel width to the

half in the “two to one” device in Figure 8.2 (b), and to the quarter in the “four to three” device in Figure 8.2 (c).

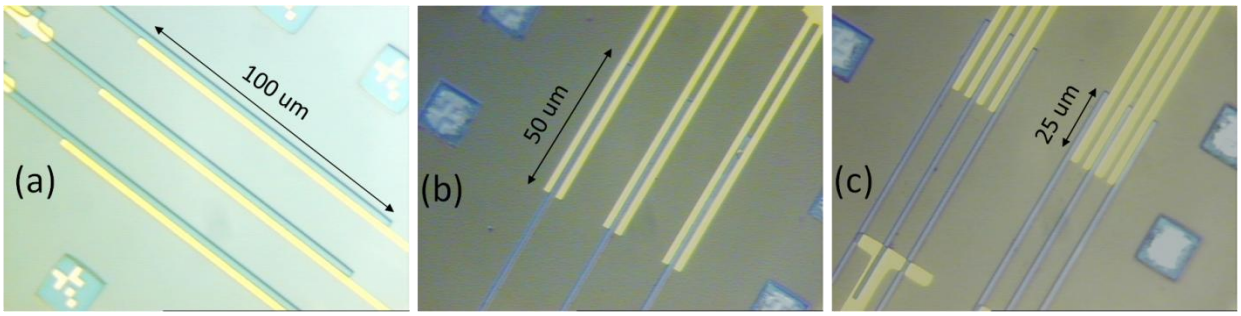

Figure 8.2 P-OPV device with Au/Ti electrodes in three different hole-collector (anode) to electron collector (cathode) electrodes ratio: (a) regular device 1:1, (b) 2:1, and (c) 4:3. Different colors are for different metals Au and Ti.

The I-V measurement for these devices made with Au and Ti were carried out for two devices of each after spin coating the P3HT:PCBM with 1:2 ratio. Figure 8.3 shows I-V curves under dark and under 100 mW/cm^2 illumination.

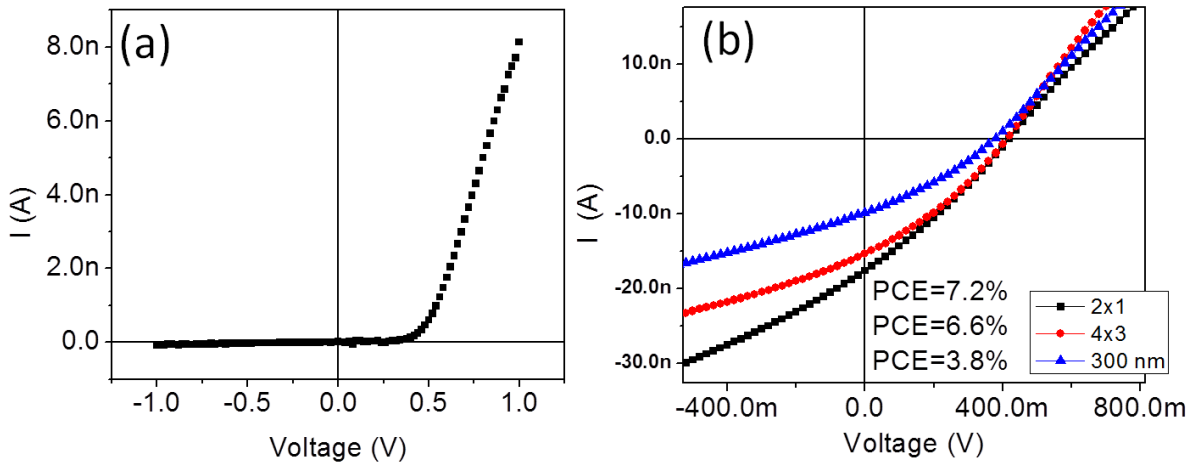

Figure 8.3 (a) Dark current, and (b) I-V curves for the three P-OPV devices with three different hole-collector to electron collector electrodes ratios. Device structure was Au/ P3HT:PCBM (1:2)/Ti with active layer thickness of 200 nm and channel length 300 nm.

All devices exhibited the same V_{oc} value about 0.4 V while I_{SC} values were 10, 15, and 18 nA leading to overall PCE values of 3.8%, 6.6%, and 7.2% for 1:1, 4:3, and 2:1 anode to cathode number of electrodes ratio, respectively. Results clearly show higher current and efficiency for the devices with higher hole-collector ratio. However, in order to test if these higher values are due to higher hole-collector ratio or because the inter-digetated design, more experiments are needed for more devices and with different designs such as having more electron collector than hole collector and compare with existing results.

REFERENCES

[1] E. Lorenzo, *Solar Electricity: Eng. Of Photovoltaic System.* (Progensa, 1994)

[2] D. Anderson, *Clean Electricity from Photovoltaics.* (London Imperial College Press, 2011)

[3] Green, M. A., Emery, K., Hishikawa, Y., & Warta, W. (2010). Solar cell efficiency tables (version 36). *Progress in Photovoltaics: Research and Applications*, *18*, 346-352.

[4] Green M.A., Emery K., King D. L., Igari S., and Warta W., Prog. Photovolt: Res. Appl. 2001, 9, 287.

[5] Kalowekamo, J., Baker, E., Estimating the manufacturing cost of purely organic solar cells, Sol. Energy (2009), doi:10.1016/j.solener.2009.02.003

[6] A. Slaoui, R.T. Collins, Advanced inorganic materials for photovoltaics, MRS Bull. 32 (2007) 211–218.

[7] F.C. Krebs, J. Fyenbo, M. Jorgensen, Product integration of compact roll-to-roll processed polymer solar cell modules: methods and manufacture using flexographic printing, slot-die coating and rotary screen printing, J. Mater. Chem. 20 (2010) 8994–9001.

[8] Minnaert B, Burgelman M (2007) Efficiency potential of organic bulk heterojunction solar cells. Prog Photovolt Res App 15:741–748

[9] Dennler G, Scharber MC, Brabec CJ (2009) Polymer-fullerene bulk heterojunction solar cells. Adv Mater 21:1323–1338

[10] Servaites JD, Yeganeh S, Marks TJ et al (2010) Efficiency enhancement in organic photovoltaic cells: consequences of optimizing series resistance. Adv Func Mat 20:97–104

[11] http://en.wikipedia.org/wiki/Solar_cell_efficiency

[12] Ma WL, Yang CY, Gong X et al (2005) Thermally stable, efficient polymer solar cells with nanoscale control of the interpenetrating network morphology. Adv Func Mat 15:1617–1622

[13] Wang X, Liu D, Li J (2010) Organic photovoltaic materials and thin film solar cells. Front Chem China 5:45–60

[14] Huynh WU, Dittmer JJ, Alivisatos AP (2002) Hybrid nanorod polymer solar cells. Science 295:2425–2427

[15] Coakley KM, McGehee MD (2003) Photovoltaic cells made from conjugated polymers infiltrated into mesaporous Titania. Appl Phys Lett 83:3380–3383

[16] Wienk MM, Turbiez MGR, Struijk MK et al (2006) Low-band gap poly(di-2 thienylthienopyrazine):fullerene solar cells. Appl Phys Lett 88:153511–153514

[17] Hou J, Chen HY, Zhang S et al (2008) Synthesis, characterization, and photovoltaic properties of a low band gap polymer based on silole-containing polythiophenes and 2, 1, 3- benzothiadiazole. J Am Chem Soc 130:16144–16145

[18] Koetse MM, Sweelsson J, Hoekerd KT et al (2006) Efficient polymer:polymer bulk heterojunction solar cells. Appl Phys Lett 88:083504–083507

[19] Tada K, Hirohata, Hosada M et al (1997) Donor polymer (PAT6)—acceptor polymer (CNPPV) fractal network photocells. Synth Met 85:1305–1306

[20] Liao H, Chen LM, Xu Z et al (2008) Highly efficient inverted polymer solar cell by low temperature annealing of CS2CO3 interlayer. Appl Phys Lett 92:173303–173306

[21] Kim, J.Y.;et.al. Science. 317, 222 – 225.2007.

[22] Kim JY, Lee K, Coates NE et al (2007) Efficient tandem polymer solar cells fabricated by all-solution processing. Science 317:222–225

[23] H. Hoppe, N. Arnold, N.S. Sariciftci, D. Meissner, Sol. Energy Mater. Sol. Cells **80**, 105 (2003).

[24] M. M. Mandoc, L. J. A. Koster, and P. W. M. Blom, Appl. Phys. Lett. **90**, 133504 (2007).

[25] C. Deibel, A. Wagenpfahl, and V. Dyakonov, phys. stat. sol. (RRL) **2**, 175 (2008).

[26] A. J. Moule, J. B. Bonekamp, and K. Meerholz, J. Appl. Phys. **100**, 094503 (2006).

[27] I. Riedel, and V. Dyakonov, phys. stat. sol. A 201, **1332** (2004).

[28] Douglas W. Sievers, Vishal Shrotriya, and Yang Yang, J. Appl. Phys. 100, 114509 (2006)

[29] http://en.wikipedia.org/wiki/Electrical_resistivity_and_conductivity

[30] R. Koeppe, D. Hoeglinger, P.A. Troshin, R.N. Lyubovskaya, V.F. Razumov, N.S. Sariciftci, Organic solar cells with semitransparent metal back contacts for power window applications, ChemSusChem 2 (2009) 309–313.

[31] Y. Galagan, J.-E.J.M. Rubingh, R. Andriessen, C.-C. Fan, P.W.M. Blom, S.C. Veenstra, J.M. Kroon, ITO-free flexible organic solar cells with printed current collecting grids, Solar Energy Materials and Solar Cells 95 (2011) 1339–1343

[32] M. Al-Ibrahim, S. Sensfuss, J. Uziel, G. Ecke, O. Ambacher, Comparison of normal and inverse poly(3-hexylthiophene)/fullerene solar cell architectures, Solar Energy Materials and Solar Cells 85 (2005) 277–283

[33] J. Meiss, M.K. Riede, K. Leo, Towards efficient tin-doped indium oxide (ITO)- free inverted organic solar cells using metal cathodes, Applied Physics Letters 94 (2009) 013303

[34] J.-Y. Lee, S.T. Connor, Y. Cui, P. Peumans, Solution-processed metal nanowire mesh transparent electrodes, Nano Letters 8 (2008) 689–692

[35] W. Gaynor, J.-Y. Lee, P. Peumans, Fully solution-processed inverted polymer solar cells with laminated nanowire electrodes, ACS Nano 4 (2010) 30–34

[36] G. Dennler, M. C. Scharber, and C. J. Brabec, Adv. Mater. **21**, 1323 (2009).

[37] R.A. Street, S. Cowan, A.J. Heeger, Experimental test for geminate recombination applied to organic solar cells, Physical Review B 82 (2010) 121301.

[38] C. Lombardo, A. Dodabalapur, Nongeminate carrier recombination rates in organic solar cells, Applied Physics Letters 97 (2010) 233302–233303.

[39] Z.-E. Ooi, R. Jin, J. Huang, Y. F. Loo, A. Sellinger, and J. C. deMello, J. Mater. Chem. 18, 1644 (2008).

[40] M. Campoy-Quiles, T. Ferenczi, T. Agostinelli, P. G. Etchegoin, Y. Kim, T. D. Anthopoulos, P. N. Stavrinou, D. D. C. Bradley, and J. Nelson, Nat. Mater. 7, 158 (2008).

[41] Z. Xu, L.-M. Chen, G. Yang, C.-H. Huang, J. Hou, Y. Wu, G. Li, C.-S. Hsu, and Y. Yang, Adv. Funct. Mater. 19, 1227 (2009).

[42] Mauro Morana, Peter Koers, Christoph Waldauf, Markus Koppe, David Muehlbacher, Patrik Denk, Markus Scharber, David Waller, and Christoph Brabec, *Adv. Funct. Mater.* **2007**, *17*, 3274–3283

[43] Y. Kim et al., Nat. Mater. 5, 197 (2006).

[44] C-W. Chu, C.-W. Chen, S.-H. Li, E. H.-En Wu, and Y. Yang, Appl. Phys. Lett. **86**, 253503 _2005_.

[45] J. Zaumseil, R. H. Friend, and H. Sirringhaus, Nat. Mater. **5**, 69 _2006_.

[46] H. Kim, J. Y. Kim, S. H. Park, K. Lee, Y. Jin, J. Kim, and H. Suh, Appl. Phys. Lett. **86**, 183502 _2005_.

[47] S. Cho, J. Yuen, J. Y. Kim, K. Lee, and A. J. Heeger, Appl. Phys. Lett **90**, 063511 (2007)

[48] J. Gao, J. Hui, Y. Hou, and S. Alem, J. Appl. Phys. **104**, 084512 (2008)

[49] Heremans P, Cheyns D, Rand BP (2009) Strategies for increasing the efficiency of heterojunction organic solar cells: material selection and device architecture. Acc Chem Res 42:1740–1747

[50] P. Peumans et al., J. Mater. Res. 19, 7 (2004)

[51] P. E. Shaw, A. Ruseckas, and I. D. W. Samuel, Adv. Mater. **20**, 3516 (2008).

[52] C. Deibel1 and V. Dyakonov, Rep. Prog. Phys. **73**, 096401 (2010).

[53] Heremans P, Cheyns D, Rand BP (2009) Strategies for increasing the efficiency of heterojunction organic solar cells: material selection and device architecture. Acc Chem Res 42:1740–1747

[54] Koster LJA, Smits ECP, Mihailetchi VD et al (2005) Device model for the operation of polymer/fullerene bulk heterojunction solar cells. Phys Rev B 72:085205–085214

[55] Andre Moliton, and Jean-Michel Nunzi, *Polymer Int.* 55, 583 (2006).

[56] Koster LJA, Mihailetchi VD, Ramaker R et al (2005) Light intensity dependence of open circuit voltage of polymer:fullerene solar cells. Appl Phys Lett 86:123509–123512

[57] Brabec CJ, Cravino A, Meissner D et al (2001) Origin of the open circuit voltage of plastic solar cells. Adv Func Mat 11:374–380

[58] Dutta U, Chatterjee P (2004) The open circuit voltage in amorphous silicon p-i-n solar cells and its relationship to material, device and dark diode parameters. J Appl Phys 96:2261–2272

[59] D. S. Germack, C. K. Chan, B. H. Hamadani, L. J. Richter, D. A. Fischer, D. J. Gundlach, D. M. DeLongchamp, Appl. Phys. Lett. 94, 233303 (2009).

[60] Marks RN, Halls JJM, Bradley DDC et al (1994) The photovoltaic response in poly(pphenylene vinylene) thin film devices. J Phys Condens Matter 6:1379–1394

[61] Cravino A, Schilinsky P, Brabec C (2007) Characterization of organic solar cells: the importance of device layout. Adv Func Mat 17:3906–3910

[62] Mihailetchi VD, Blom PWM, Hummelen JC et al (2003) Cathode dependence of the opencircuit voltage of polymer:fullerene bulk heterojunction solar cells. J Appl Phys 94:6849–6855

[63] Scharber MC, Mühlbacher D, Koppe M et al (2006) Design rules for donors in bulk heterojunction solar cells-towards 10% energy conversion efficiency. Adv Func Mat 18:789–794

[64] Malliaras GG, Salem JR, Brock PJ et al (1998) Photovoltaic measurement of the built-in potential in organic light emitting diodes and photodiodes. J Appl Phys 84:1583–1588

[65] Gregg B (2003) Exitonic solar cells. J Phys Chem B 107:4688–4698

[66] Ramsdale CM, Barker JA, Arias AC et al (2002) The origin of the open circuit voltage in polyfluorene-based photovoltaic devices. J Appl Phys 92:4266–4271

[67] Brabec CJ, Cravino A, Meissner D et al (2001) Origin of the open circuit voltage of plastic solar cells. Adv Func Mat 11:374–380

[68] Gadisa A, Svensson M, Andersson MR et al (2004) Correlation between oxidation potential and open circuit voltage of composite solar cells based on blends of polythiophenes/ fullerene derivative. Appl Phys Lett 84:1609–1612

[69] Frohne H, Shaheen S, Brabec C et al (2002) Influence of anodic work function on the performance of organic solar cells. Chem Phys Chem 3:795–799

[70] Liu J, Shi Y, Yang Y (2001) Solvation induced morphology effects on the performance of polymer-based photovoltaic devices. Adv Func Mat 11:420–424

[71] Koster LJA, Mihailetchi VD, Ramaker R et al (2005) Light intensity dependence of open circuit voltage of polymer:fullerene solar cells. Appl Phys Lett 86:123509–123512

[72] Moule AJ, Bonekamp BJ, Meerholtz K (2006) The effect of active layer thickness and composition on the performance of bulk heterojunction solar cells. J Appl Phys 100:094503–094510

[73] Hoppe H, Sariciftci NS, Meissner D (2003) Modeling the optical absorption within conjugated polymer/fullerene-based bulk-heterojunction organic solar cells. Sol Energy Mater Sol Cells 80:105–113

[74] Soci C, Hwang IW, Moses D et al (2007) Photoconductivity of a low-bandgap conjugated polymer. Adv Func Mat 17:632–636

[75] Nunzi JM (2002) Organic photovoltaic materials and devices. C R Physique 3:523–542

[76] Campos L, Tontcheva A, Günes S et al (2005) Extended photocurrent spectrum of a low band gap polymer in a bulk heterojunction solar cell. Chem Mater 17:4031–4033

[77] Perzon E, Wang X, Admassic S et al (2006) An alternating low band-gap polyfluorene for optoelectronic devices. Polymer 47:4261–4268

[78] Wienk M, Struijk M, Janssen R (2006) Low band gap polymer bulk heterojunction solar cells. Chem Phys Lett 422:488–491

[79] Bundgaard E, Krebs F (2007) Large-area photovoltaics based on low band gap copolymers of thiophene and benzothiadiazole or benzo-bis(thiadiazole). Sol Energy Mater Sol Cells 91:1019–1025

[80] Winder C, Matt G, Hummelen JC et al (2002) Sensitization of low bandgap polymer bulk heterojunction solar cells. Thin Solid Films 403–404:373–379

[81] Gupta D, Mukhopadhyay S, Narayan K S (2010) Fill factors in organic solar cells. solar energy materials and solar cells. 94:1309–1313

[82] S.-S. Li, K.-H. Tu, C.-C. Lin, C.-W. Chen, and M. Chhowalla, ACSNANO **6**, 3169 (2010).

[83] S. Han, W. S. Shin, M. Seo, D. Gupta, S.-J. Moon, and S. Yoo, Organic Electronics **10**, 791 (2009).

[84] F. Liu, S. Shao, X. Guo, Y. Zhao, Z. Xie, Sol. Energy Mater. Sol. Cells **94**, 842 (2010).

[85] Gupta D, Mukhopadhyay S, Narayan K S (2010) Fill factors in organic solar cells. solar energy materials and solar cells. 94:1309–1313

[86] M-Su Kim, B-Gi Kim, Kim J (2009) Effective variables to control the fill factor of organic photovoltaic cells. Appl Mater Interf 1:1264–1269

[87] Hoppe H, Sariciftci NS (2004) Organic solar cells: an overview. J Mater Chem 19:1924–1945

[88] Heeger AJ (2001) Nobel lecture: semiconducting and metallic polymers: the fourth generation of polymeric materials. Rev Mod Phys 73:681–700

[89] Hoppe H, Sariciftci NS (2004) Organic solar cells: an overview. J Mater Chem 19:1924–1945

[90] Borroughes JH, Bradley DDC, Brown AR et al (1990) Light emitting diodes based on conjugated polymers. Nature 347:539–541

[91] Berggren M, Gustafsson G, Ingaenes O et al (1994) Green electroluminescence in Poly-(3-cyclohexylthiophene) light-emitting diodes. Adv Mater 6:488–490

[92] Gadisa A, Person E, Andersson MR et al (2007) Red and near infrared polarized light emissions from polyfluorene copolymer based light emitting diodes. Appl Phys Lett 90:113510–113513

[93] Bao Z, Dodabalapur A, Lovinger A et al (1996) Soluble and processable regioregular poly(3-hexylthiophene) for thin film field-effect transistor applications with high mobility. Appl Phys Lett 69:4108–4111

[94] Sirringhaus H, Tessler N, Friend RH (1998) Integrated optoelectronic devices based on conjugated polymers. Science 280:1741–1744

[95] Neugebauer H, Brabec C, Hummelen JC, Sariciftci NS (2000) Stability and photodegradation mechanisms of conjugated polymer/fullerene plastic solar cells 61:35–42

[96] Kanicki J (1986) Handbook of conducting polymers Marcel Dekker, New York, p 544

[97] Sariciftci NS, Smilowitz L, Heeger AJ et al (1992) Photoinduced electron transfer from a conducting polymer to buckminsterfullerene. Science 258:1474–1476

[98] Smilowitz L, Sariciftctci NS, Wu R et al (1993) Photoexcitation spectroscopy of conducting-polymer–C60 composites: photoinduced electron transfer. Phys Rev B 47:13835–13842

[99] Kraabel B, Hummelen JC, Vacar D et al (1996) Subpicosecond photoinduced electron transfer from conjugated polymers to functionalized fullerenes. J Chem Phys 104:4267–4274

[100] Morita S, Zakhidov AA, Yoshino K (1992) Doping effect of Buckminsterfullerene in conducting polymer: change of absorption spectrum and quenching of luminescene. Solid State Commun 82:249–252

[101] Yoshino K, Yin XH, Morita S et al (1993) Enhanced photoconductivity of C60 doped Poly(3-alkylthiophene). Solid State Commun 85:85–88

[102] Wudl F (1992) The chemical properties of Buckminsterfullerene (C60) and the birth and infancy of fulleroids. Acc Chem Res 25:157–161

[103] Na S, Kim S, Jo J et al (2008) Efficient and flexible ITO free organic solar cells using highly conductive polymer anodes. Adv Mater 20:4061–4067

[104] Zhang F, Johansson M, Andersson MR et al (2002) Polymer photovoltaic cells with conducting polymer anodes. Adv Mater 14:662–665

[105] Hiramoto M, Fujiwara H, Yokoyama M et al (1991) Three-layered organic solar cell with a photoactive interlayer of codeposited pigments. Appl Phys Lett 58:1062–1065

[106] Huang J, Miller PF, Wilson JS et al (2005) Investigation of the effects of doping and postdeposition treatments on the conductivity, morphology, and work function of poly(3, 4-ethylenedioxythiophene)/poly(styrene sulfonate) films. Adv Func Mater 15:290–296

[107] Jong D, Friedlein MP, Osikowicz RW et al (2006) Ultraviolet photoelectron spectroscopy of polymers. Mol Cryst Liq Cryst 455:193–203

[108] Brabec CJ, Shaheen SE, Winder C et al (2002) Effect of LiF/metal electrodes on the performance of plastic solar cells. App Phys Lett 0:1288–1291

[109] Hung LS, Tang CW, Mason NG (1997) Enhanced electron injection in organic electroluminescence devices using an Al/LiF electrode. App Phys Lett 70:152–155

[110] Jabbour GE, Kawahe Y, Shaheen S et al (1997) Highly efficient and bright organic electroluminescent devices with an aluminum cathode. Appl Phys Lett 71:1762–1765

[111] Horowitz G (1990) Organic semiconductors for new electronic devices. Adv Mater 2:287–292

[112] Glenis S, Tourillon G, Garnier F (1984) Electrochemically grown polythiophene and Poly (3-methylthiophene) organic photovoltaic cells. Thin Solid Films 111:93–103

[113] Yu G, Zhang C, Heeger AJ (1994) Dual function semiconducting polymer devices light emitting and photodetecting diodes. Appl Phys Lett 64:154–1540

[114] R. N. Marks et al., J. Phy.: Condens Matter 6, 1379 (1994)

[115] Antoniadis H, Hsieh BR, Abkowitz MA et al (1994) Photovoltaic and photoconductive properties of aluminum/poly(p-phenylene vinylene) interfaces. Synt Metals 62:265–271

[116] Hoppe H, Sariciftci NS (2008) Polymer solar cells. Adv Poly Sci Springer Berlin Heidelberg 1–86

[117] Yamashita Y, Takashima W, Kaneto K (1993) Characteristics of heterojunction diode of C60/tetratiafulvalene (TTF). Jpn J Appl Phys 32:L1017–L1020

[118] Sariciftci NS, Braun D, Zhang C et al (1993) Semiconducting polymer-buckminster fullerene heterojunctions: diodes, photodiodes and photovoltaic cells. Appl Phys Lett 62:585–587

[119] Smilowitz L, Sariciftctci NS, Wu R et al (1993) Photoexcitation spectroscopy of conducting-polymer–C60 composites: photoinduced electron transfer. Phys Rev B 47:13835–13842

[120] Kraabel B, Hummelen JC, Vacar D et al (1996) Subpicosecond photoinduced electron transfer from conjugated polymers to functionalized fullerenes. J Chem Phys 104:4267–4274

[121] Tang CW (1986) Two layer organic photovoltaic cell. App Phys Lett 43:183–186

[122] C.W. Tang: Two-layer organic photovoltaic cell. *Appl. Phys. Lett.* **48,** 183 (1986).

[123] M. Hiramoto, Y. Kishigami, and M. Yokoyama: Doping effect on the two-layer organic solar cell. *Chem. Lett.* **19,** 119 (1990).

[124] J. Rostalski and D. Meissner: Photocurrent spectroscopy for the investigation of charge carrier generation and transport mechanisms in organic p/n-junction solar cells. *Sol. Energy Mater. Sol. Cells* **63,** 37 (2000).

[125] A.J. Breeze, A. Salomon, D.S. Ginley, B.A. Gregg, H. Tillmann, and H-H. Ho¨rhold: Polymer-perylene diimide heterojunction solar cells. *Appl. Phys. Lett.* **81,** 3085 (2002).

[126] J.J.M. Halls, K. Pichler, R.H. Friend, S.C. Moratti, and A.B. Holmes: Exciton diffusion and dissociation in a poly(pphenylenevinylene)/ C60 heterojunction photovoltaic cell. *Appl. Phys. Lett.* **68,** 3120 (1996).

[127] L.S. Roman, W. Mammo, L.A.A. Petterson, M.R. Andersson, and O. Ingana¨s: High quantum efficiency polythiophene/C60 photodiodes. *Adv. Mater.* **10,** 774 (1998).

[128] S.A. Jenekhe and S. Yi: Efficient photovoltaic cells from semiconducting polymer heterojunctions. *Appl. Phys. Lett.* **77,** 2635 (2000).

[129] P. Peumanns and S.R. Forrest: Very-high-efficiency doubleheterostructure copper phthalocyanine/C60 photovoltaic cells. *Appl. Phys. Lett.* **79,** 126 (2001).

[130] P. Peumans and S.R. Forrest: Erratum: Very-high-efficiency double-heterostructure copper phthalocyanine/C60 photovoltaic cells. *Appl. Phys. Lett.* **79,** 126 (2001).

[131] J. Xue, S. Uchida, B.P. Rand, and S.R. Forrest: 4.2% efficient organic photovoltaic cells with low series resistances. *Appl Phys. Lett.* **84,** 3013 (2004).

[132] Brabec CJ, Sariciftci NS, Hummelen JC (2001) Plastic solar cells. Adv Func Mater 11:15–26

[133] Brabec CJ, Sariciftci NS, Hummelen JC (2001) Plastic solar cells. Adv Func Mater 11:15–26

[134] Rep. Prog. Phys. **73** (2010) 096401.

[135] Van Duren JKJ, Yang XN, Loos J et al (2004) Relating the morphology of Poly(pphenylenevinylene)/methanofullerene blends to solar-cell performance. Adv Func Mat 14:425–434

[136] Martens T, Dhaen J, Munters T et al (2003) Disclosure of the nanostructure of MDMOPPV: PCBM bulk hetero-junction organic solar cells by a combination of SPM and TEM).Synth Met 138:243–247

[137] Mihailetchi VD, Blom PWM, Hummelen JC et al (2003) Cathode dependence of the opencircuit voltage of polymer:fullerene bulk heterojunction solar cells. J Appl Phys 94:6849–6855

[138] Brabec CJ, Cravino A, Meissner D et al (2001) Origin of the open circuit voltage of plastic solar cells. Adv Func Mat 11:374–380

[139] Mihailetchi VD, Koster LJA, Blom PWM (2004) Effect of metal electrodes on the performance of polymer:fullerene bulk eterojunction solar cells. Appl Phys Lett 85:970–973

[140] Hoppe H, Niggemann M, Winder C et al (2004) Nanoscale morphology of conjugated polymer/fullerene based bulk heterojunction solar cells. Adv Func Mat 14:1005

[141] Padinger F, Rittberger RS, Sariciftci NS (2003) Effects of post production treatment on plastic solar cells. Adv Func Mat 13:85–88

[142] Schilinsky P, Waldauf C, Brabec CJ (2002) Recombination and loss analysis in polythiophene based bulk heterojunction hotodetectors. Appl Phys Lett 81:3885–3888

[143] Kim JY, Kim SH, Lee HH et al (2006) New architecture for high efficiency polymer photovoltaic cells using solution based titanium xide as an optical spacer. Adv Mat 18:572–576.

[144] F. Padinger, R.S. Rittberger, and N.S. Sariciftci: Effects of postproduction treatment on plastic solar cells. *Adv. Funct. Mater.***13,** 1 (2003).

[145] Jin Young Kim, Kwanghee Lee, Nelson E. Coates, Daniel Moses, Thuc-Quyen Nguyen, Mark Dante, and Alan J. Heeger, Science 2007 317 222-225.

[146] Hiramoto, M., Suezaki, M., & Yokoyama, M. (1990). Effect of thin gold interstitial-layer on the photovoltaic properties of tandem organic solar cell. *Chemistry Letters*, *3*, 327-330.

[147] Xue, J., Uchida, S., Rand, B. P., & Forrest, S. R. (2004). Asymmetric tandem organic photovoltaic cells with hybrid planar-mixed molecular heterojunctions. *Applied Physics Letters*, *85*, 5757-5759.

[148] Heliatek. Heliatek and IAPP achieve production-relevant efficiency record for organic photovoltaic cells. Retrieved November 8, 2010, from http://www.heliatek.com/news-19

[149] Yakimov, A., & Forrest, S. R. (2002). High photovoltage multiple-heterojunction organic solar cells incorporating interfacial metallic nanoclusters. *Applied Physics Letters*, *80*, 1667-1669.

[150] Drechsel, J., Männig, B., Kozlowski, F., Gebeyehu, D., Werner, A., Koch, M., Leo, K., & Pfeiffer, M. (2004). High efficiency organic solar cells based on single or multiple PIN structures. *Thin Solid Films, 451-452,* 515-517.

[151] Schueppel, R., Timmreck, R., Allinger, N., Mueller, T., Furno, M., Uhrich, C., Leo, K., & Riede, M. (2010). Controlled current matching in small molecule organic tandem solar cells using doped spacer layers. *Journal of Applied Physics*, *107*.

[152] Inoue, J., Yamagishi, K., & Yamashita, M. (2007). Photovoltaic properties of multilayer organic thin films. *Journal of Crystal Growth*, *298*, 782-786.

[153] Cheyns, D., Gommans, H., Odijk, M., Poortmans, J., & Heremans, P. (2007). Stacked organic solar cells based on pentacene and C60. *Solar Energy Materials and Solar Cells*, *91*, 399-404.

[154] Taima, T., Yamanari, T., Sakai, J., & Yoshida, Y. (2010). Tandem organic photovoltaic cells based on low-molecular-weight semiconductors. *Japanese Journal of Applied Physics*, *49*, 01AC04.

[155] Xue, J., Uchida, S., Rand, B. P., & Forrest, S. R. (2004). Asymmetric tandem organic photovoltaic cells with hybrid planar-mixed molecular heterojunctions. *Applied Physics Letters*, *85*, 5757-5759.

[156] Schueppel, R., Timmreck, R., Allinger, N., Mueller, T., Furno, M., Uhrich, C., Leo, K., & Riede, M. (2010). Controlled current matching in small molecule organic tandem solar cells using doped spacer layers. *Journal of Applied Physics*, *107*.

[157] Kim, J. Y., Lee, K., Coates, N. E., Moses, D., Nguyen, T.-Q., Dante, M., & Heeger, A. J. (2007). Efficient tandem polymer solar cells fabricated by all solution processing. *Science*, *317*, 222-225.

[158] L Dou et. al. Nature Photonics, 6, 180,2012

[159] Spanggaard H, Krebs F (2004) A brief history of the development of organic and polymeric photovoltaics. Sol Energy Mater Sol Cells 83:125–146

[160] Shrotriya V, Li G, Yao Y et al (2006) Accurate measurement and characterization of organic solar cells. Adv Func Mat 16:2016–2023

[161] Shrotriya V, Li G, Yao Y et al (2006) Accurate measurement and characterization of organic solar cells. Adv Func Mat 16:2016–2023

[162] Dutta U, Chatterjee P (2004) The open circuit voltage in amorphous silicon p-i-n solar cells and its relationship to material, device and dark diode parameters. J Appl Phys 96:2261–2272

[163] Shrotriya V, Li G, Yao Y et al (2006) Accurate measurement and characterization of organic solar cells. Adv Func Mat 16:2016–2023

[164] Liang, Y. Y.*;* Xu, Z.*;* Xia, J. B.*;* Tsai, S. T.*;* Wu, Y.*;* Li, G.*;* Ray, C.*;* Yu, L. P. Adv. Mater. 2010, 22, E135.

[165] G. Li, V. Shrotriya, Y. Yao, Y. Yang, J. Appl. Phys. 2005, 94, 043704.

[166] X. Yang, J. Loos, S. C. Veenstra, W. J. H. Verhees, M. M. Wienk, J. M. Kroon, M. A. J. Michels, R. A. J. Janssen, Nano Lett. 2005, 5, 579.

[167] Y. Kim, S. Cook, S. M. Tuladhar, S. A. Choulis, J. Nelson, J. R. Durrant, D. D. C. Bradley, M. Giles, I. McCulloch, C.-S. Ha, M. Ree, Nat. Mater. 2006, 5, 197.

[168] M. D. Irwin, D. B. Buchholz, A. W. Hains, R. P. H. Chang, T. J. Marks, PNAS, 2008, 105, 2783.

[169] M. S. White, D. C. Olson, S. E. Shaheen, N. Kopidakis, D. S. Ginley, Appl.Phys. Lett. 2006, 89, 143517.

[170] L Zeng et .al. Applied Physics Letters, 97, 053305,2010

[171] S Lee et.al. Applied Physics Letters, 97, 103503, 2010

[172] W. L. Ma, C. Y. Yang, X. Gong, K. Lee, and A. J. Heeger, Adv. Funct. Mater. **15**, 1617 (2005)

[173] G. Li, S. Shrotriya, J. S. Huang, Y. Yao, T. Moriarty, K. Emery, and Y. Yang, Nature Mater. **4**, 864 (2005).

[174] M. Morana, M. Wegscheider, A. Bonanni, N. Kopidakis, S. Shaheen, M. Scharber, Z. Zhu, D. Waller, R. Gaudiana, C. J. Brabec, Adv. Funct. Mater. 2008, 18, 1757.

[175] H. Hoppe, S. Sariciftci, Adv. Polym. Sci. 2007, 12, 121.

[176] M. Riedel, V. Dyakonov, Phys. Status Solidi A 2004, 201, 1332.

[177] P. Schilinsky, C. Waldauf, C. J. Brabec, Appl. Phys. Lett. 2002, 81, 3885.

[178] S.-S. Li, K.-H. Tu, C.-C. Lin, C.-W. Chen, and M. Chhowalla, ACSNANO **6**, 3169 (2010).

[179] S. Han, W. S. Shin, M. Seo, D. Gupta, S.-J. Moon, and S. Yoo, Organic Electronics **10**, 791 (2009).

[180] F. Liu, S. Shao, X. Guo, Y. Zhao, Z. Xie, Sol. Energy Mater. Sol. Cells **94**, 842 (2010).

[181] Cravino A, Schilinsky P, Brabec C (2007) Characterization of organic solar cells: the importance of device layout. Adv Func Mat 17:3906–3910

[182] Kim M-S, Kang M-G, Guo L-J et al (2008) Choice of electrode geometry for accurate measurement of organic photovoltaic cell performance. Appl Phys Lett 92:133301–133304

[183] Li G, Shrotriya V, Huang J et al (2005) High-efficiency solution processable polymer photovoltaic cells by self-organization of polymer blends. Nat Mater 4:864–868

[184] Miller S, Fanchini G, Lin Y-Y et al (2008) Investigation of nanoscale morphological changes in organic photovoltaics during solvent vapor annealing. J Mater Chem 18:306–312

[185] Shaheen SE, Brabec C, Padinger F et al (2001) 2.5% efficient organic plastic solar cells. Appl Phys Lett 78:841–843

[186] Neugebauer H, Brabec C, Hummelen JC, Sariciftci NS (2000) Stability and photodegradation mechanisms of conjugated polymer/fullerene plastic solar cells 61:35–42

[187] Dennler G, Lungenschmied C, Neugebauer H et al (2006) A new encapsulation solution for flexible organic solar cells. Thin Solid Films 511:349–353

[188] B. Crone , A. Dodabalapur , Y.-Y. Lin , R. W. Filas , Z. Bao , A. LaDuca , R. Sarpeshkar , H. E. Katz , W. Li , *Nature* **2000** , *403* , 521 .

[189] T. Someya , T. Sekitani , S. Iba , Y. Kato , H. Kawaguchi , T. Sakurai , *Proc. Natl. Acad. Sci USA* **2004** , *101* , 9966 .

[190] S. Cho, J. Yuen, J. Y. Kim, K. Lee, and A. J. Heeger, Appl. Phys. Lett **90**, 063511 (2007).

[191] J. Gao, J. Hui, Y. Hou, and S. Alem, J. Appl. Phys. **104**, 084512 (2008).

[192] L. L. Chua, J. Zaumseil, J-F. Chang, E. C.-W. Ou, P. K.-H. Ho, H. Sirringhaus, and R. H. Friend, Nature (London) **434**, 194 (2005).

[193] C. D. Müller, A. Falcou, N. Reckefuss, M. Rojahn, V. Wiederhirn, P. Rudati, H. Frohne, O. Nuyken, H. Becker, and K. Meerholz, Nature (London) **421**, 829 (2003).

[194] Eo, Y.S.; Rhee, H.W.; Chin, B.D.; Yu, J.-W. Influence of metal cathode for organic photovoltaic device performance. *Synth. Met.* **2009**, *159*, 1910-1913.

[195] V. D. Mihailetchi, P. W. M. Blom, J. C. Hummelen, and M. T. Rispens J. Appl. Phys. 94, 6849 (2003)

[196] C. M. Ramsdale, J. A. Barker, A. C. Arias, J. D. MacKenzie, R. H. Friend, and N. C. Greenham J. Appl. Phys. **92**, 4266 (2002);

[197] N. S. Lewis, SCIENCE **315**, 798 (2007).

[198] B. Tian, X. Zheng, T. J. Kempa, Y. Fang, N. Yu, G. Yu, J. Huang, and C. M. Lieber, Nature **449**, 885 (2007).

[199] S. Cho, J. Yuen, J. Y. Kim, K. Lee, and A. J. Heeger, Appl. Phys. Lett **90**, 063511 (2007).

[200] S. Nagata, G. M. Atkinson, D. Pestov, G. C. Tepper, and J. T. McLeskey Jr, Sol. Energy Mater. Sol. Cells **95**, 1594 (2011).

[201] J. Gao, J. Hui, Y. Hou, and S. Alem, J. Appl. Phys. **104**, 084512 (2008).

[202] C. Deibel, T. Strobel, and V. Dyakonov, Adv. Mater. **22**, 4097 (2010).

[203] S. Cho, J. Yuen, J. Y. Kim, K. Lee, and A. J. Heeger, Appl. Phys. Lett **90**, 063511 (2007).

[204] J. Gao, J. Hui, Y. Hou, and S. Alem, J. Appl. Phys. **104**, 084512 (2008).

[205] S.W. Tong, C.F. Zhang, C.Y. Jiang, G. Liu, Q.D. Ling, E.T. Kang, D.S.H. Chan , and C. Zhu, Chemical Phys. Lett. **453**, 73 (2008).

[206] V. Shrotriya, G. Li, Y. Yao, C.-W. Chu, and Y. Yang, Appl. Phys. Lett. **88**, 073508 (2006).

[207] J. S. Kim, J. H. Park, J. H. Lee, J. Jo, D.-Y. Kim, and K. Cho, Appl. Phys. Lett. **91**, 112111 (2007).

[208] J. Kim, D.-Y. Khang, J.-H. Kim, and H. H. Lee, Appl. Phys. Lett. **92**, 133307 (2008).

[209] S. Han, W. S. Shin, M. Seo, D. Gupta, S.-J. Moon, S. Yoo, Organic Electronics **10**, 791 (2009).

[210] S.-S. Li, K.-H. Tu, C.-C. Lin, C.-W. Chen, and M. Chhowalla, ACS Nano **4**, 3169 (2010).

[211] W.-T. Chiang, S.-H. Su, Y.-F. Lin, and M. Yokoyama, J. J. of Appl. Phys. **49**, 0DK14 (2010).

[212] F. Liu, S. Shao, X. Guo, Y. Zhao, Z. Xie, Sol. Energy Mater. Sol. Cells **94**, 842 (2010).

[213] S.W. Tong, C.F. Zhang, C.Y. Jiang, G. Liu, Q.D. Ling, E.T. Kang, D.S.H. Chan , and C. Zhu, Chemical Phys. Lett. **453**, 73 (2008).

[214] F. L. Zhang, A. Gadisa, O. Inganas, M. Svensson, and M. R. Andersson, Appl. Phys. Lett. **84**, 3906 (2004).

[215] R. Steim, F. R. Kogler, and C. J. Brabec, J. Mater. Chem., **20**, 2499 (2010).

[216] H. Ma, H.-L. Yip, F. Huang, and A. K.-Y. Jen, Adv. Funct. Mater. **20**, 1371 (2010).

[217] J. Y. Kim, S. H. Kim, H.-Ho. Lee, K. Lee, W. Ma, X. Gong, A. J. Heeger, Adv. Mater. 2006, 18, 572.

[218] W.Ma, C. Yang, X. Gong, K. Lee, A. J.Heeger, Adv. Funct. Mater. 2005, 15, 1617.

[219] M. D. Irwin, D. B. Buchholz, A. W. Hains, R. P. H. Chang, T. J. Marks, PNAS, 2008, 105, 2783.

[220] J. C. Blakesley, and D. Neher, Phys. Rev. B **84**, 075210 (2011).

[221] A. Maurano, R. Hamilton, C. G. Shuttle, A. M. Ballantyne, J. Nelson, B. O'Regan, W. Zhang, L. McCulloch, H. Azimi, M. Morana, C. J. Brabec, and J. R. Durrant, Adv. Mater. **22**, 4987 (2010).

[222] G. Dennler, M. C. Scharber, and C. Brabec, Adv Mater. **21**, 1323 (2009).

[223] Y. Shen, K. Li, N. Majumdar, J. C. Campbell, and M. C. Gupta, Sol. Energy Mater. Sol. Cells **95**, 2314 (2011).

[224] J. Xue, S. Uchida, B. P. Rand, and S. R. Forrest, Appl. Phys. Lett. 84, 3013 (2004).

[225] P. Schilinsky, C. Waldauf, J. Hauch, and C. J. Brabec, J. Appl. Phys. **95**, 2816 (2004).

[226] M. Morana, P. Koers, C. Waldauf, M. Koppe, D. Muehlbacher, P. Denk, M. Scharber, D. Waller, and C. Brabec, Adv. Funct. Mater. **17**, 3274 (2007).

[227] V. D. Mihailetchi, L. J. A. Koster, J. C. Hummelen, and P.W.M. Blom, Phys. Rev. Lett. 93, 216601-1 (2004)

[228] A. J. Moule, J. B. Bonekamp, and K. Meerholz, J. Appl. Phys. **100**, 094503 (2006)

[229] J. R. Tumbleston, D.-H. Ko, E. T. Samulski, and R. Lopez, Phys. Rev. B 82, 205325 (2010)

[230] G. Li, V. Shrotriya, Y. Yao, and Y. Yang, J. Appl. Phys. 98, 043704 (2005).

[231] D. W. Sievers, V. Shrotriya, and Y. Yang, J. Appl. Phys. 100, 114509 (2006).

[232] A. J. Moule, J. B. Bonekamp, and K. Meerholz, J. Appl. Phys. **100**, 094503 (2006).

[233] V. Shrotriya, G. Li, Y. Yao, T. Moriarty, K. Emery, and Y. Yang, Adv. Func. Mater. 16, 2016 (2006).

[234] K. Emery, C. Osterwald, in Current Topics in Photovoltaics Vol.3, Academic London 1988, Ch.4.

[235] J. Gao, J. Hui, Y. Hou, and S. Alem, J. Appl. Phys. **104**, 084512 (2008).

[236] S. Nagata, G. M. Atkinson, D. Pestov, G. C. Tepper, and J. T. McLeskey Jr, Sol. Energy Mater. Sol. Cells **95**, 1594 (2011)

[237] G. Dennler, M. C. Scharber, and C. J. Brabec, Adv. Mater. 21, 1323–1338 (2009)

[238] S. Cho, J. Yuen, J. Y. Kim, K. Lee, and A. J. Heeger, Appl Phys. Lett. **90**, 063511 (2007

[239] P. E. Shaw, A. Ruseckas, and I. D. W. Samuel, Adv. Mater. **20**, 3516 (2008).

[240] C. Deibel1 and V. Dyakonov, Rep. Prog. Phys. **73**, 096401 (2010).

[241] S. E. Shaheen, C. J. Brabec, N. S. Sariciftci, F. Padinger, T. Fromherz, and J. C. Hummelen, Appl. Phys. Lett. **78**, 841 (2001).

[242] Y. Xie, P. Dutta, D. Cengher, V. Bommisetty, J. Li, D. Galipeau, Q. Qiao, Proc. SPIE **7416**, 74161Q (2009).

[243] W. Ma, C. Yang, X. Gong, K. Lee, A. J. Heeger, Adv. Funct. Mater **15**, 1617 (2005).

[244] R. D. Bettignies, J. Leroy, M. Firon, C. Sentein, Synthetic Metals **156**, 510 (2006).

[245] D. Chirvase, J. Parisi, J. C. Hummelen, V. dyakonov, nanotechnology **15**, 1317 (2004).

[246] M. C.-Quiles, T. Ferenczi, T. Agostinelli, P. G. Etchegoin, Y. Kim, T. D. Anthopoulos, P. N. Stavrinou, D. D. C. Bradley, J. Nelson, Nature Materials **7**, 158 (2008).

[247] G. Dennler, M. C. Scharber, and C. Brabec, Adv Mater. **21**, 1323 (2009).

[248] R. Giridharagopal, and D. S. Ginger, J. Phys. Chem. Lett. **1**, 1160 (2010).

[249] Y. Kim, S. Cook, S. M. Tuladhar, S. A. Choulis, J. Nelson, J. R. Durrant, D. D. C. Bradley, M. Giles, I. Mcculloch, C.-S. HA, and M. Ree, nature materials **5**, 197(2006).

[250] D. Chirvase, J. Parisi, J. C. Hummelen, V. dyakonov, nanotechnology **15**, 1317 (2004).

[251] R. D. Bettignies, J. Leroy, M. Firon, C. Sentein, Synthetic Metals **156**, 510 (2006).

[252] F.-C. Chen, C.-J. Ko, J.-L. Wu, and W.-C. Chen, Sol. Energy Mater. Sol. Cells **94**, 2426 (2010).

[253] S. H. Park, A. Roy, S. Beaupre, S. Cho, N. Coates, J. S. Moon, D. Moses, M. Leclerc, K. Lee, A. J. Heeger Nature Photonics **3**, 297 (2009).

[254] G. Li, V. Shrotriya, J. Huang, Y. Yao, T. Moriarty, K. Emery, and Y. Yang, Nature Materials **4**, 864 (2005).

[255] D. S. Germack, C. K. Chan, B. H. Hamadani, L. J. Richter, D. A. Fischer, D. J. Gundlach, D. M. DeLongchamp, Appl. Phys. Lett. 94, 233303 (2009).

[256] D. S. Germack, C. K. Chan, B. H. Hamadani, L. J. Richter, D. A. Fischer, D. J. Gundlach, D. M. DeLongchamp, Appl. Phys. Lett. 94, 233303 (2009).

[257] A. J. Parnell, A. D. F. Dunbar, A. J. Pearson, P. A. Staniec, A. J. C. Dennison, H. Hamamatsu, M. W. A. Skoda, D. G. Lidzey, and R. A. L. Jones, Adv. Mater. **22**, 2444 (2010).

[258] M. C.-Quiles, T. Ferenczi, T. Agostinelli, P. G. Etchegoin, Y. Kim, T. D. Anthopoulos, P. N. Stavrinou, D. D. C. Bradley, J. Nelson, Nature Materials **7**, 158 (2008).

[259] Y. Ding, P. Lu, and Q. Chen, Proc. Of SPIE **7099**, 709919 (2008).

[260] D. S. Germack, C. K. Chan, B. H. Hamadani, L. J. Richter, D. A. Fischer, D. J. Gundlach, D. M. DeLongchamp, Appl. Phys. Lett. 94, 233303 (2009).

[261] G. Dennler, M. C. Scharber, and C. Brabec, Adv Mater. **21**, 1323 (2009).

[262] S.-S. Li, K.-H. Tu, C.-C. Lin, C.-W. Chen, and M. Chhowalla, ACSNANO **6**, 3169 (2010).

[263] S. Han, W. S. Shin, M. Seo, D. Gupta, S.-J. Moon, and S. Yoo, Organic Electronics **10**, 791 (2009).

[264] F. Liu, S. Shao, X. Guo, Y. Zhao, Z. Xie, Sol. Energy Mater. Sol. Cells **94**, 842 (2010).

[265] G. Li, V. Shrotriya, J. Huang, Y. Yao, T. Moriarty, K. Emery, and Y. Yang, Nature Materials **4**, 864 (2005).

[266] Y. Shen, K. Li, N. Majumdar, J. C. Campbell, and M. C. Gupta, Sol. Energy Mater. Sol. Cells **95**, 2314 (2011).

[267] D. Chirvase, J. Parisi, J. C. Hummelen, V. dyakonov, nanotechnology **15**, 1317 (2004).

[268] E. V. Hauff, J. Parisi, V. Dyakonov, Thin Solid Films **511-512**, 506 (2006).

[269] M. M. Mandoc, L. J. A. Koster, and P. W. M. Blom, Appl. Phys. Lett. **90**, 133504 (2007).